Let’s talk about AVO

Quick Recap of AVO

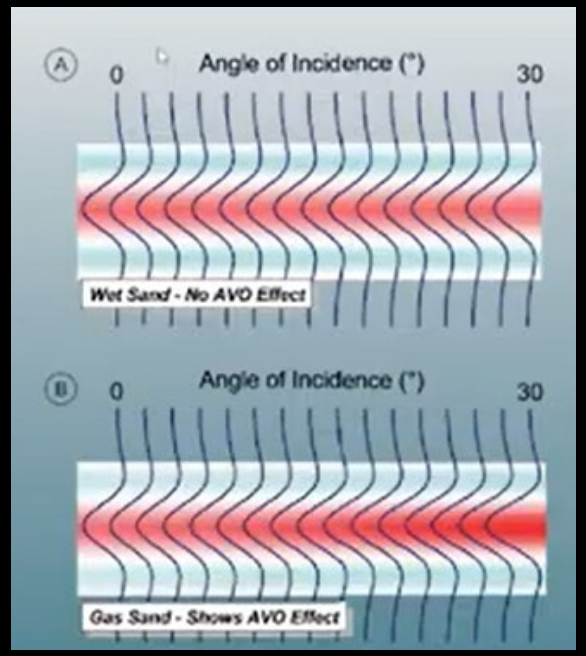

Reflection Coefficients for vertical rays

$$R_i = \frac{I_{i+1} - I_i}{I_{i+1} + I_i} \qquad I = \begin{cases} \text{Acoustic Impedance} \\ \text{or} \\ \text{Shear Impedance} \\ \text{or} \\ \text{Elastic Impedance} \end{cases}$$

Acoustic Impedance = ρV_P

Shear Impedance = ρV_S

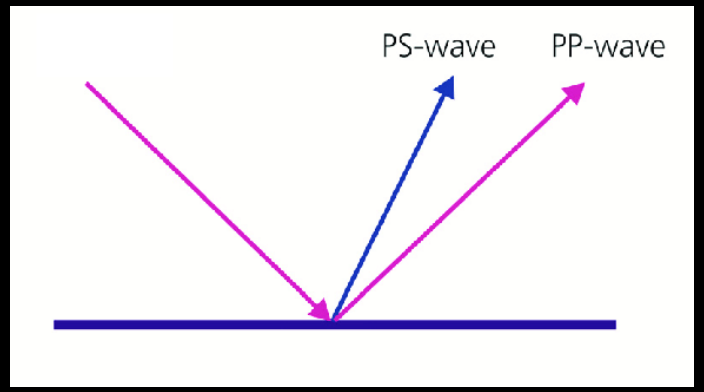

This partitioning has been quantified

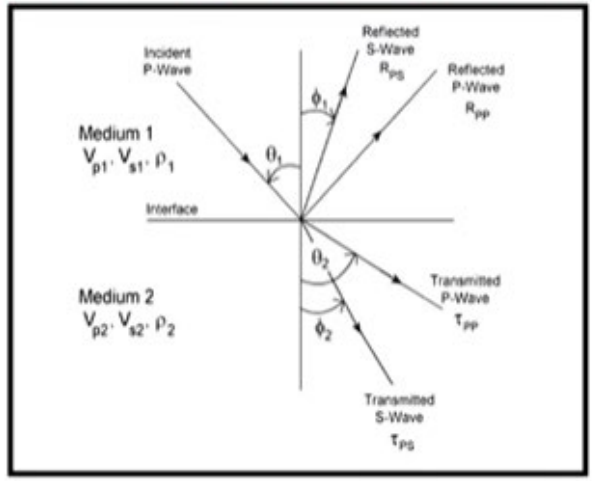

Zoeppritz (1919) published the solution

$$\begin{bmatrix} R_P \\ R_S \\ T_P \\ T_S \end{bmatrix} = \begin{bmatrix} -\sin\theta_1 & -\cos\phi_1 & \sin\theta_2 & \cos\phi_2 \\ \cos\theta_1 & -\sin\phi_1 & \cos\theta_2 & -\sin\phi_2 \\ \sin 2\theta_1 & \frac{V_{P1}}{V_{S1}}\cos 2\phi_1 & \frac{\rho_2 V_{S2}^2 V_{P1}}{\rho_1 V_{S1}^2 V_{P2}}\sin 2\theta_2 & \frac{\rho_2 V_{S2} V_{P1}}{\rho_1 V_{S1}^2}\cos 2\phi_2 \\ -\cos 2\phi_1 & \frac{V_{S1}}{V_{P1}}\sin 2\phi_1 & \frac{\rho_2 V_{P2}}{\rho_1 V_{P1}}\cos 2\phi_2 & -\frac{\rho_2 V_{S2}}{\rho_1 V_{P1}}\sin 2\phi_2 \end{bmatrix}^{-1} \begin{bmatrix} \sin\theta_1 \\ \cos\theta_1 \\ \sin 2\theta_1 \\ \cos 2\phi_1 \end{bmatrix}$$

But these equations are complex so we need to simplify them

2-term and 3-term AVO approximations

$$R(\theta) = A + B \sin^2\theta$$

$$R(\theta) = A + B \sin^2\theta + C \tan^2\theta \sin^2\theta$$

For large recording offsets we extend the analysis. The 3-term equation is required for angles > 35 degrees.

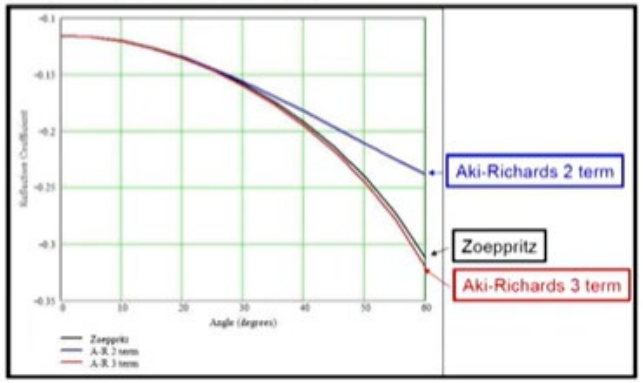

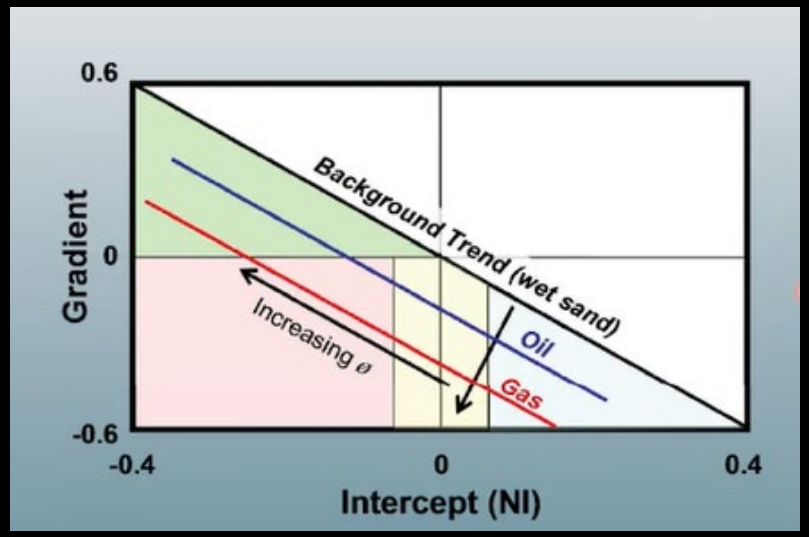

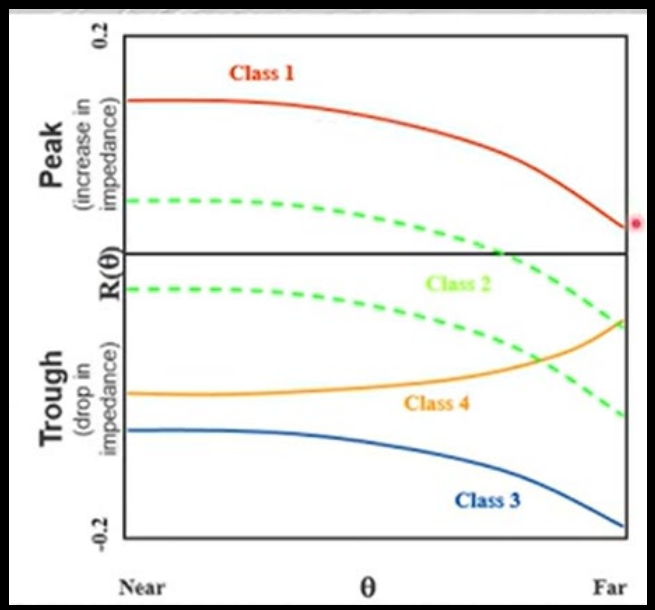

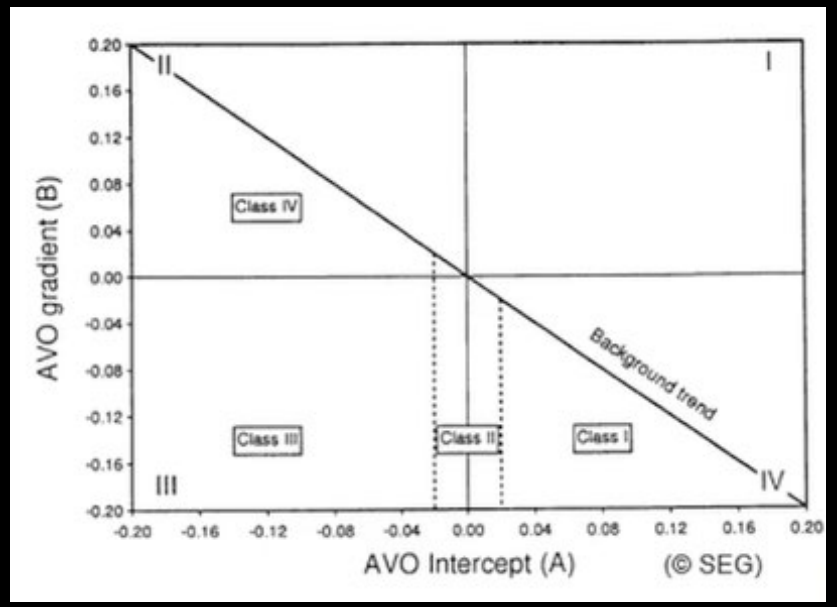

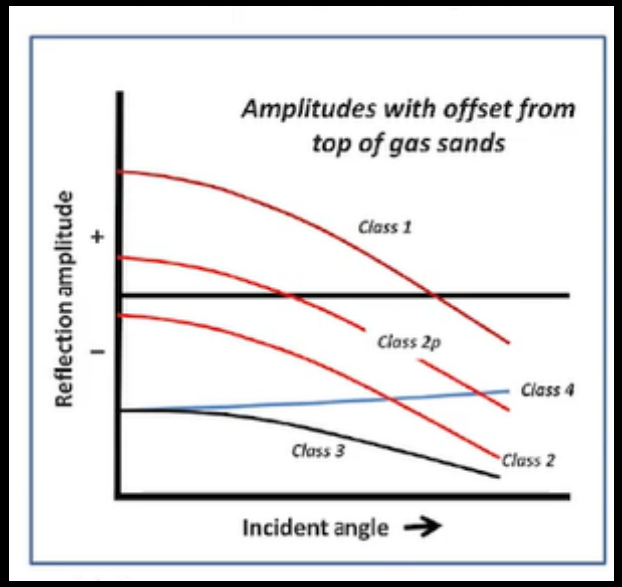

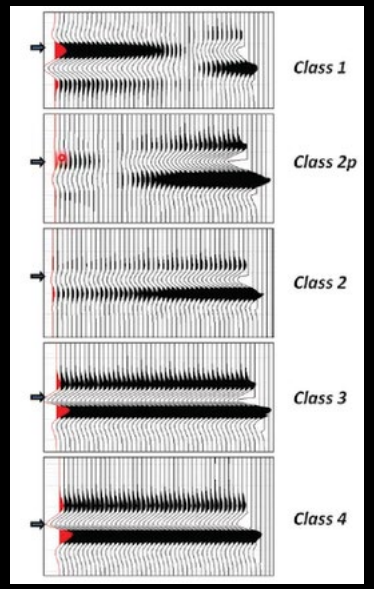

A simple AVO model – gathers

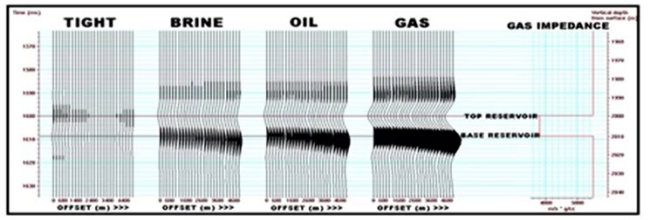

The model is a 10m thick sand for four different reservoir scenarios. Each yields a different seismic brightness and offset (angle) dependent reflectivity.

A simple AVO model - analysis

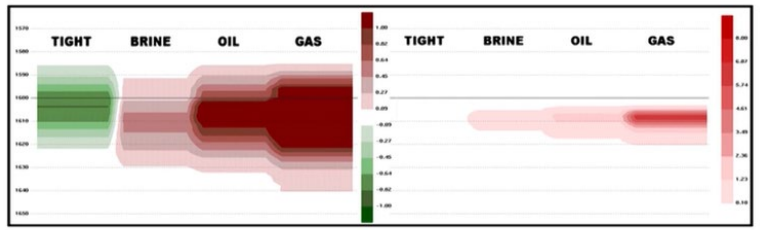

Traditional reflectivity AVO
Interfaces and low resolution

Incorporating inversion
Layers and high resolution

Do you see a Channel?

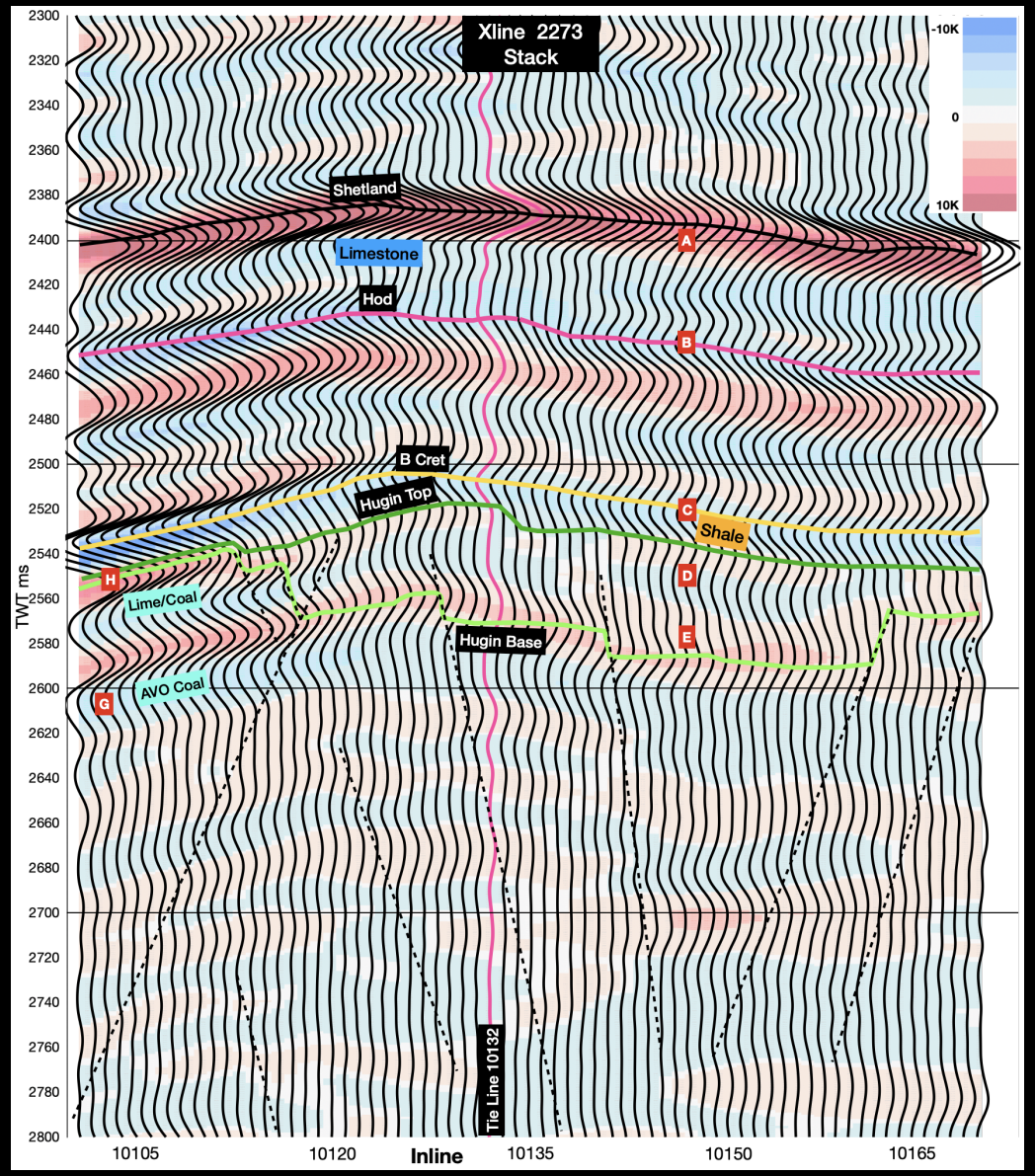

Do you see a Channel?

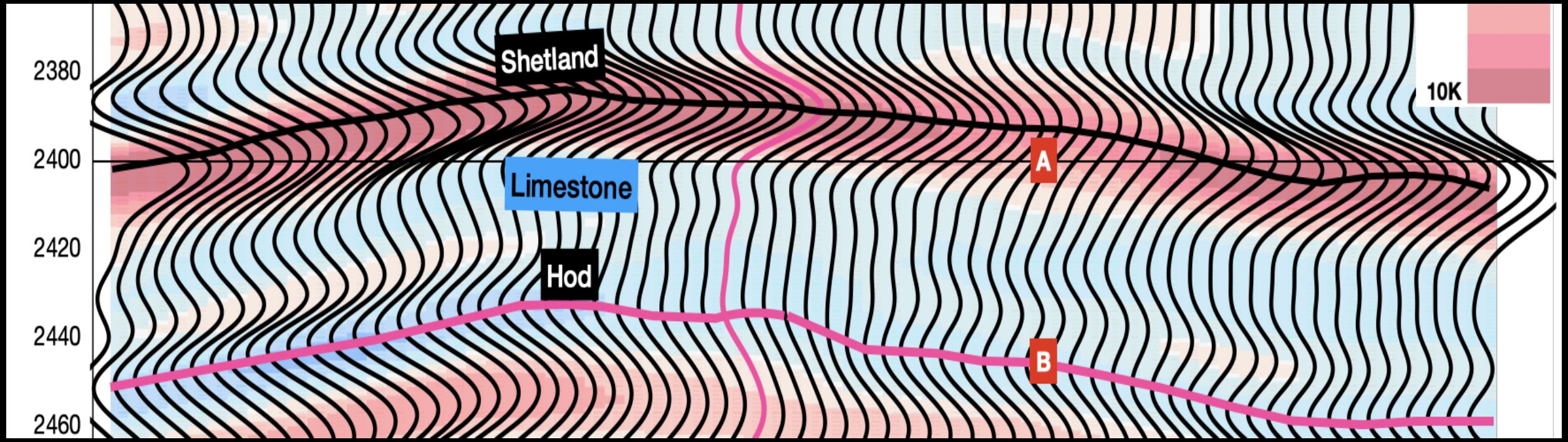

Do you see a Channel?

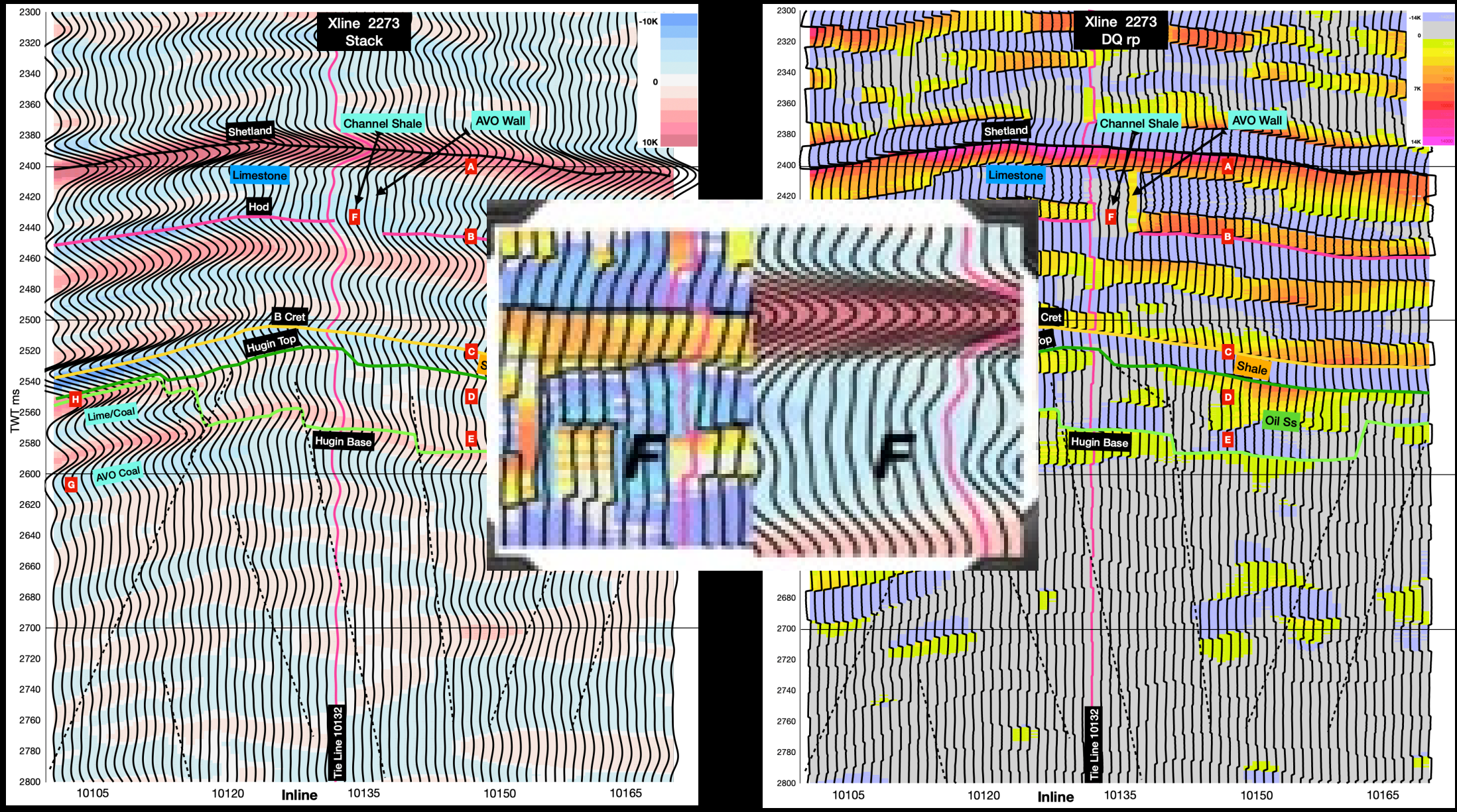

Do you see Oil Water Contact

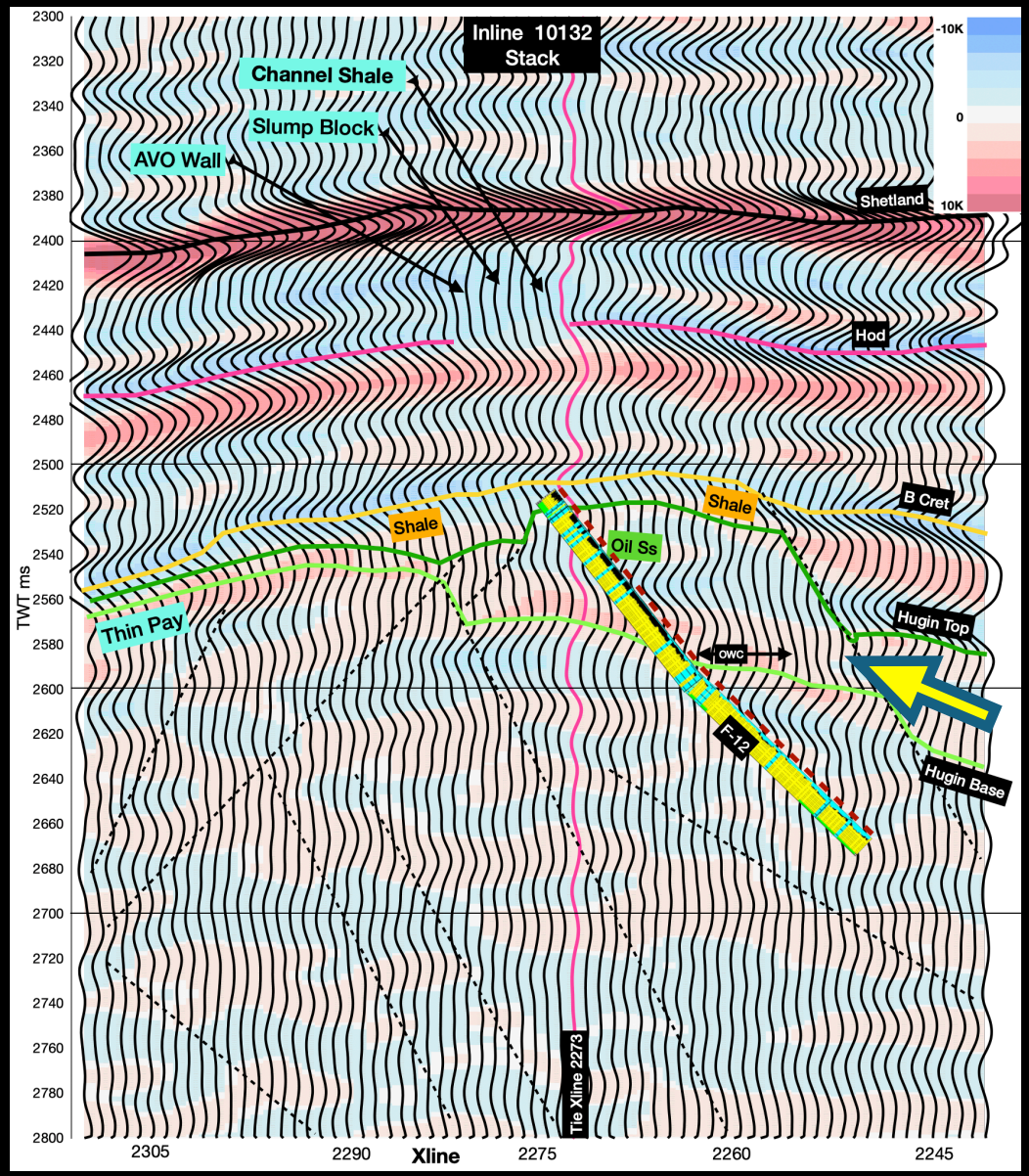

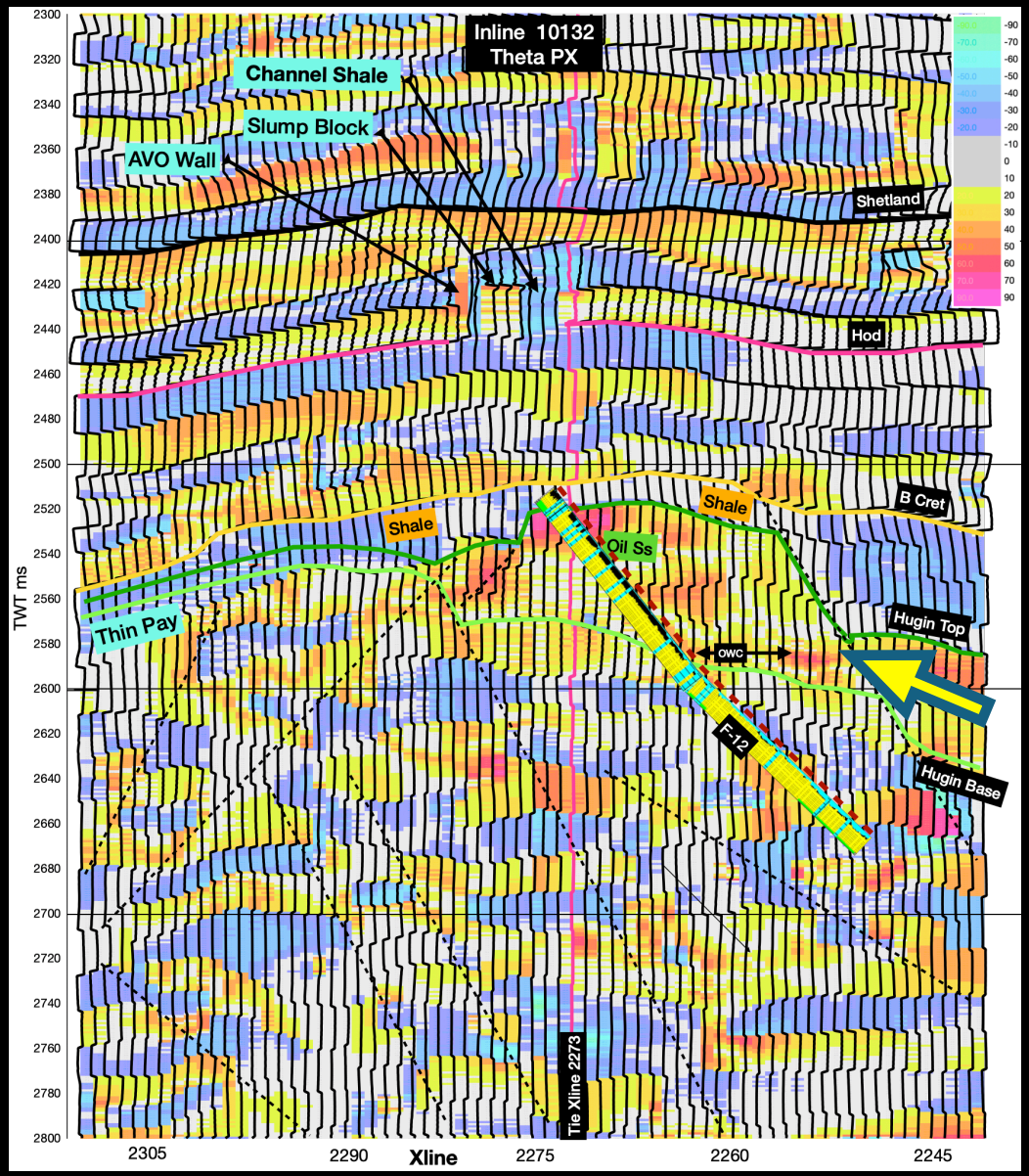

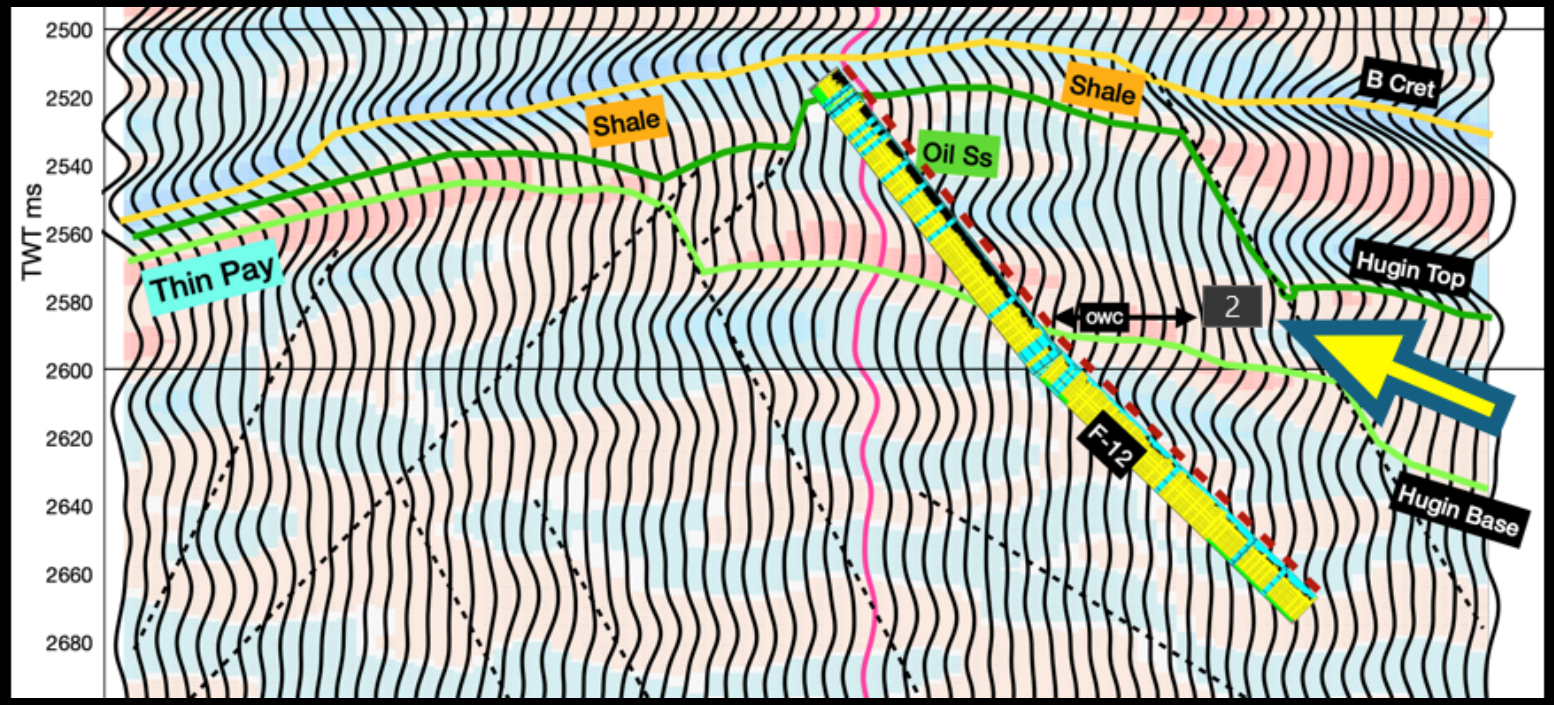
TWT ms
2500
2520
2540
2560
2580
2600
2620
2640
2660
2680
Shale
Shale
Oil Ss
B Cret
Thin Pay
Hugin Top
OWC
2
F-12
Hugin Base

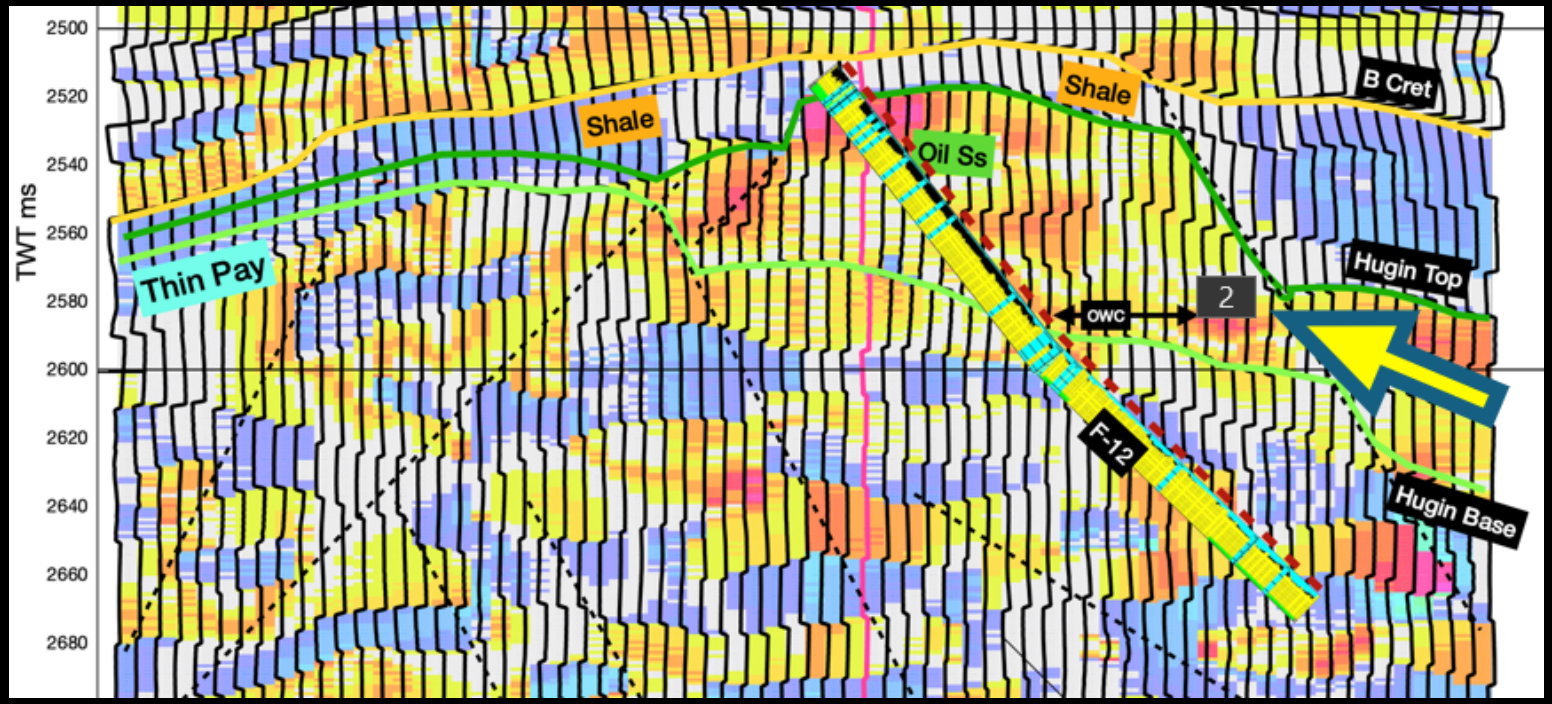
TWT ms
2500
2520
2540
2560
2580
2600
2620
2640
2660
2680
Shale
Shale
Oil Ss
B Cret
Thin Pay
Hugin Top
OWC
2
F-12
Hugin Base

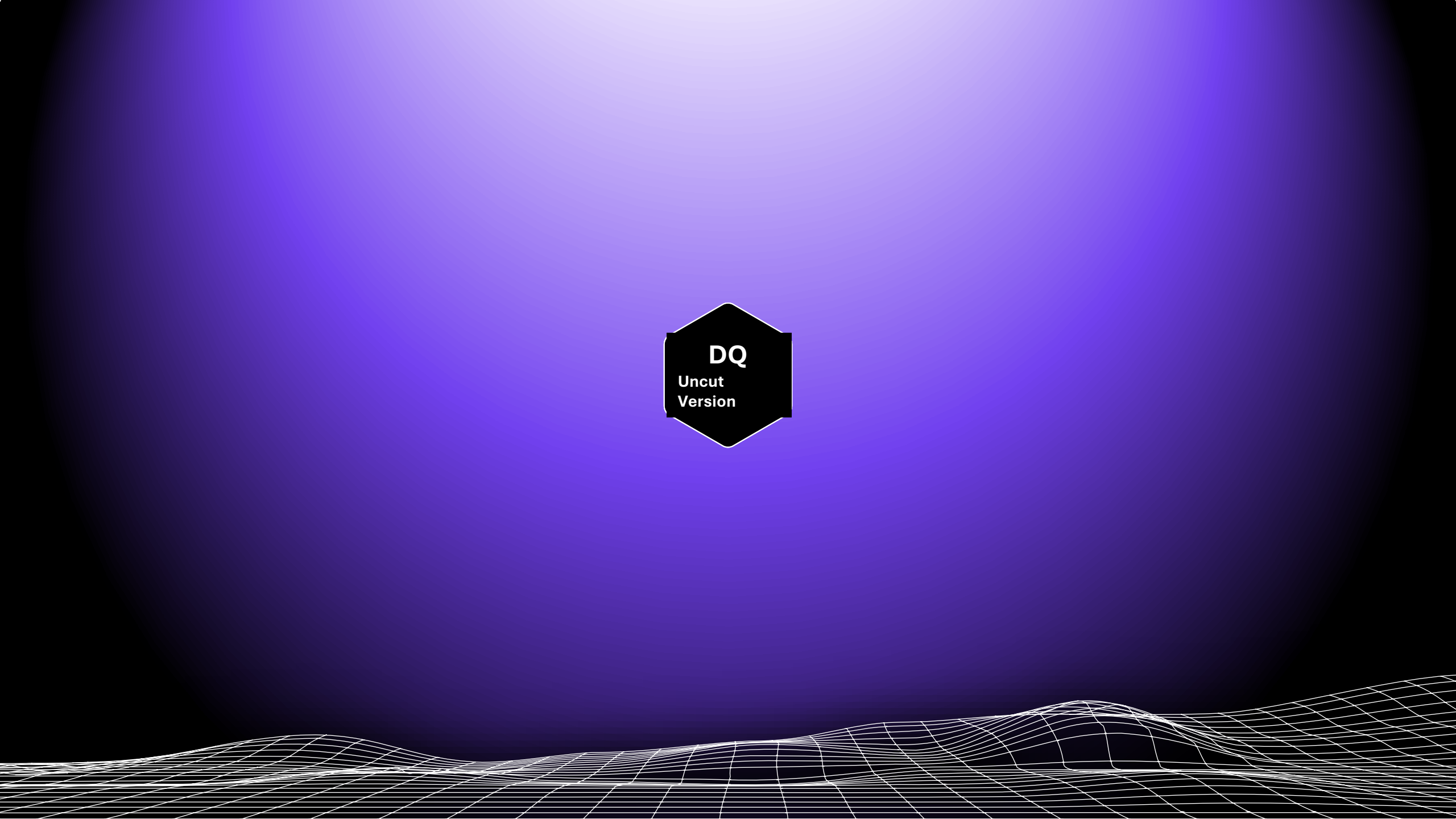
DQ
Uncut
Version


Step 3
Step 2
Step 4
Stick o gram
Step 6
Step 5
Step 7

Step 1

Step 1

In the basic two-term AVO equation;
$R(0) = A + B \sin^2\theta$, DQ uses approximations for A and B given as:

A = Near Partial Stack Trace
B = (Far - Near) Partial Stack Traces

These input traces allow us to also apply eight phase-shift filters that convert the Near/Far seismic traces to a DQ relative porosity trace.

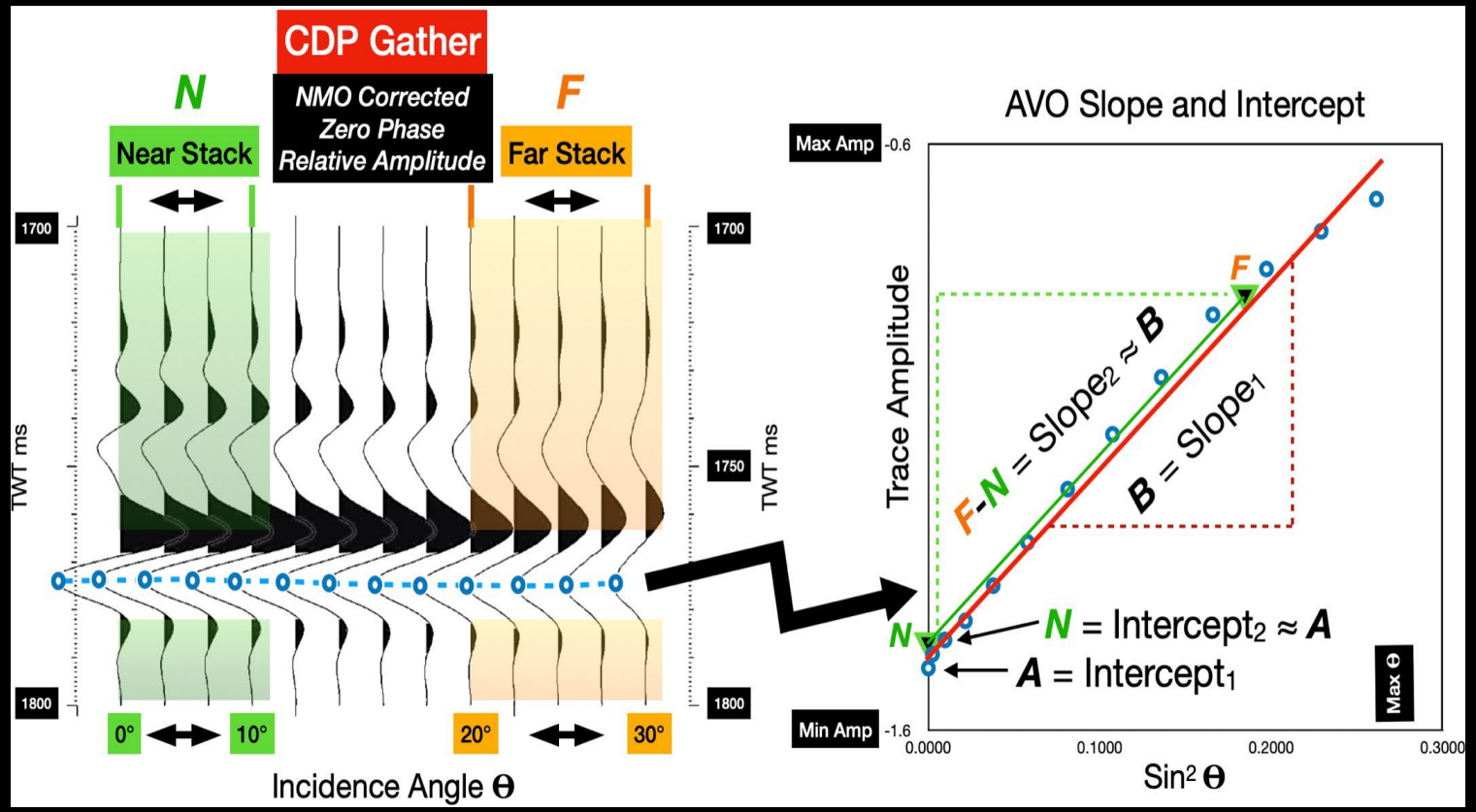

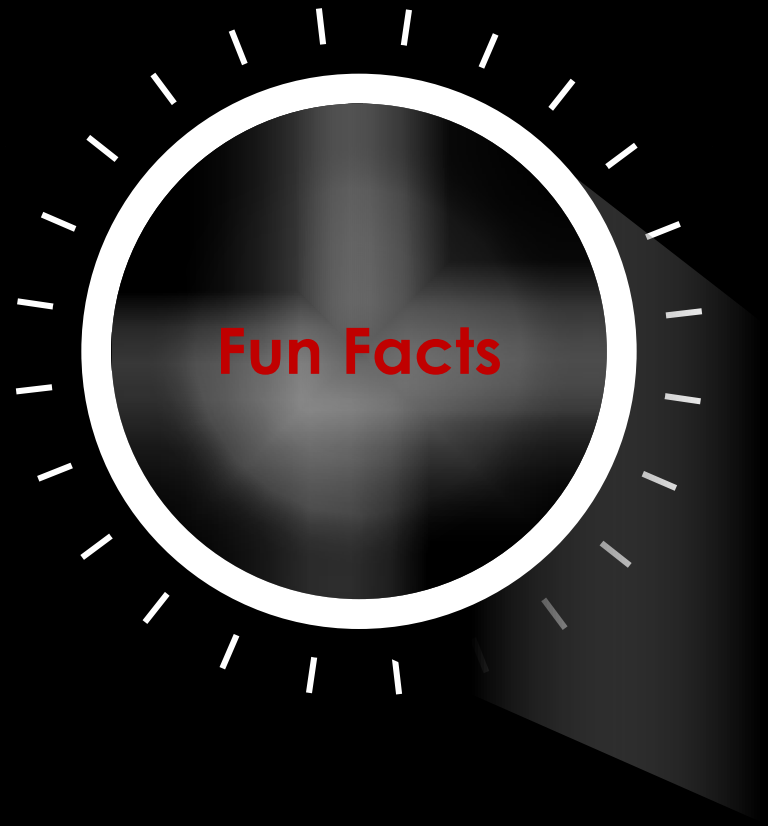
Fun Facts

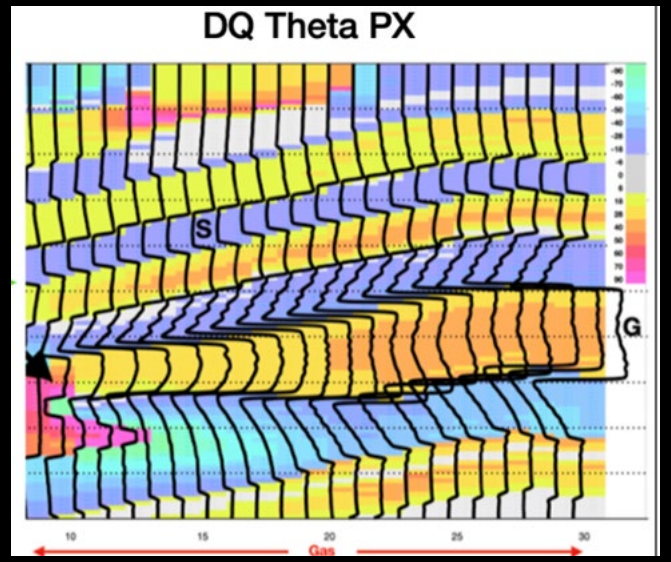

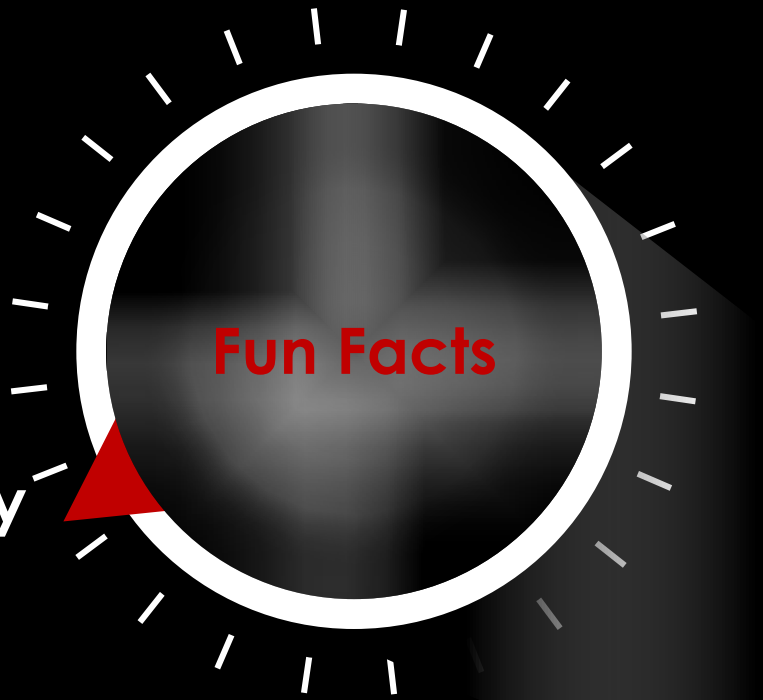

- DQ is a layer-based display of relative porosity. It is a preconditioning step to an AVO quantitative petrophysical inversion for pseudo-porosity/HPV.

- ThetaPX is an AVO Elastic Impedance trace that also captures porosity and Hydrocarbon Pore Volume (HPV) effects. It is combined with DQ and Half Isochron in an ML or inversion program.

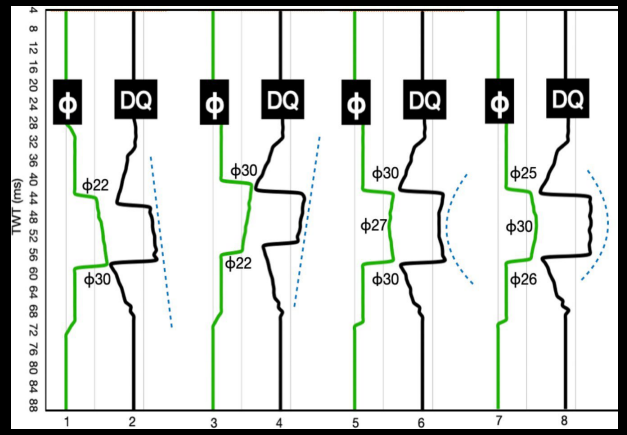

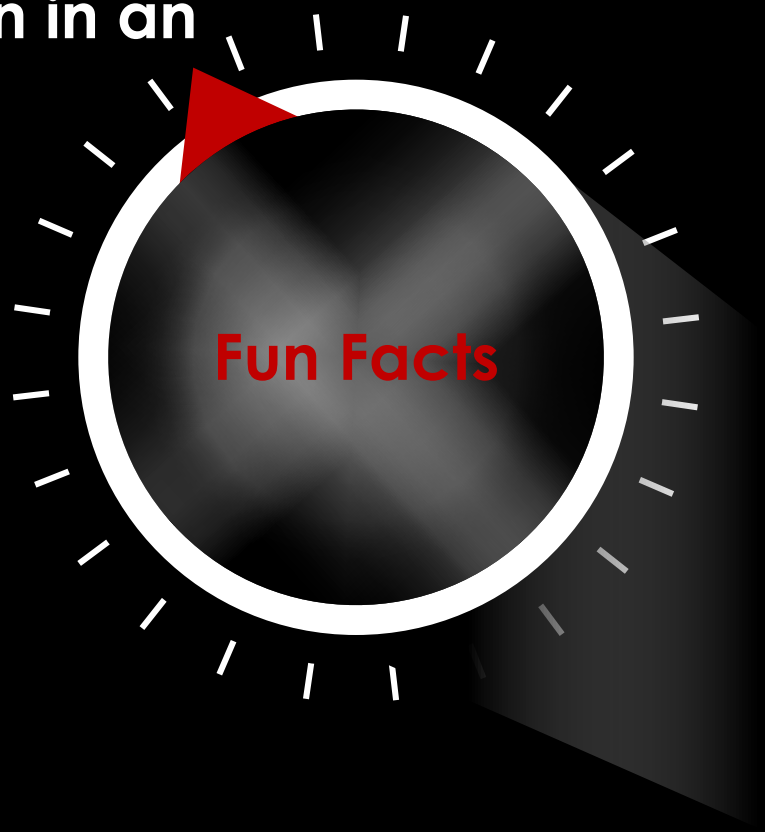

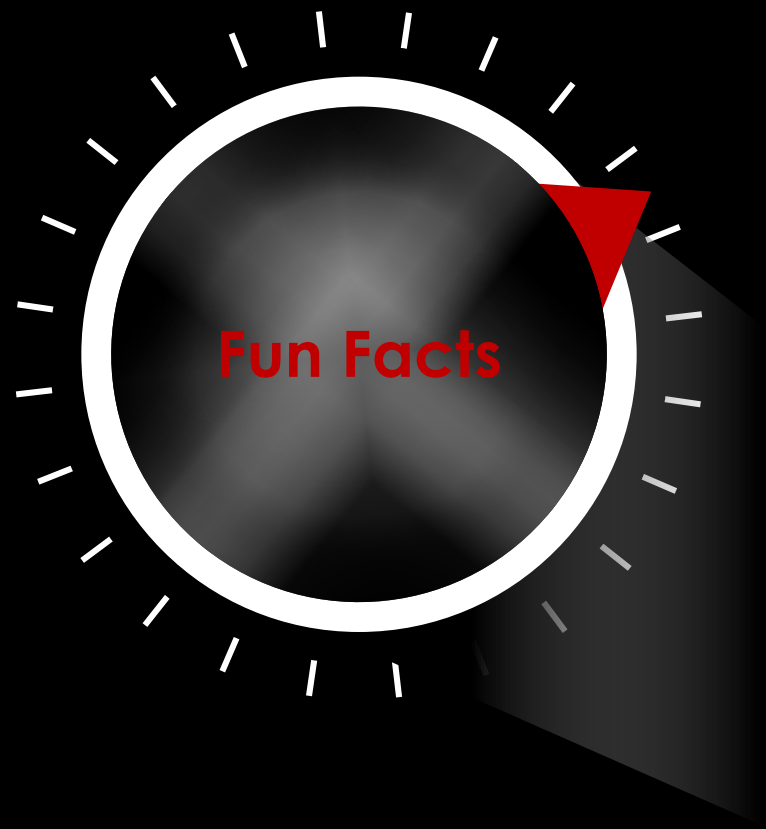

- The DQ family of attributes are intermediate products that support advanced ML and inversion programs.

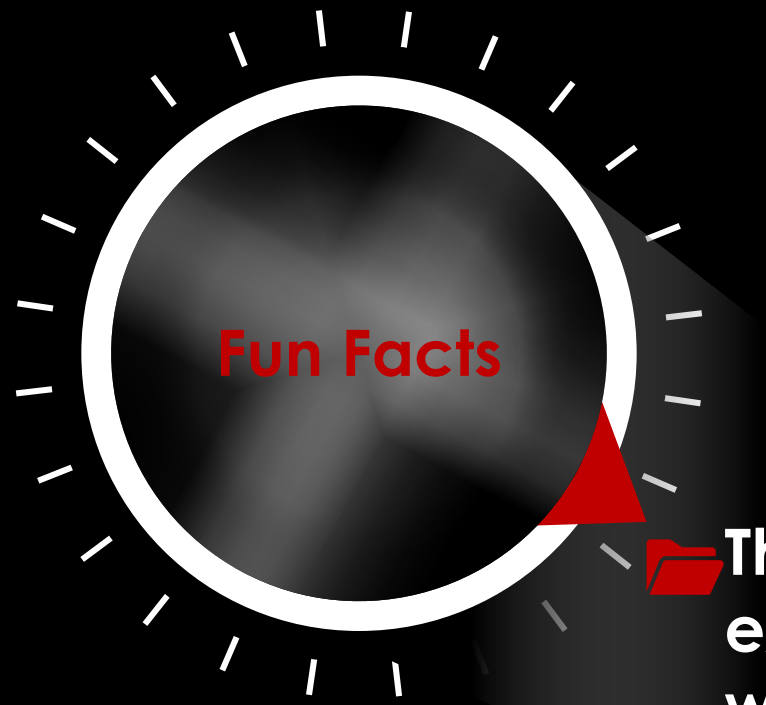

They intentionally have exceptional utility for basic workstation interpretation processes.

Define Acoustic Layers with Peak - Trough - Zero Crossings.
DQ: 1) picks all zero-crossings 2) picks all Peaks/Troughs.

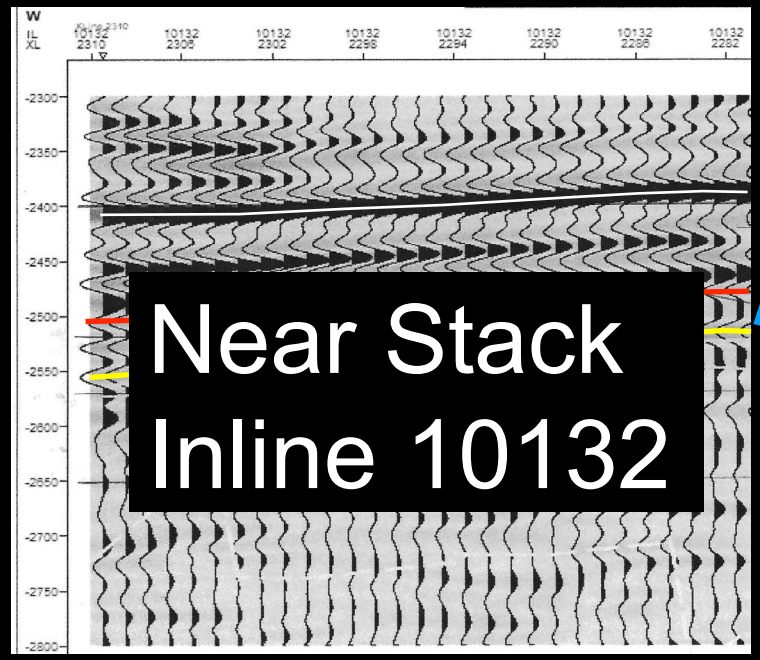

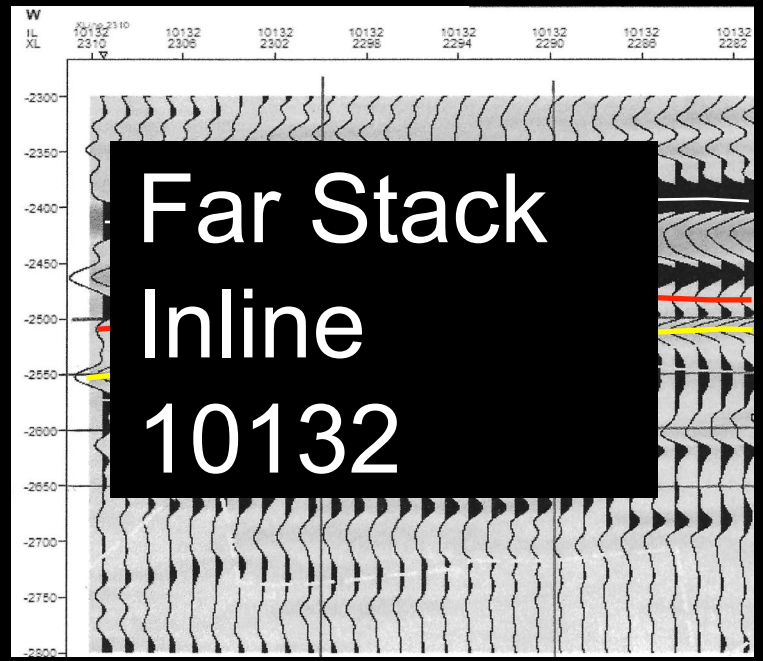

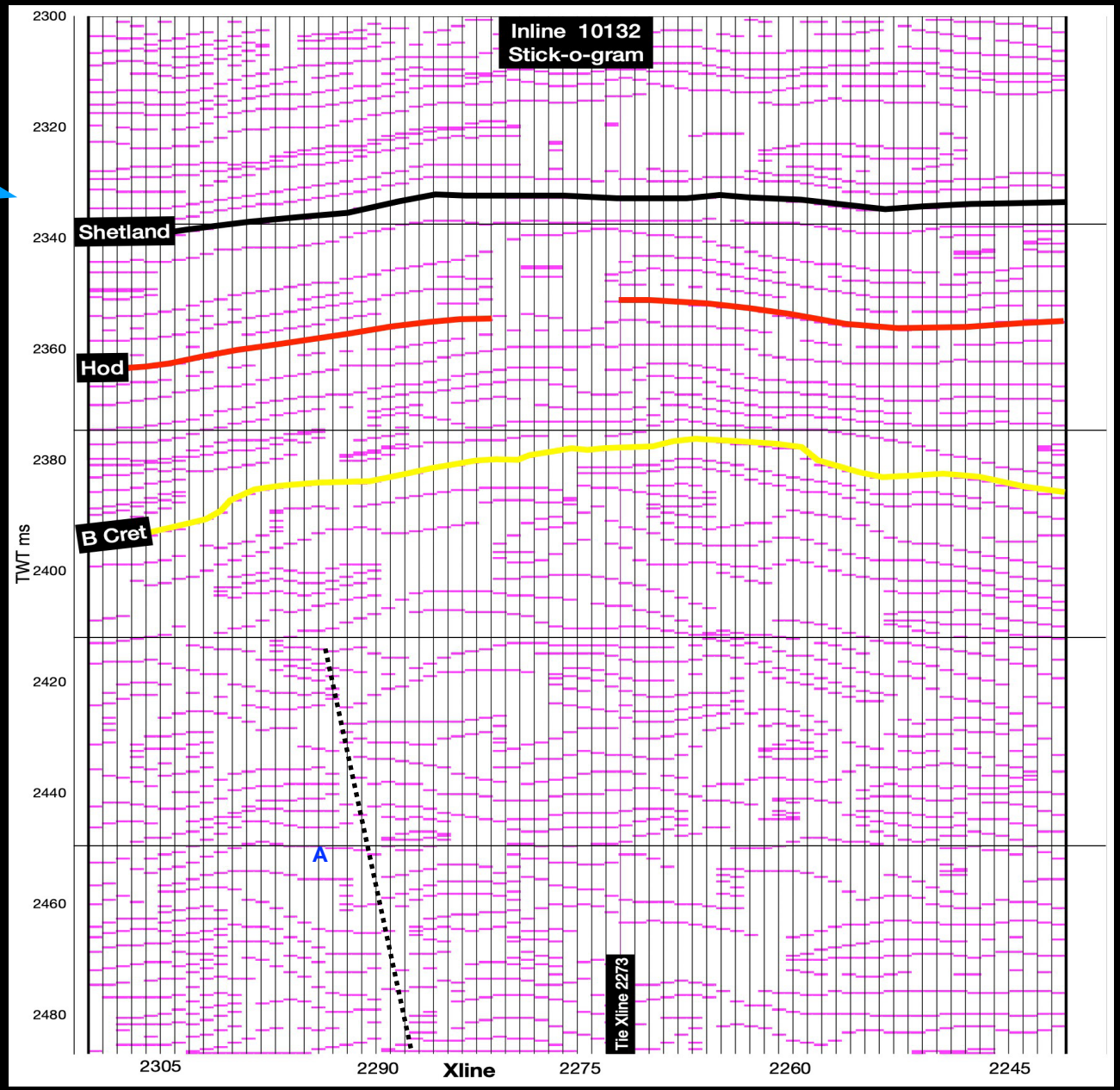

Define Acoustic Layers with Peak - Trough - Zero Crossings.
DQ: 1) picks all zero-crossings 2) picks all Peaks/Troughs.

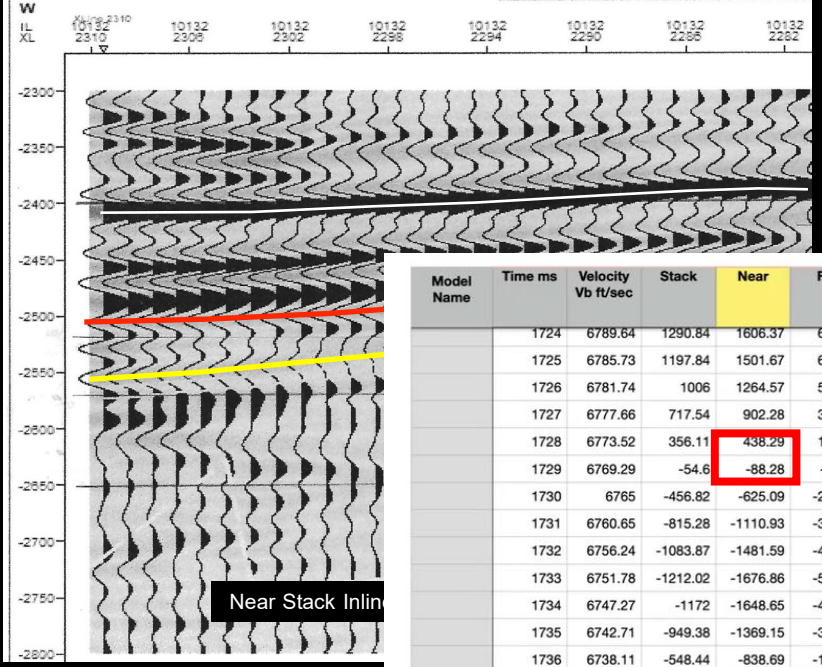

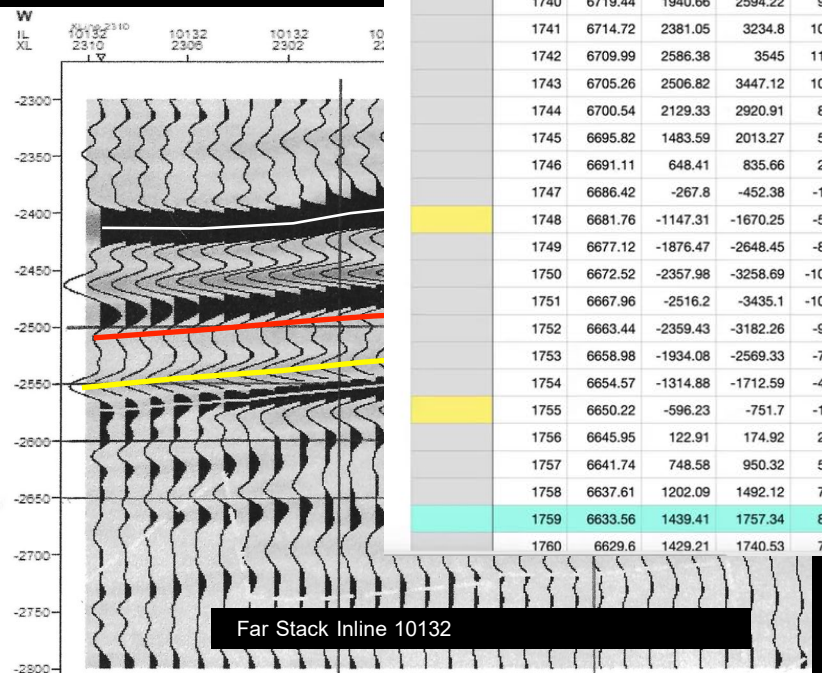

Model Name	Time ms	Velocity Vb ft/sec	Stack	Near	Far	Far-Near BA	ABD	Near Quadrant	Far-Near BA Quad	DQ	Quadrant	Slope	1/2 Isochron	Isochron	Vss %	PorE %	Shc %	HPVThick. PorFT	Thicknes s feet	Depth	Lith Symbol	X	Nea Amplit
	1724	6789.64	1290.84	1606.37	696.58	-909.8	1848.12	1606.37	-909.8	1846.12	0	1	10	13	5.49	0	0	0	4.46	6017.74	Sh	0	1,60
	1725	6785.73	1197.84	1501.67	622.75	-878.91	1741.77	1707.81	-949.93	-1954.22	1	-1	-5	-8	6.36	0	0	0	4.47	6022.2	Sh	0	1,50
	1726	6781.74	1006	1264.57	504.99	-759.58	1477.12	1634.82	-933.76	-1882.69	1	-1	-5	-8	7.24	0	0	0	4.49	6026.68	Sh	0	1,26
	1727	6777.66	717.54	902.28	340.89	-561.39	1064.44	1711.02	-968.82	-1966.27	2	-1	-5	-8	8.14	0	0	0	4.5	6031.16	Sh	0	902
	1728	6773.52	356.11	438.29	153.54	-284.74	524.59	1736.91	-984.29	-1996.42	3	-1	-5	-8	9.03	0	0	0	4.51	6035.66	Sh	0	438
	1729	6769.29	-54.6	-88.28	-54.33	33.96	-92.55	-1735.77	1002.53	-2004.49	4	-1	-5	-8	9.99	0	0	0	4.52	6040.17	Sh	0	-88
	1730	6765	-456.82	-625.09	-233.48	391.61	-735.68	-1707.63	1029.14	-1993.77	5	-1	-3	-8	9.06	0	0	0	4.51	6044.69	Sh	0	-62
	1731	6760.65	-815.28	-1110.93	-382.36	728.57	-1326.78	-1676.82	1051.68	-1979.33	6	-1	-3	-8	8.17	0	0	0	4.5	6049.2	Sh	0	-1,1
	1732	6756.24	-1083.87	-1481.59	-483.32	998.27	-1784.6	-1658.52	1095.93	-1987.9	7	-1	-3	-8	7.27	0	0	0	4.49	6053.7	Sh	0	-1,48
	1733	6751.78	-1212.02	-1676.86	-502.14	1174.73	-2045.68	-1676.86	1174.73	2047.4	8	1	4	10	6.39	0	0	0	4.47	6058.19	Sh	0	-1,67
	1734	6747.27	-1172	-1648.65	-440.99	1207.65	-2041.76	-1725.57	1263.07	2138.45	1	1	4	10	5.51	0	0	0	4.46	6062.66	Sh	0	-1,64
	1735	6742.71	-949.38	-1369.15	-304.15	1065	-1732.91	-1729.29	1319.57	2175.25	1	1	4	10	4.63	0	0	0	4.45	6067.12	Sh	0	-1,36
	1736	6738.11	-548.44	-838.69	-100.05	738.64	-1115.74	-1870.74	1458.64	2372.19	2	1	4	10	3.76	0	0	0	4.44	6071.57	Sh	0	-83
	1737	6733.48	3.38	-91.47	155.56	247.03	-261.37	-2055.56	1611.15	2611.73	3	1	6	10	2.89	0	0	0	4.43	6076.01	Sh	0	-91
	1738	6728.82	656.26	802.26	442.95	-359.31	881.18	2320.48	-1781.73	2925.61	4	1	6	10	1.98	0	0	0	4.41	6080.43	Sh	0	802
	1739	6724.14	1340.56	1739.41	734.3	-1005.11	2010.74	2627.21	-1967.57	3282.31	5	1	6	10	2.96	0	0	0	4.43	6084.85	Sh	0	1,73
	1740	6719.44	1940.66	2594.22	949.38	-1644.84	3073.67	2931.2	-2148.35	3634.19	6	1	6	10	3.83	0	0	0	4.44	6089.27	Sh	0	2,59
	1741	6714.72	2381.05	3234.8	1081.73	-2153.07	3887.56	3251.89	-2306.82	3987.01	7	1	6	10	4.7	0	0	0	4.45	6093.71	Sh	0	3,23
	1742	6709.99	2586.38	3545	1113.05	-2431.95	4300.91	3545	-2431.95	4299	0	1	6	10	5.58	0	0	0	4.46	6098.16	Sh	0	3,54
	1743	6705.26	2506.82	3447.12	1033.69	-2413.42	4209.71	3805.92	-2535.29	-4573.04	1	-1	-5	-8	6.46	0	0	0	4.47	6102.62	Sh	0	3,44
	1744	6700.54	2129.33	2920.91	844.04	-2076.86	3585.89	3745.47	-2530.58	-4520.22	1	-1	-5	-8	13.17	0	0	0	4.56	6107.1	Sh	0	2,92
	1745	6695.82	1483.59	2013.27	552.43	-1460.84	2489.14	3971.85	-2609.48	-4752.37	2	-1	-5	-8	24.29	0	0	0	4.71	6111.66	Sh	0	2,01
	1746	6691.11	648.41	835.66	201.29	-634.37	1051.04	4099.9	-2645.86	-4879.53	3	-1	-5	-8	25.22	0	0	0	4.72	6116.37	Sh	0	836
	1747	6686.42	-267.8	-452.38	-164.45	287.93	-534.48	-4161.04	2654.96	-4935.89	4	-1	-5	-8	25.82	0	0	0	4.73	6121.09	Sh	0	-45
	1748	6681.76	-1147.31	-1670.25	-510.82	1159.43	-2031.32	-4108.7	2621.14	-4873.58	5	-1	-3	-8	22.95	0	0	0	4.69	6125.81	Sh	0	-1,67
	1749	6677.12	-1876.47	-2648.45	-809.63	1838.82	-3222.49	-3958.23	2544.01	-4705.27	6	-1	-3	-8	5.98	0	0	0	4.47	6130.5	Sh	0	-2,64
	1750	6672.52	-2357.98	-3258.69	-1017.55	2241.14	-3953.06	-3725.35	2451.06	-4459.36	7	-1	-3	-8	5	0	0	0	4.45	6134.97	Sh	0	-3,25
	1751	6667.96	-2516.2	-3435.1	-1071.94	2363.16	-4167.73	-3435.1	2363.16	4169.46	8	1	5	9	4.11	0	0	0	4.44	6139.43	Sh	0	-3,43
	1752	6663.44	-2359.43	-3182.26	-986.46	2195.79	-3864.4	-3092.76	2247.03	3822.87	1	1	5	9	3.24	0	0	0	4.43	6143.87	Sh	0	-3,18
	1753	6658.98	-1934.08	-2569.33	-787.09	1782.24	-3125.23	-2746.28	2118.85	3468.66	2	1	5	9	2.38	0	0	0	4.42	6148.3	Sh	0	-2,56
	1754	6654.57	-1314.88	-1712.59	-498.49	1214.1	-2097.39	-2432.12	1979.72	3136	3	1	5	9	2.48	0	0	0	4.42	6152.72	Sh	0	-1,7
	1755	6650.22	-596.23	-751.7	-154.46	597.24	-958.41	2133.62	-1805.33	2794.91	4	1	5	9	3.34	0	0	0	4.43	6157.14	Sh	0	-75
	1756	6645.95	122.91	174.92	205.26	30.34	181.4	1904.89	-1601.56	2488.7	5	1	4	9	4.21	0	0	0	4.44	6161.57	Sh	0	175
	1757	6641.74	748.58	950.32	528.39	-421.93	1041.75	1778.56	-1404.65	2266.34	6	1	4	9	5.09	0	0	0	4.46	6166.01	Sh	0	950
	1758	6637.61	1202.09	1492.12	755.67	-736.44	1666.03	1728.88	-1170.24	2087.7	7	1	4	9	5.99	0	0	0	4.47	6170.47	Sh	0	1,49
	1759	6633.56	1439.41	1757.34	858.19	-899.15	1975.88	1757.34	-899.15	1974.01	8	1	4	9	6.98	0	0	0	4.48	6174.94	Sh	0	1,75
	1760	6629.6	1429.21	1740.53	793.77	-946.76	1983.38	1871.87	-625.14	-1973.5	1	-1	-7	-11	7.86	0	0	0	4.49	6179.42	Sh	0	1,74

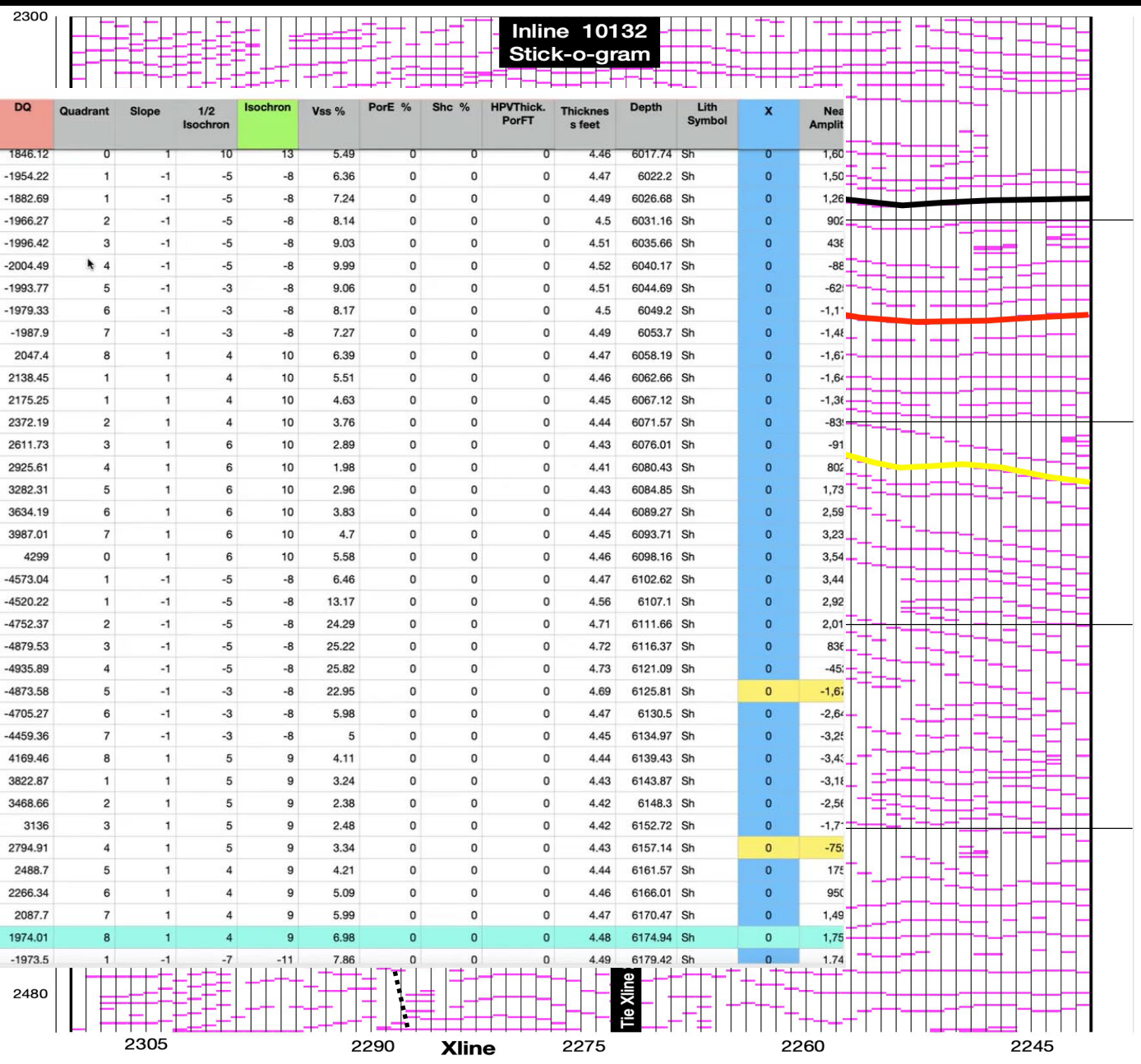

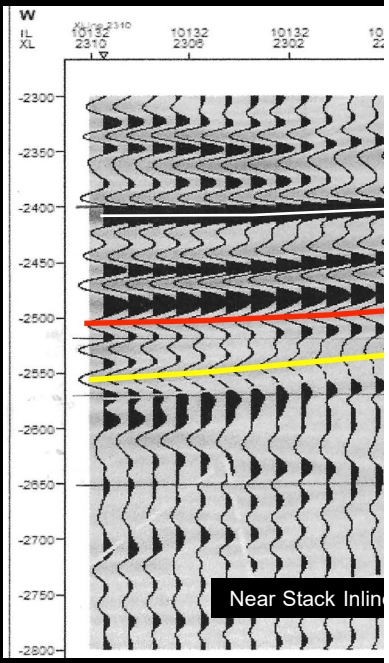

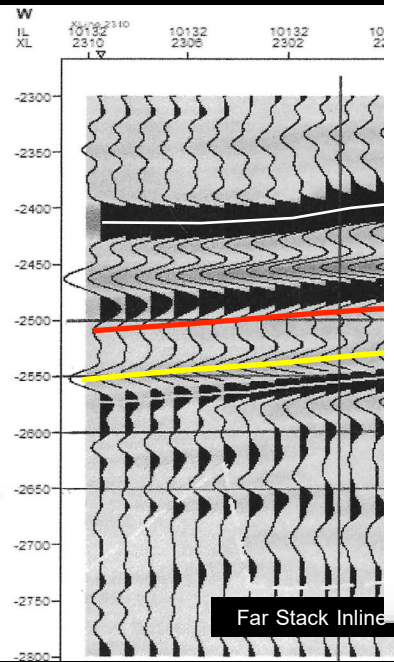

Model Name	Time ms	Velocity Vb ft/sec	Stack	Near	Far	Far-Near BA	ABD	Near Quadrant	Far-Near BA Quad	DQ	Quadrant
	1724	6789.64	1290.84	1606.37	696.58	-909.8	1848.12	1606.37	-909.8	1846.12	0
	1725	6785.73	1197.84	1501.67	622.75	-878.91	1741.77	1707.81	-949.93	-1954.22	1
	1726	6781.74	1006	1264.57	504.99	-759.58	1477.12	1634.82	-933.76	-1882.69	1
	1727	6777.66	717.54	902.28	340.89	-561.39	1064.44	1711.02	-968.82	-1966.27	2
	1728	6773.52	356.11	438.29	153.54	-284.74	524.59	1736.91	-984.29	-1996.42	3
	1729	6769.29	-54.6	-88.28	-54.33	33.96	-92.55	-1735.77	1002.53	-2004.49	4
	1730	6765	-456.82	-625.09	-233.48	391.61	-735.68	-1707.63	1029.14	-1993.77	5
	1731	6760.65	-815.28	-1110.93	-382.36	728.57	-1326.78	-1676.82	1051.68	-1979.33	6
	1732	6756.24	-1083.87	-1481.59	-483.32	998.27	-1784.6	-1658.52	1095.93	-1987.9	7
	1733	6751.78	-1212.02	-1676.86	-502.14	1174.73	-2045.68	-1676.86	1174.73	2047.4	8
	1734	6747.27	-1172	-1648.65	-440.99	1207.65	-2041.76	-1725.57	1263.07	2138.45	1
	1735	6742.71	-949.38	-1369.15	-304.15	1065	-1732.91	-1729.29	1319.57	2175.25	1
	1736	6738.11	-548.44	-838.69	-100.05	738.64	-1115.74	-1870.74	1458.64	2372.19	2
	1737	6733.48	3.38	-91.47	155.56	247.03	-261.37	-2055.56	1611.15	2611.73	3
	1738	6728.82	656.26	802.26	442.95	-359.31	881.18	2320.48	-1781.73	2925.61	4
	1739	6724.14	1340.56	1739.41	734.3	-1005.11	2010.74	2627.21	-1967.57	3282.31	5
	1740	6719.44	1940.66	2594.22	949.38	-1644.84	3073.67	2931.2	-2148.35	3634.19	6
	1741	6714.72	2381.05	3234.8	1081.73	-2153.07	3887.56	3251.89	-2306.82	3987.01	7
	1742	6709.99	2586.38	3545	1113.05	-2431.95	4300.91	3545	-2431.95	4299	0
	1743	6705.26	2506.82	3447.12	1033.69	-2413.42	4209.71	3805.92	-2535.29	-4573.04	1
	1744	6700.54	2129.33	2920.91	844.04	-2076.86	3585.89	3745.47	-2530.58	-4520.22	1
	1745	6695.82	1483.59	2013.27	552.43	-1460.84	2489.14	3971.85	-2609.48	-4752.37	2
	1746	6691.11	648.41	835.66	201.29	-634.37	1051.04	4099.9	-2645.86	-4879.53	3
	1747	6686.42	-267.8	-452.38	-164.45	287.93	-534.48	-4161.04	2654.96	-4935.89	4
	1748	6681.76	-1147.31	-1670.25	-510.82	1159.43	-2031.32	-4108.7	2621.14	-4873.58	5
	1749	6677.12	-1876.47	-2648.45	-809.63	1838.82	-3222.49	-3958.23	2544.01	-4705.27	6
	1750	6672.52	-2357.98	-3258.69	-1017.55	2241.14	-3953.06	-3725.35	2451.06	-4459.36	7
	1751	6667.96	-2516.2	-3435.1	-1071.94	2363.16	-4167.73	-3435.1	2363.16	4169.46	8
	1752	6663.44	-2359.43	-3182.26	-986.46	2195.79	-3864.4	-3092.76	2247.03	3822.87	1
	1753	6658.98	-1934.08	-2569.33	-787.09	1782.24	-3125.23	-2746.28	2118.85	3468.66	2
	1754	6654.57	-1314.88	-1712.59	-498.49	1214.1	-2097.39	-2432.12	1979.72	3136	3
	1755	6650.22	-596.23	-751.7	-154.46	597.24	-958.41	2133.62	-1805.33	2794.91	4
	1756	6645.95	122.91	174.92	205.26	30.34	181.4	1904.89	-1601.56	2488.7	5
	1757	6641.74	748.58	950.32	528.39	-421.93	1041.75	1778.56	-1404.65	2266.34	6
	1758	6637.61	1202.09	1492.12	755.67	-736.44	1666.03	1728.88	-1170.24	2087.7	7
	1759	6633.56	1439.41	1757.34	858.19	-899.15	1975.88	1757.34	-899.15	1974.01	8
	1760	6629.6	1429.21	1740.53	793.77	-946.76	1983.38	1871.87	-625.14	-1973.5	1

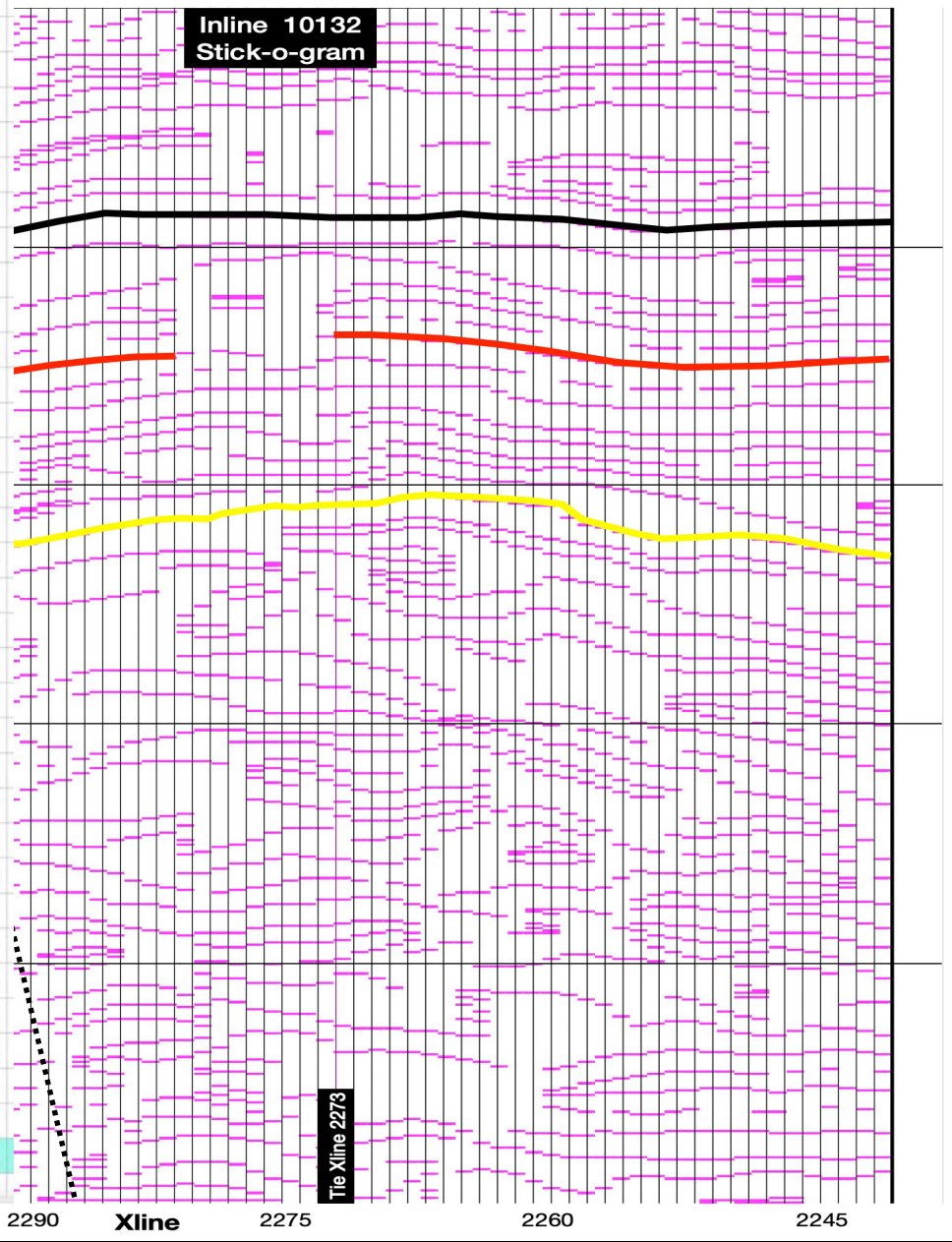

Define Acoustic Layers with Peak - Trough - Zero Crossings.
DQ: 1) picks all zero-crossings 2) picks all Peaks/Troughs.

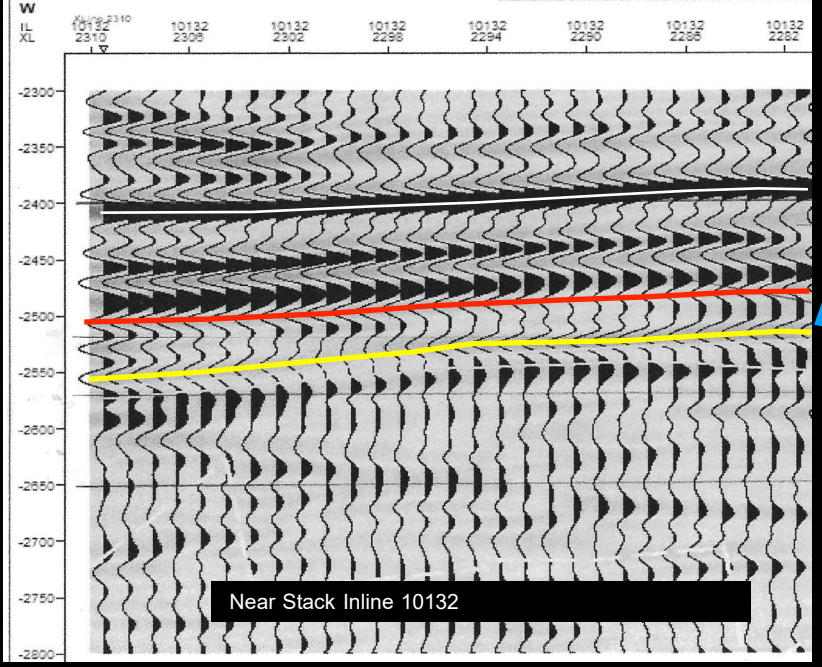

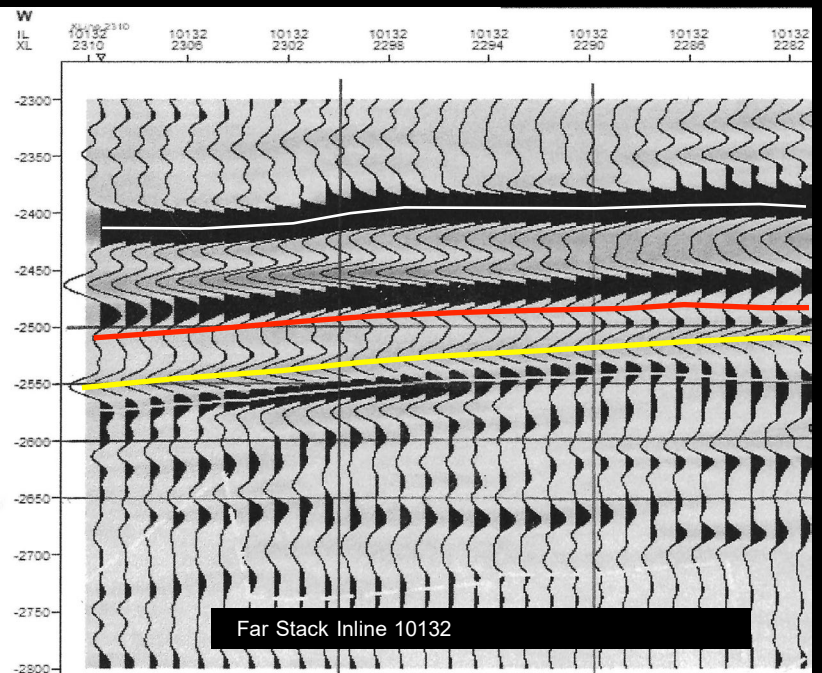

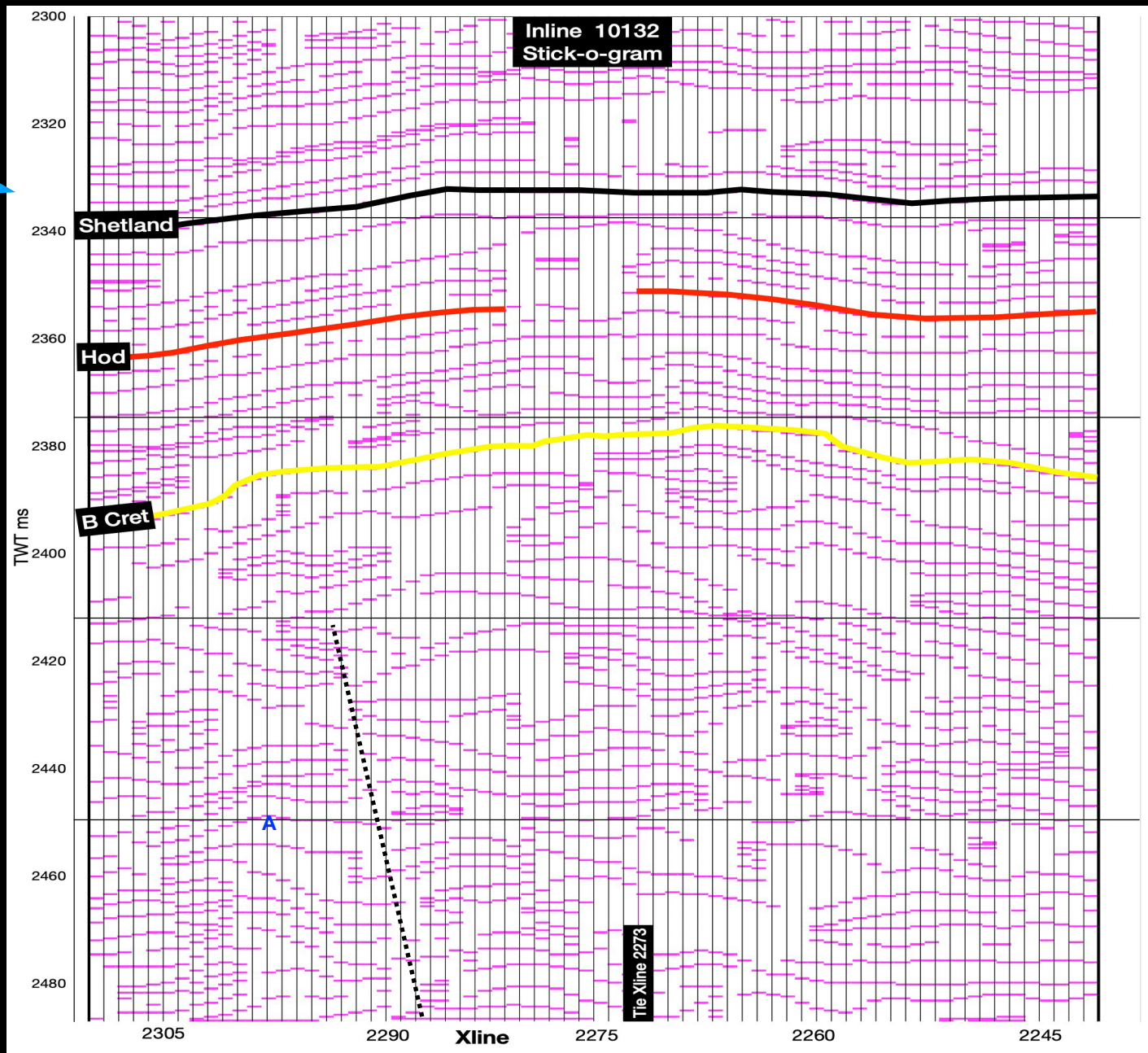

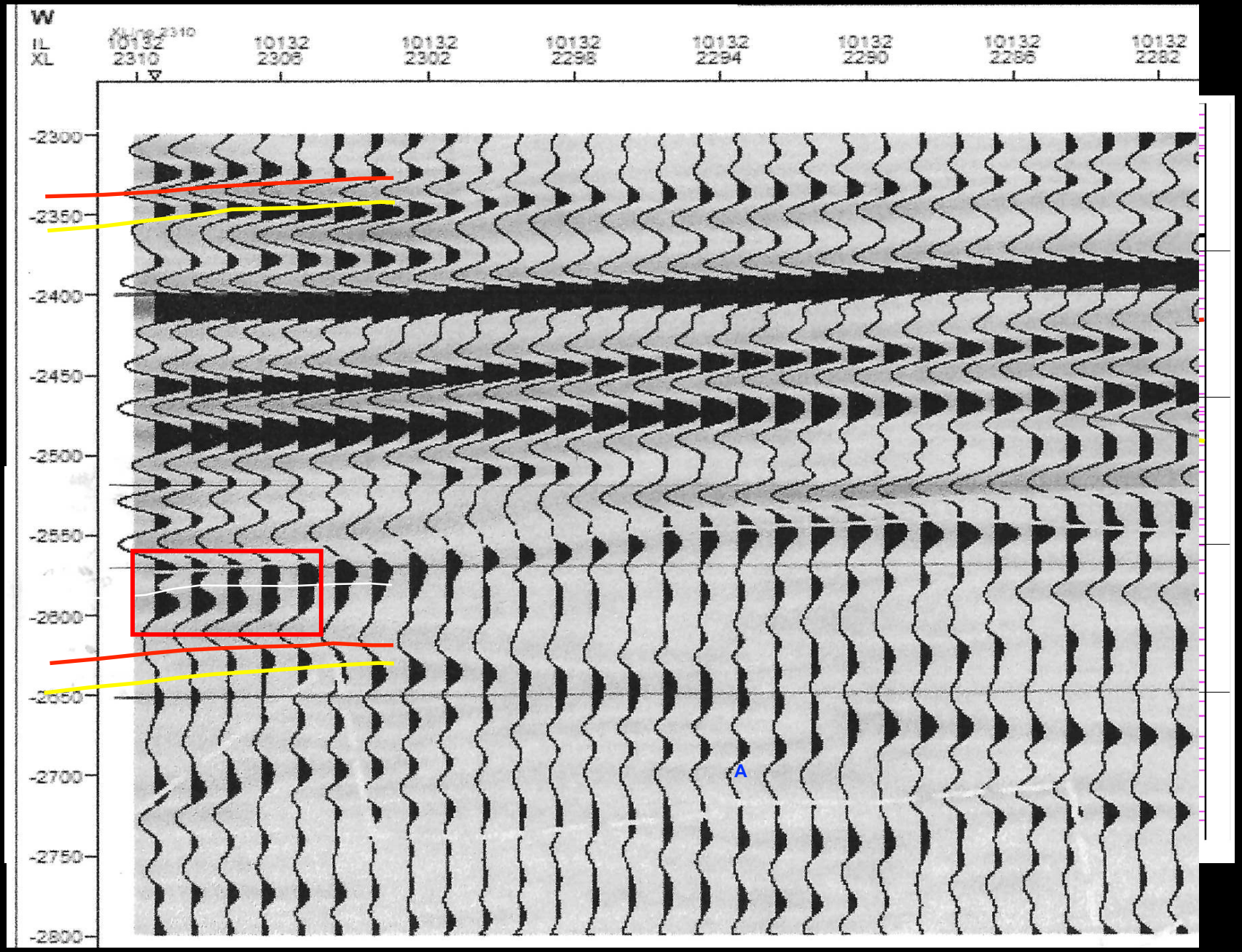
W
IL
XL
10132
2310
10132
2306
10132
2302
10132
2298
10132
2294
10132
2290
10132
2286
10132
2282
-2300
-2350
-2400
-2450
-2500
-2550
-2600
-2650
-2700
-2750
-2800
A

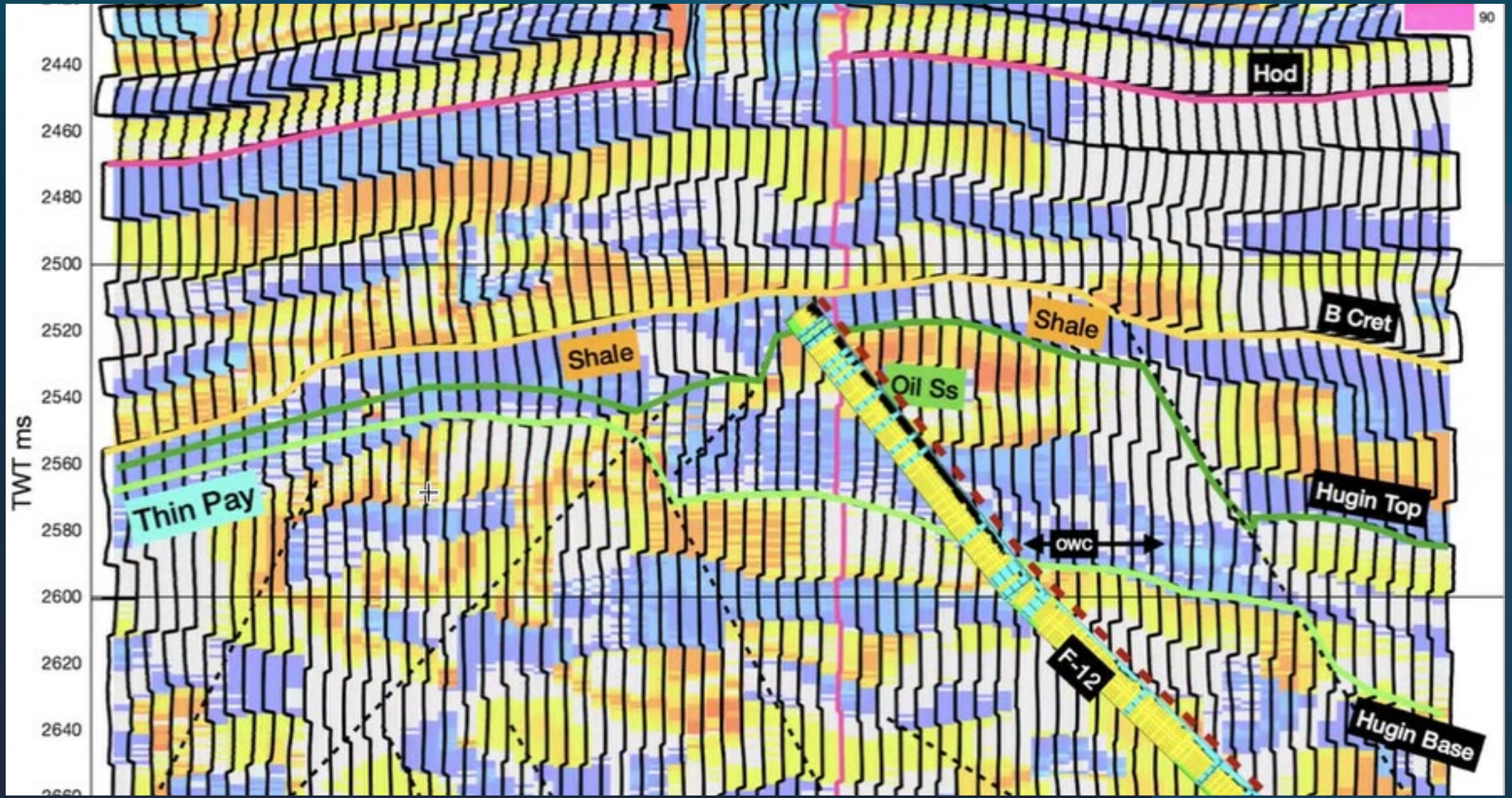
TWT ms
2440
2460
2480
2500
2520
2540
2560
2580
2600
2620
2640
90
Hod
B Cret
Shale
Shale
Oil Ss
Thin Pay
Hugin Top
OWC
F-12
Hugin Base

Let’s plot StickOgram

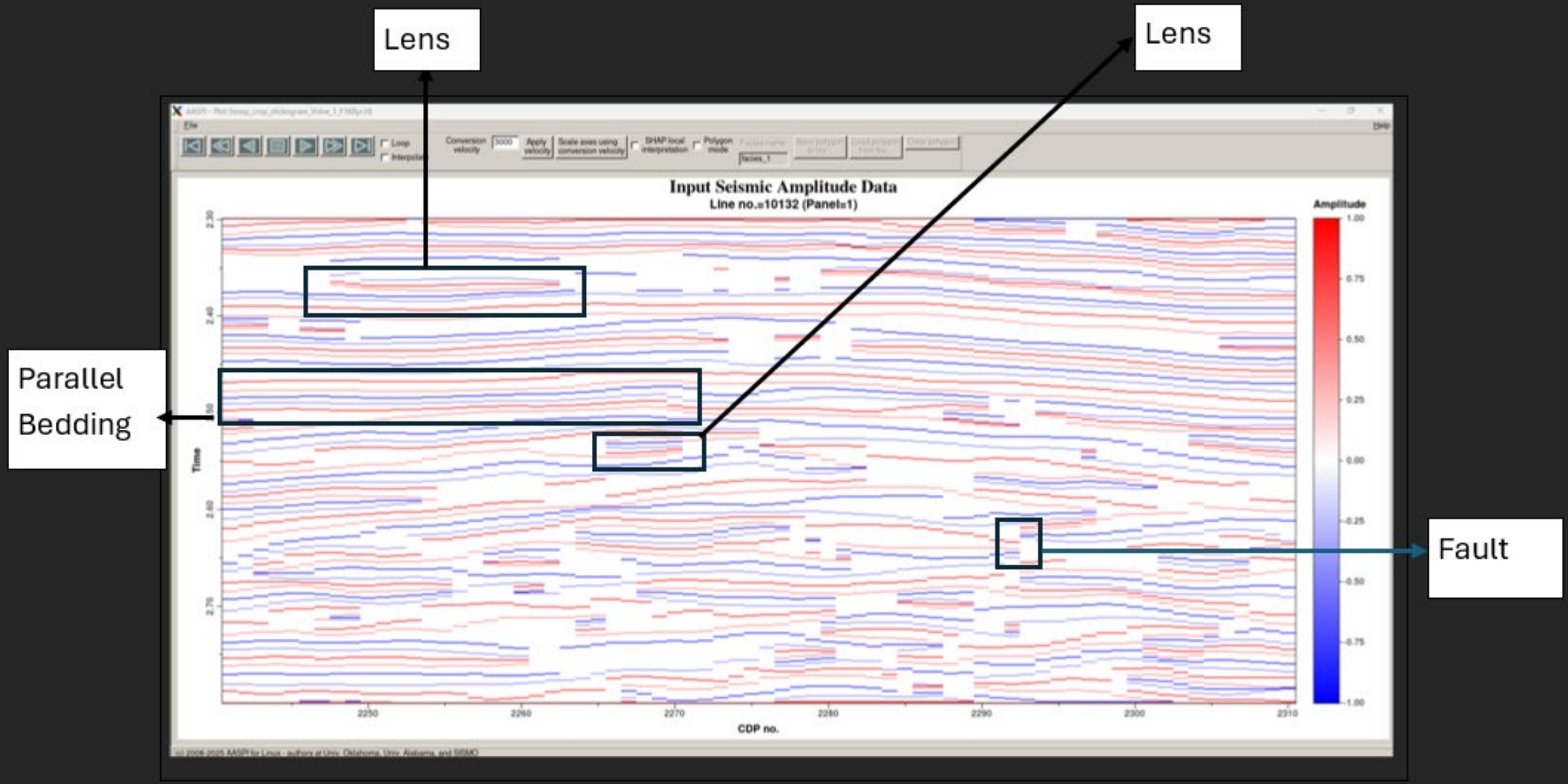
Lens
Lens
Parallel Bedding
Fault
Input Seismic Amplitude Data
Line no.=10132 (Panel=1)
Amplitude
Time
CDP no.

Stick o gram

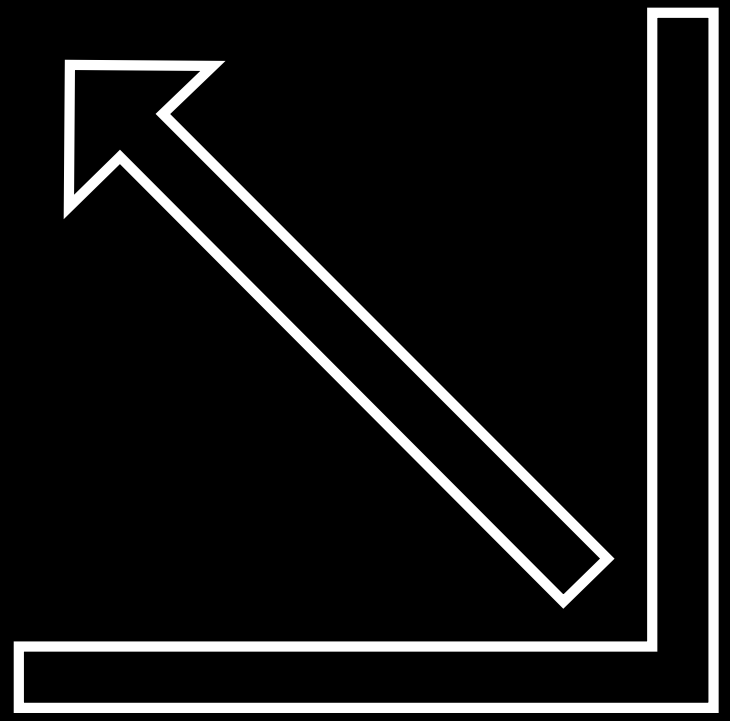

Step 2

Step 2

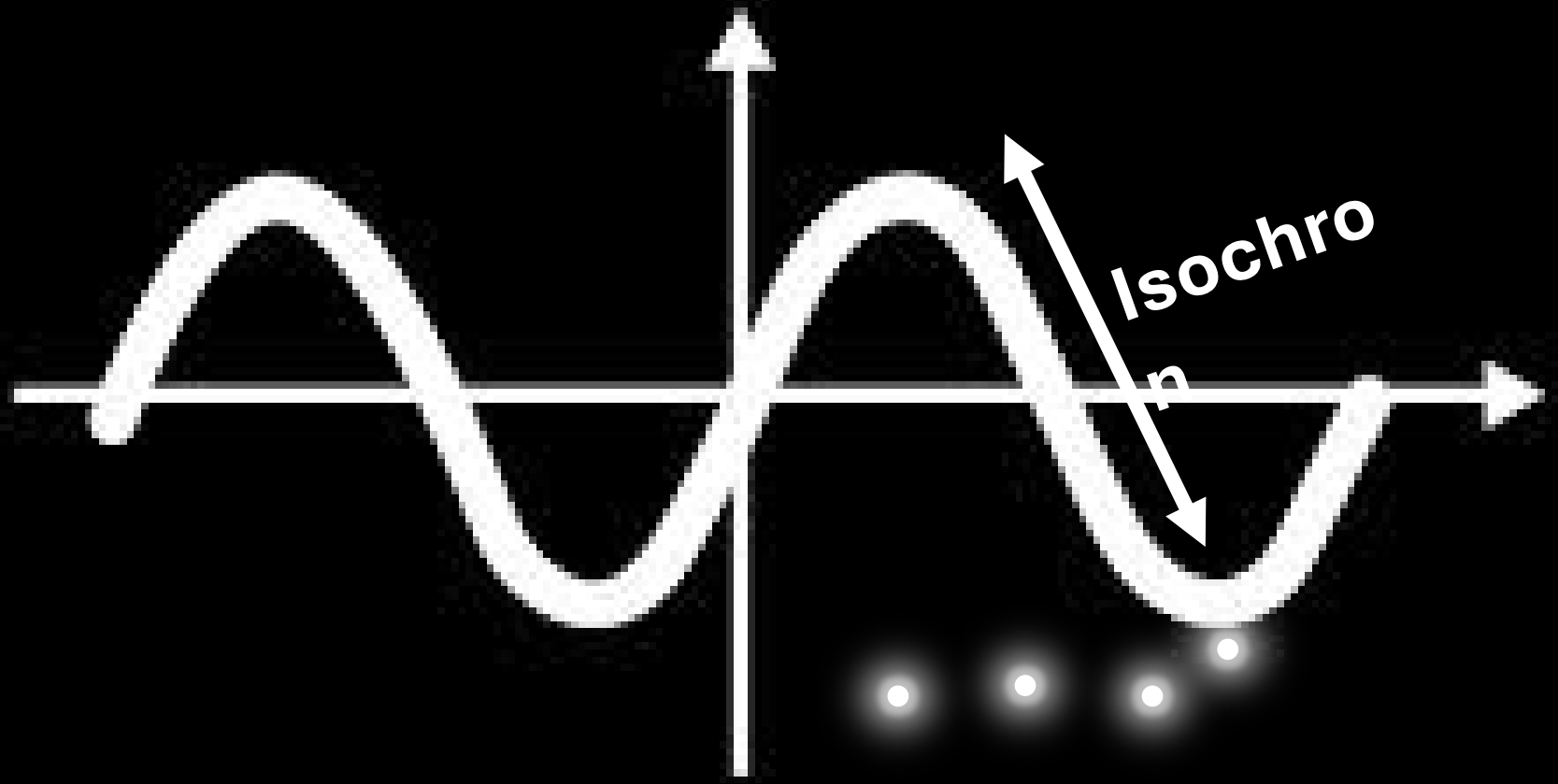

Step 2

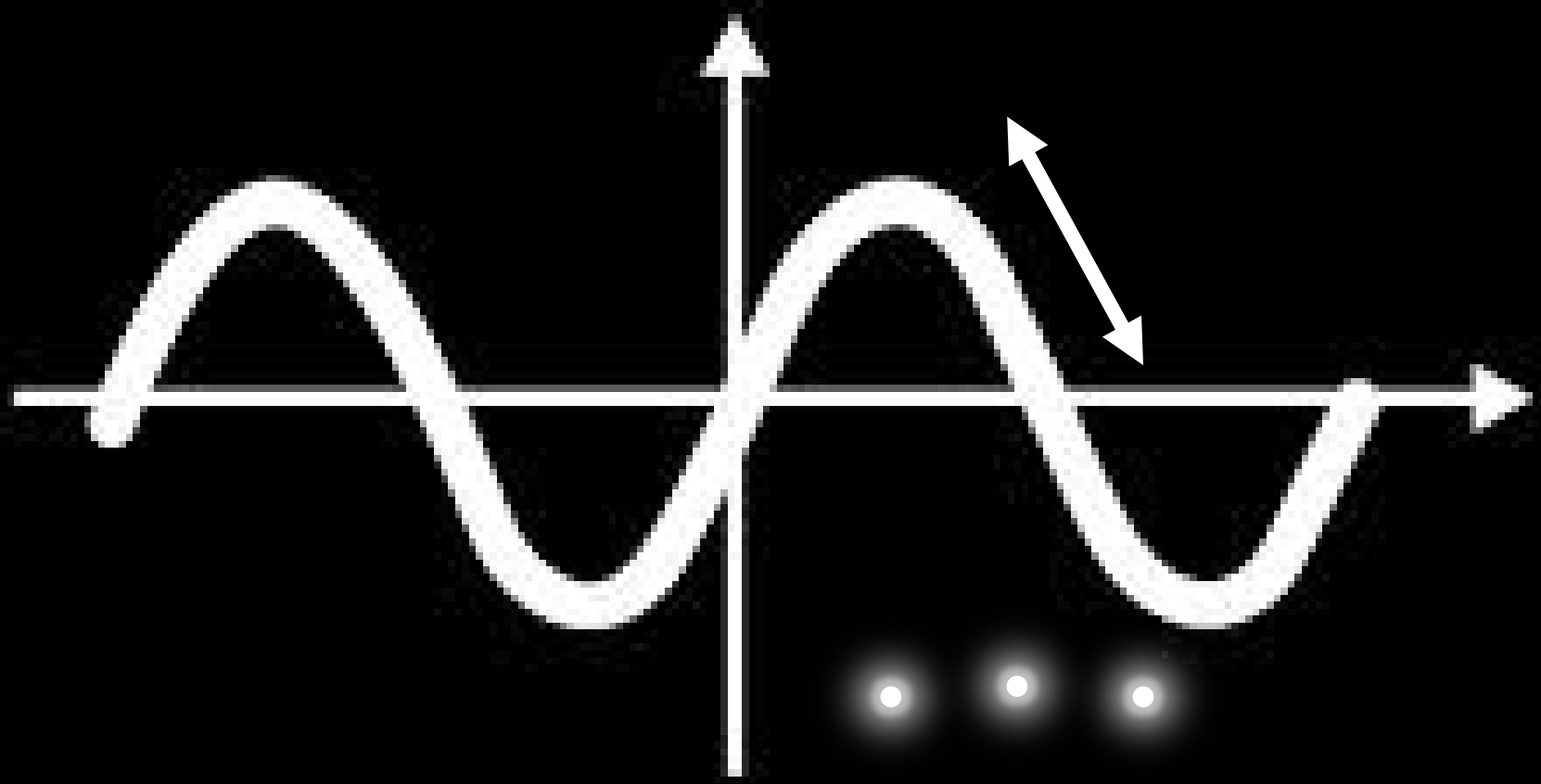

Step 2

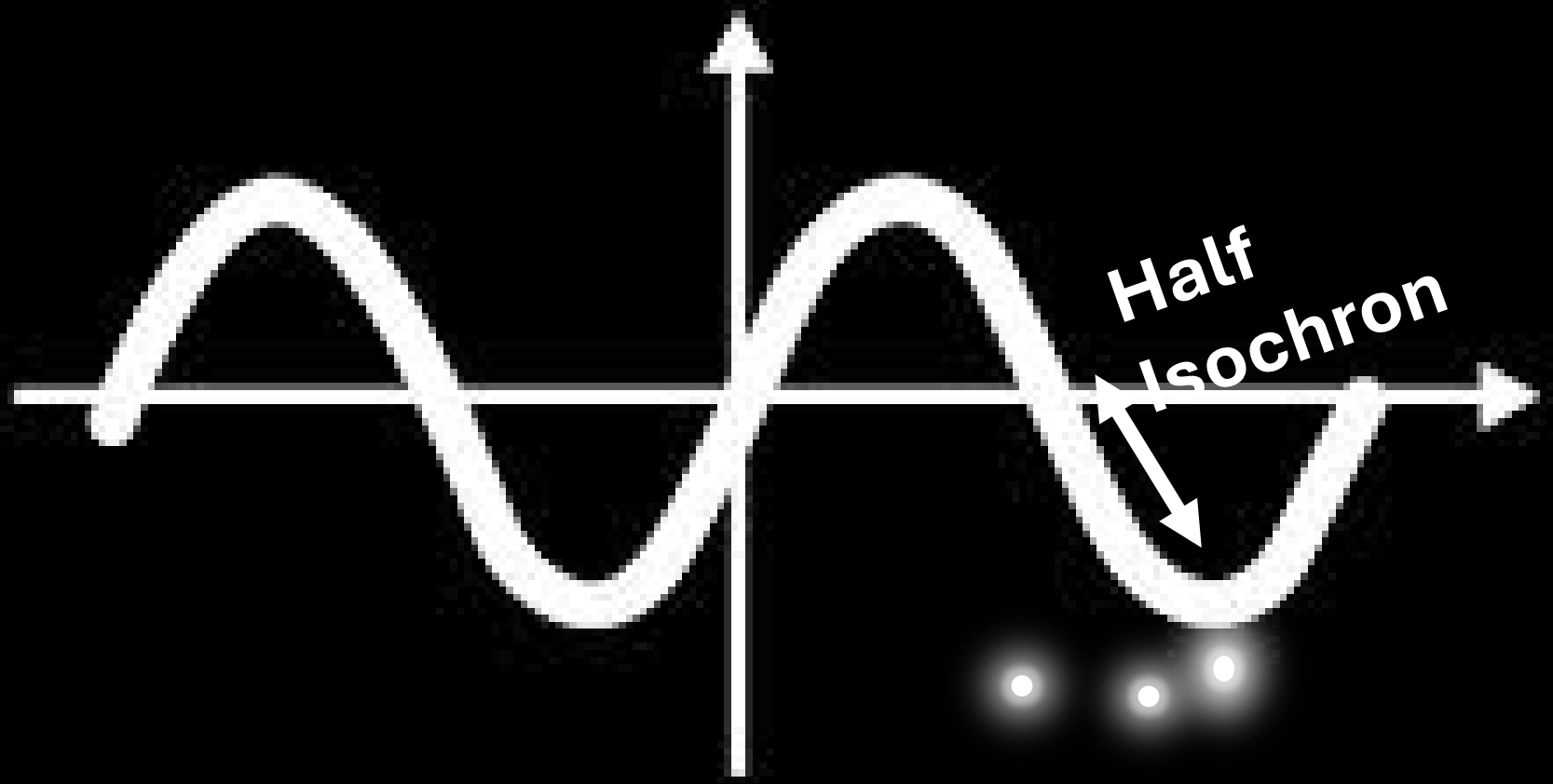

DQ calculates full isochron and half isochron values between all picks on the stick-o-gram.

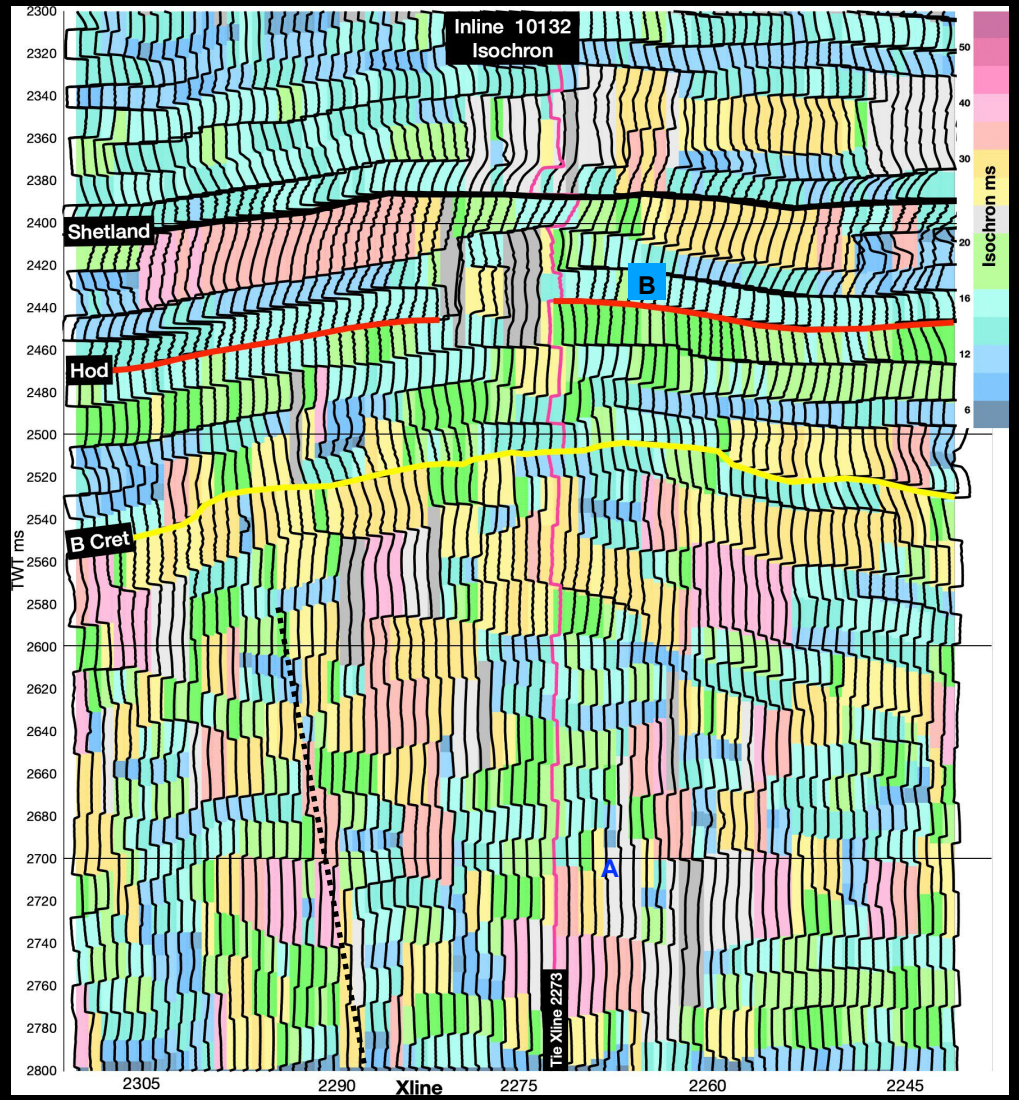

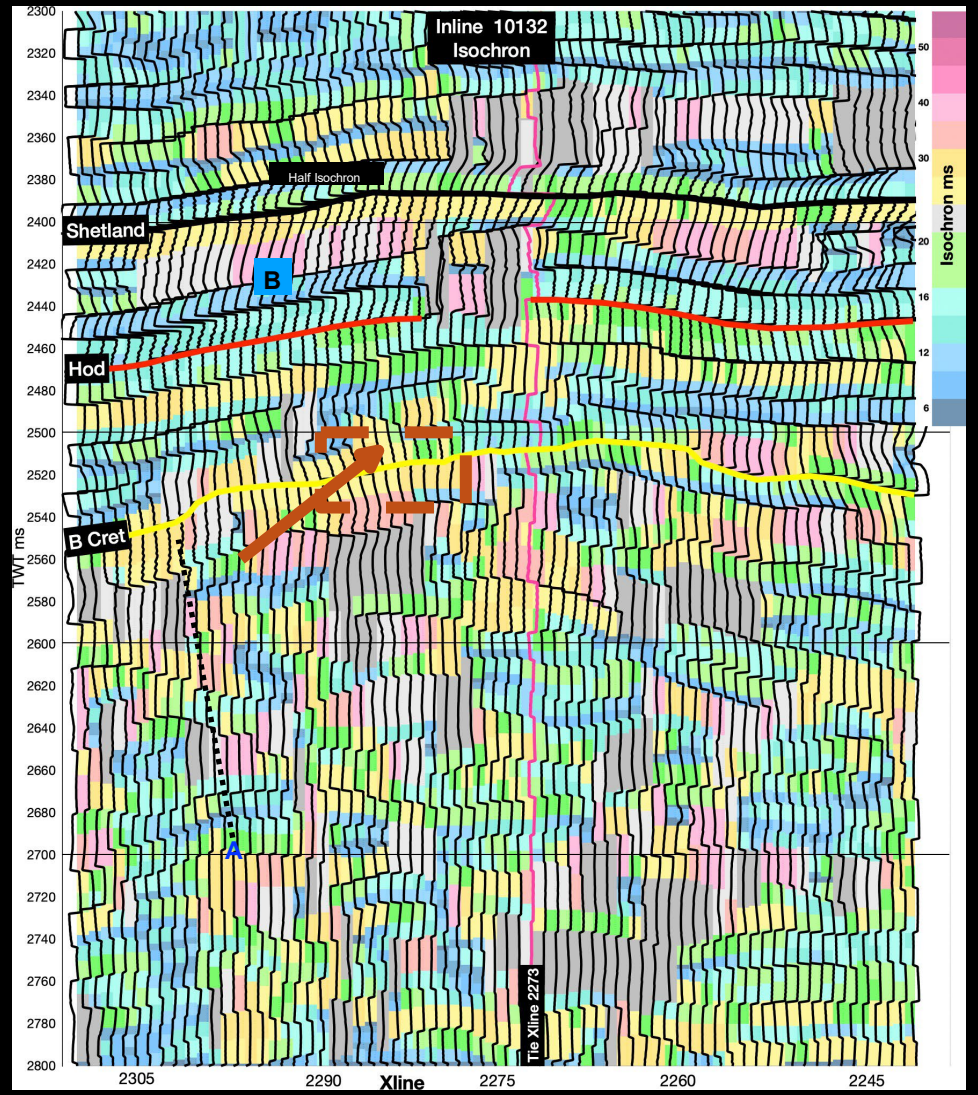

Half Isochron helps define Facies using Changing Thickness and Asymmetric Waveforms shapes. Fault zones and Channel edges also appear on the DQ isochron sections (letters A and B).

Let’s plot Isochron and Half Isochron

Downthrown has thinner isochron

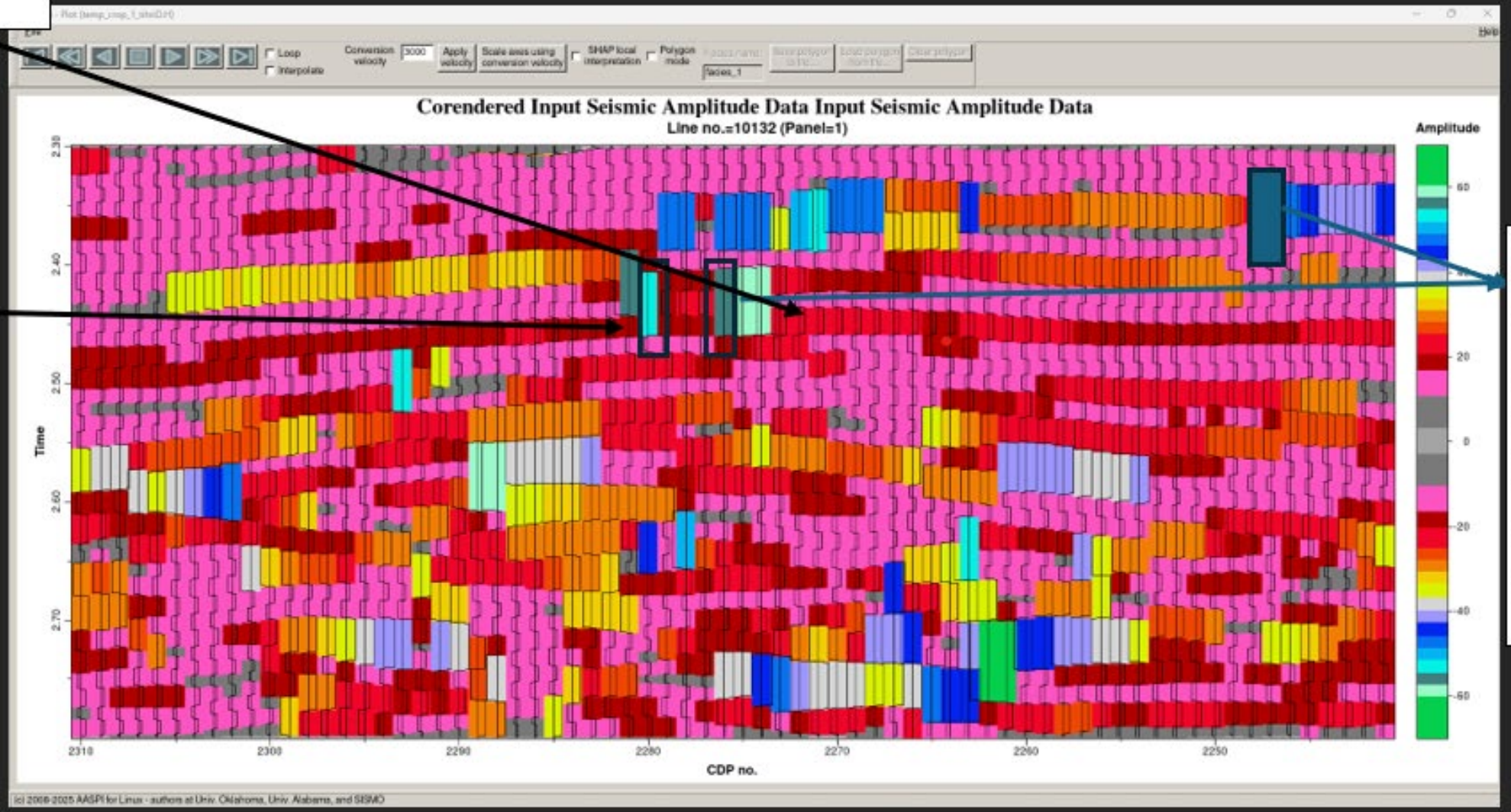

Edge of channel marked by thick isochron going into thin

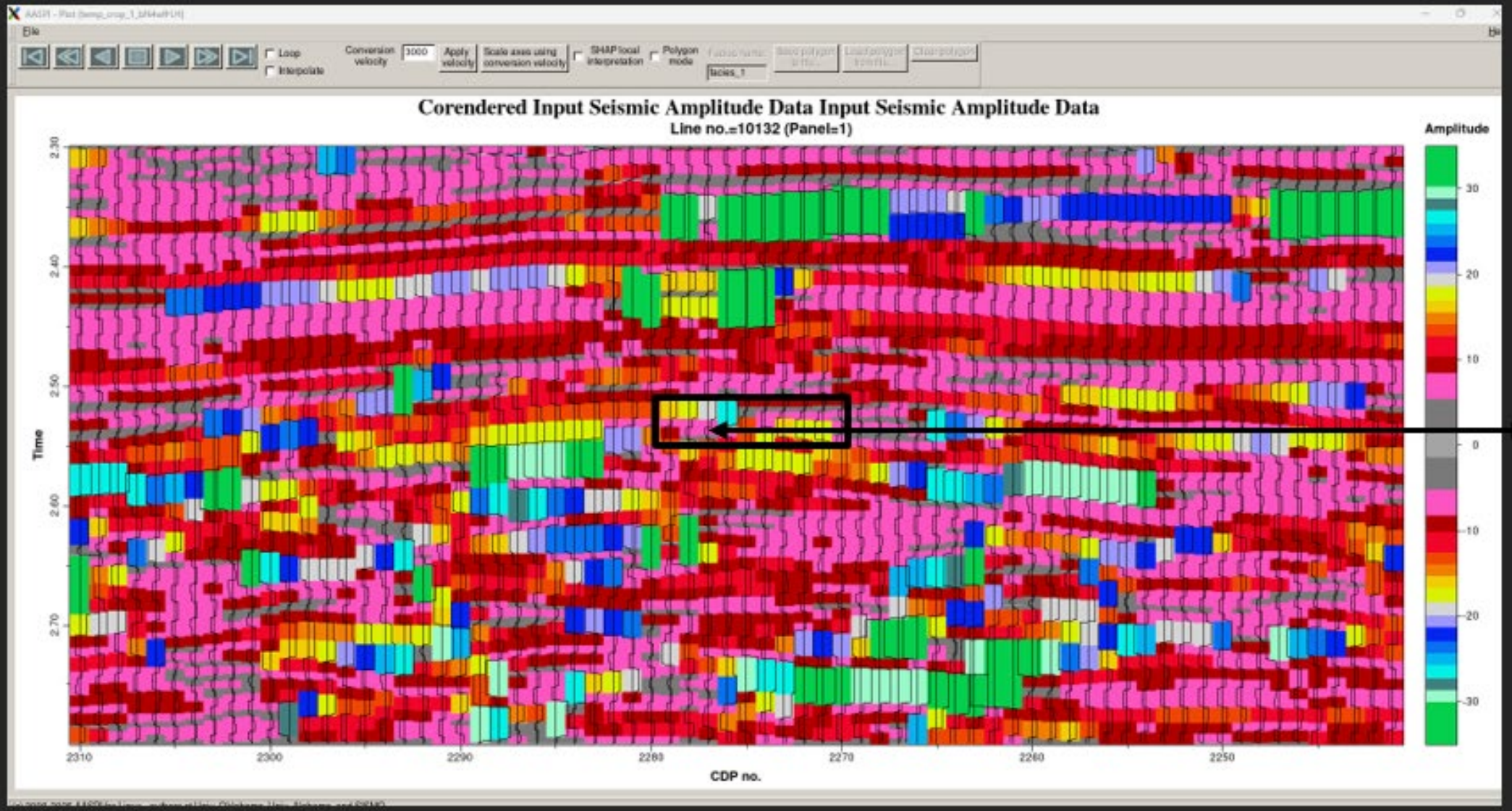

Thin isochron, limestone streak 15 ft of thickness

Asymmetry in well logs causes unequal Half Isochron layers.

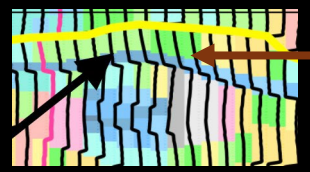

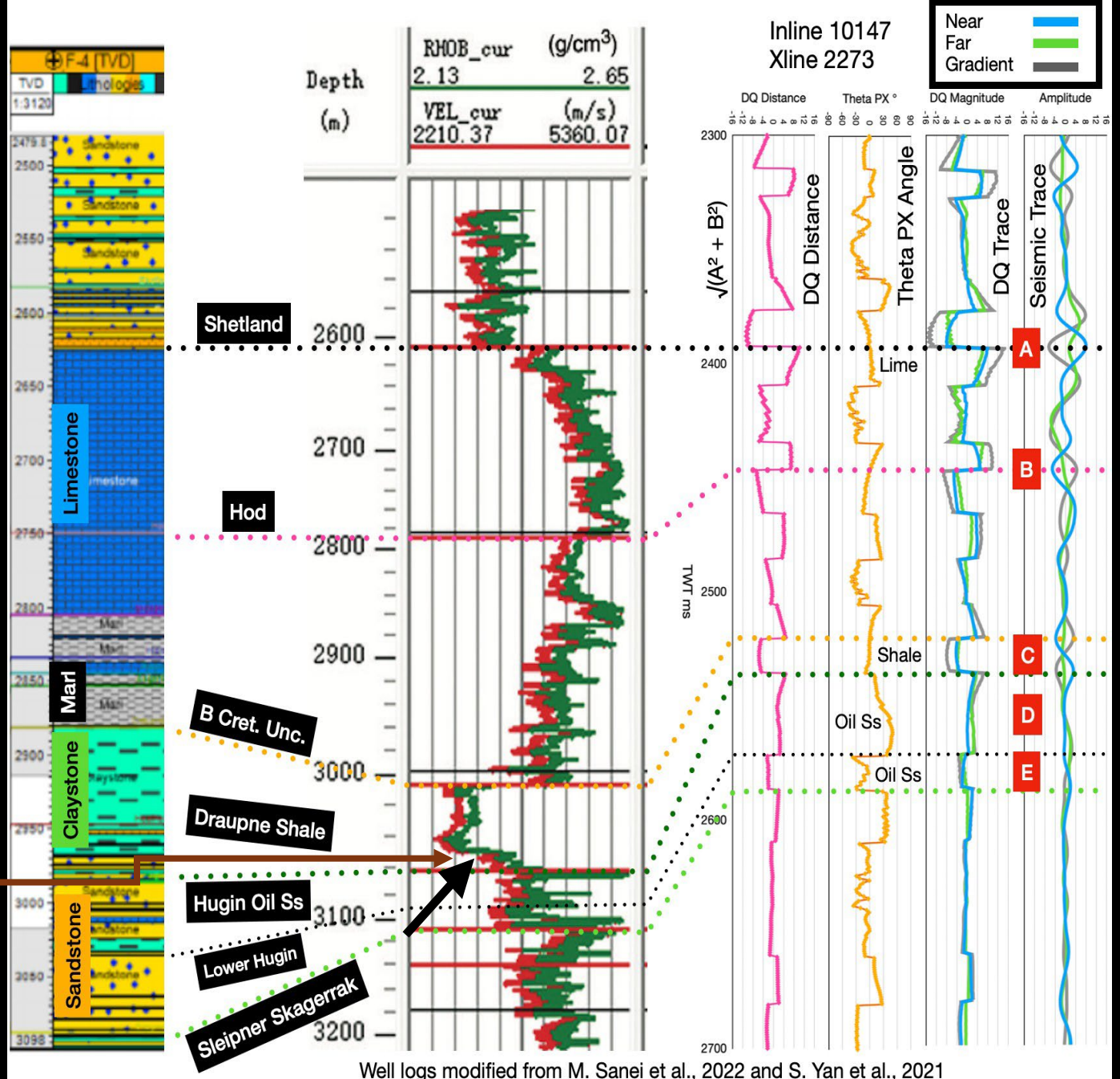

Well logs modified from M. Sanei et al., 2022 and S. Yan et al., 2021

a) b) c) d) e) f)

DQ and ThetaPX input models for quantitative petrophysical inversion of a Class 1 sand.

DQ is an intermediate product on the way to a final product.
The shapes herein are relative porosity, but without calibration to wells.

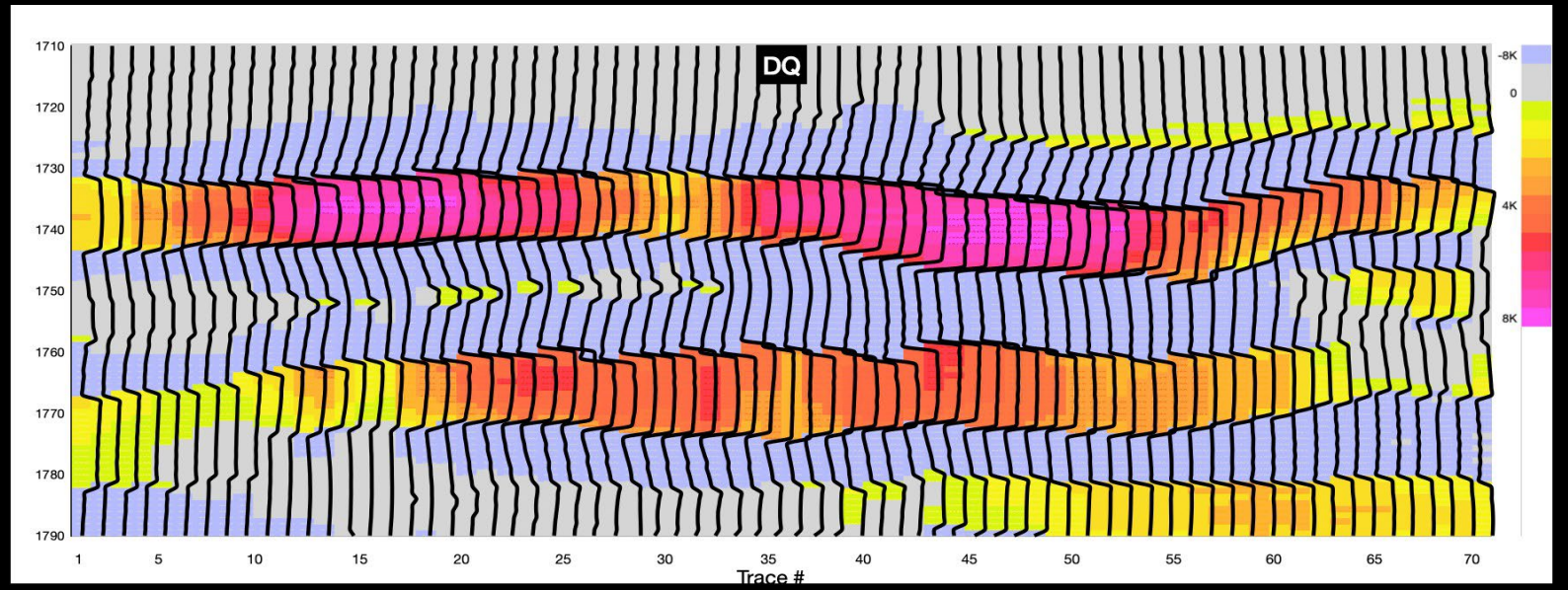

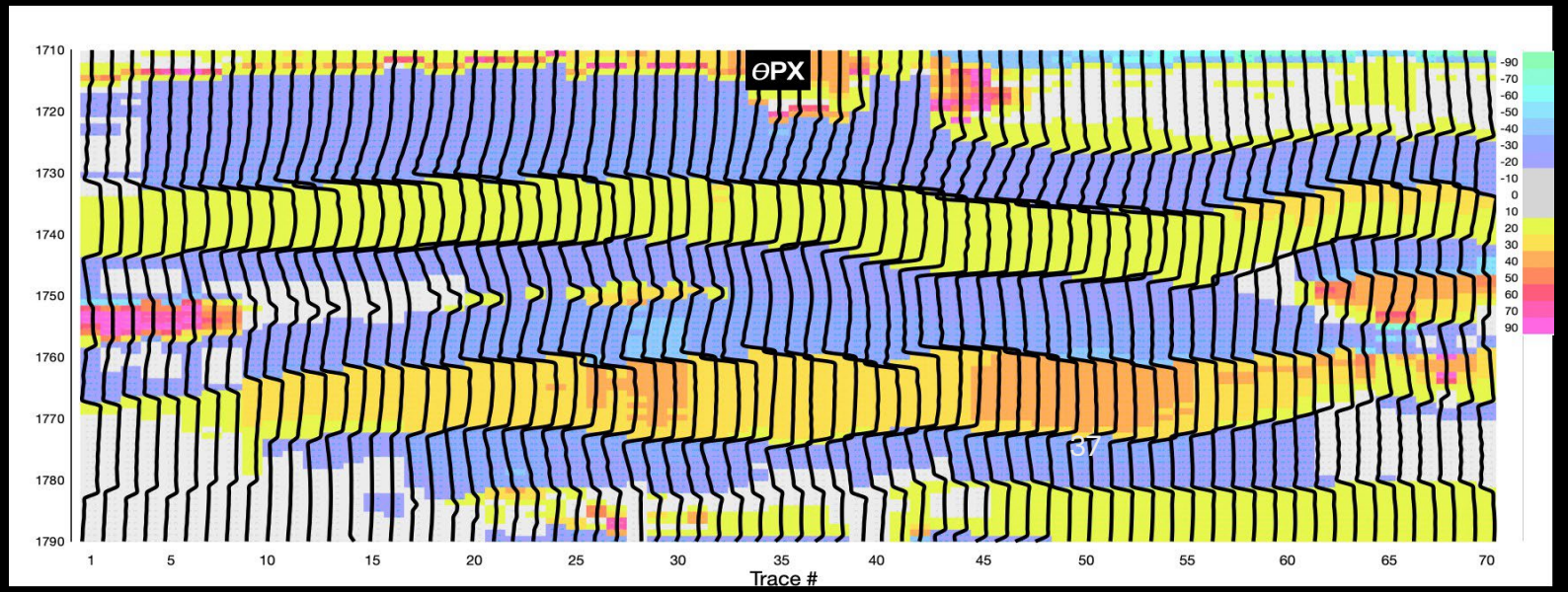

DQ Inversion is a combination of Acoustic Impedance and Elastic Impedance inversion but performed in a simultaneous manner.

Shown here are Inversion results using DQ inputs for Vsand and HPV.

DQ correctly predicted that the upper sand was wet and the lower sand had gas.

Numerical petrophysical predictions have now been assigned to each sample in the 3D cube.

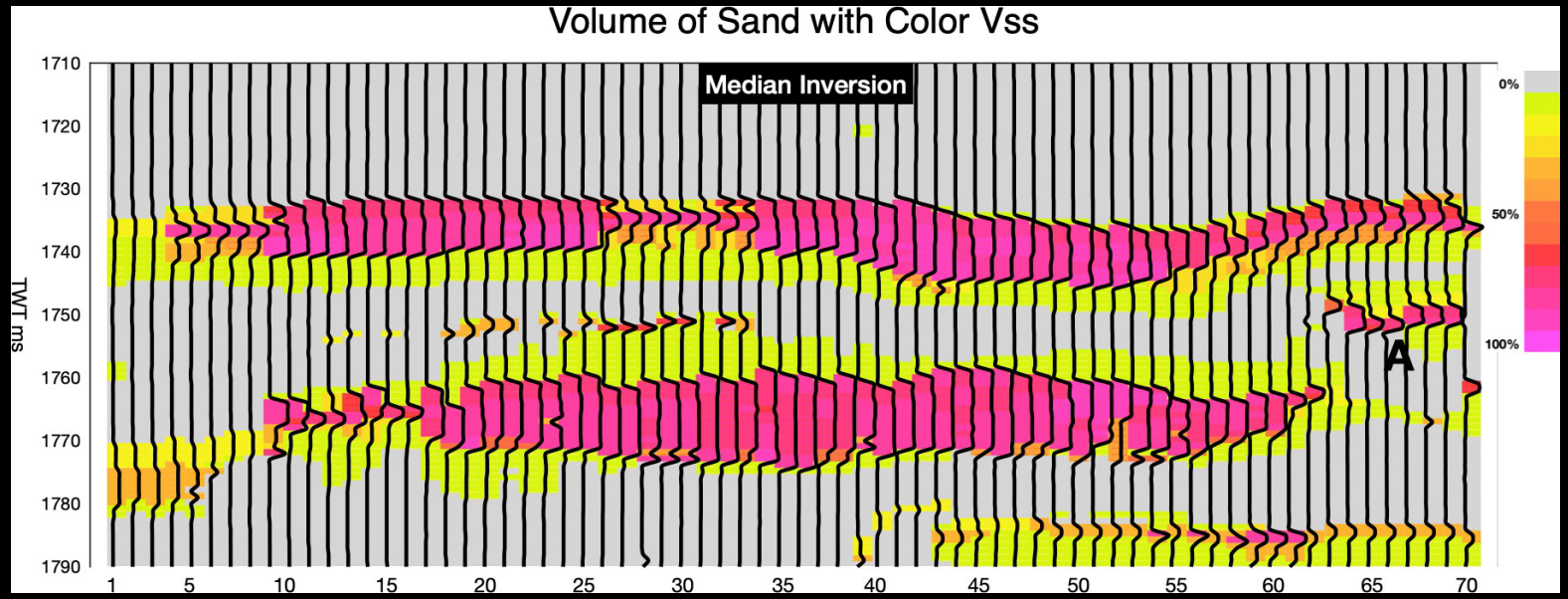

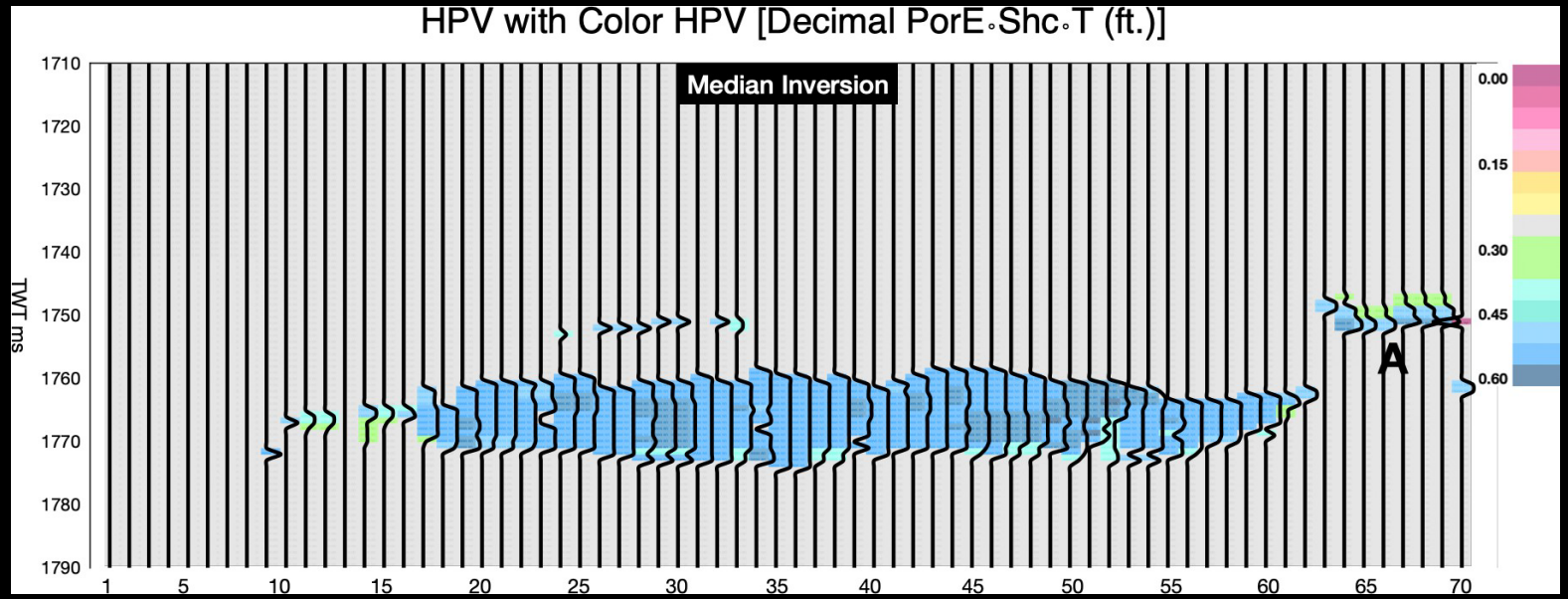

Example of Quantitative Petrophysical Inversion for Porosity and HPV using DQ wedge models.

The prediction results for this Class 3, stratigraphic pinch- out are exceptionally good.
Most inversion programs do not perform well in thin beds.

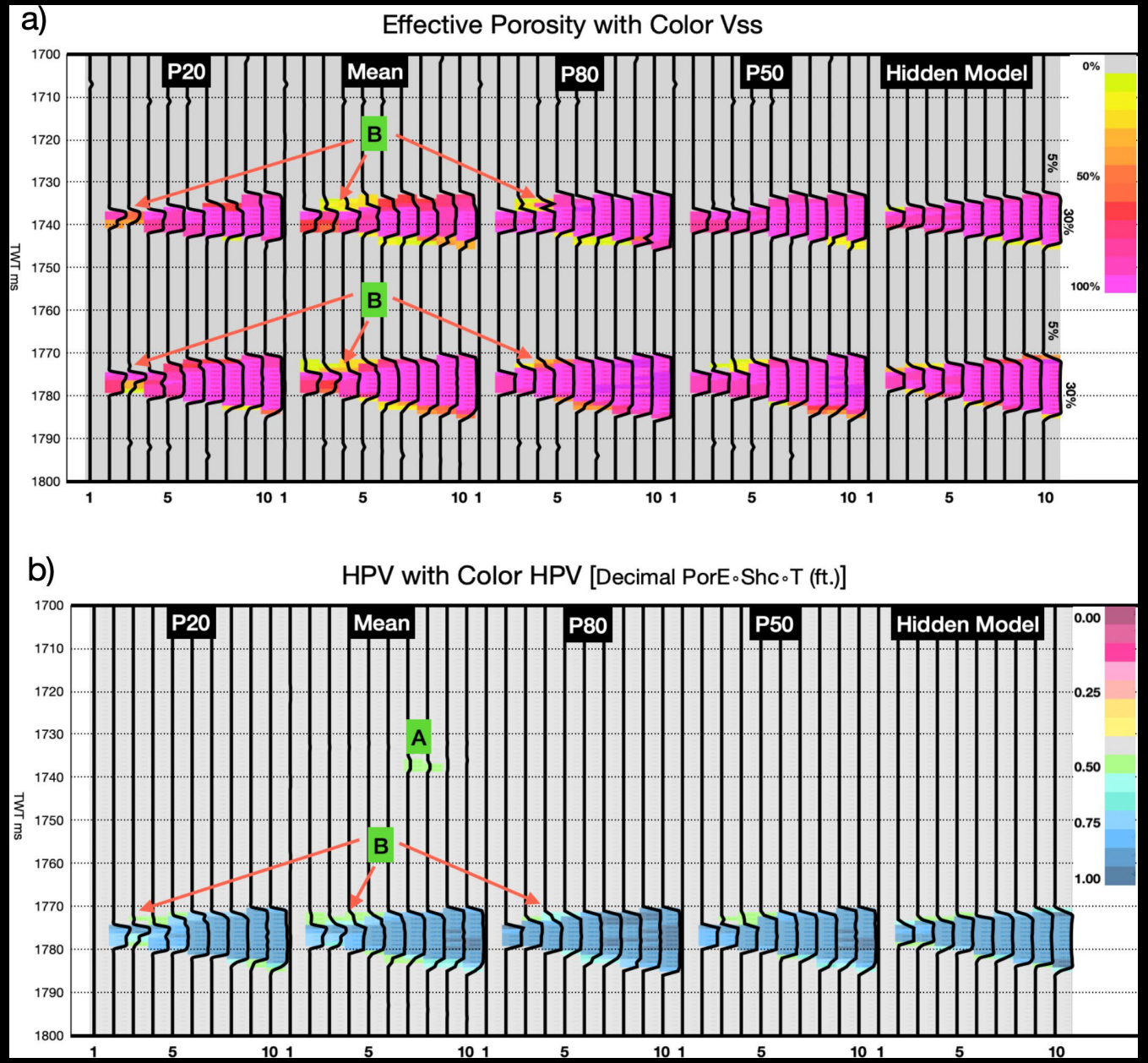

Let’s plot DQ and ThetaPX

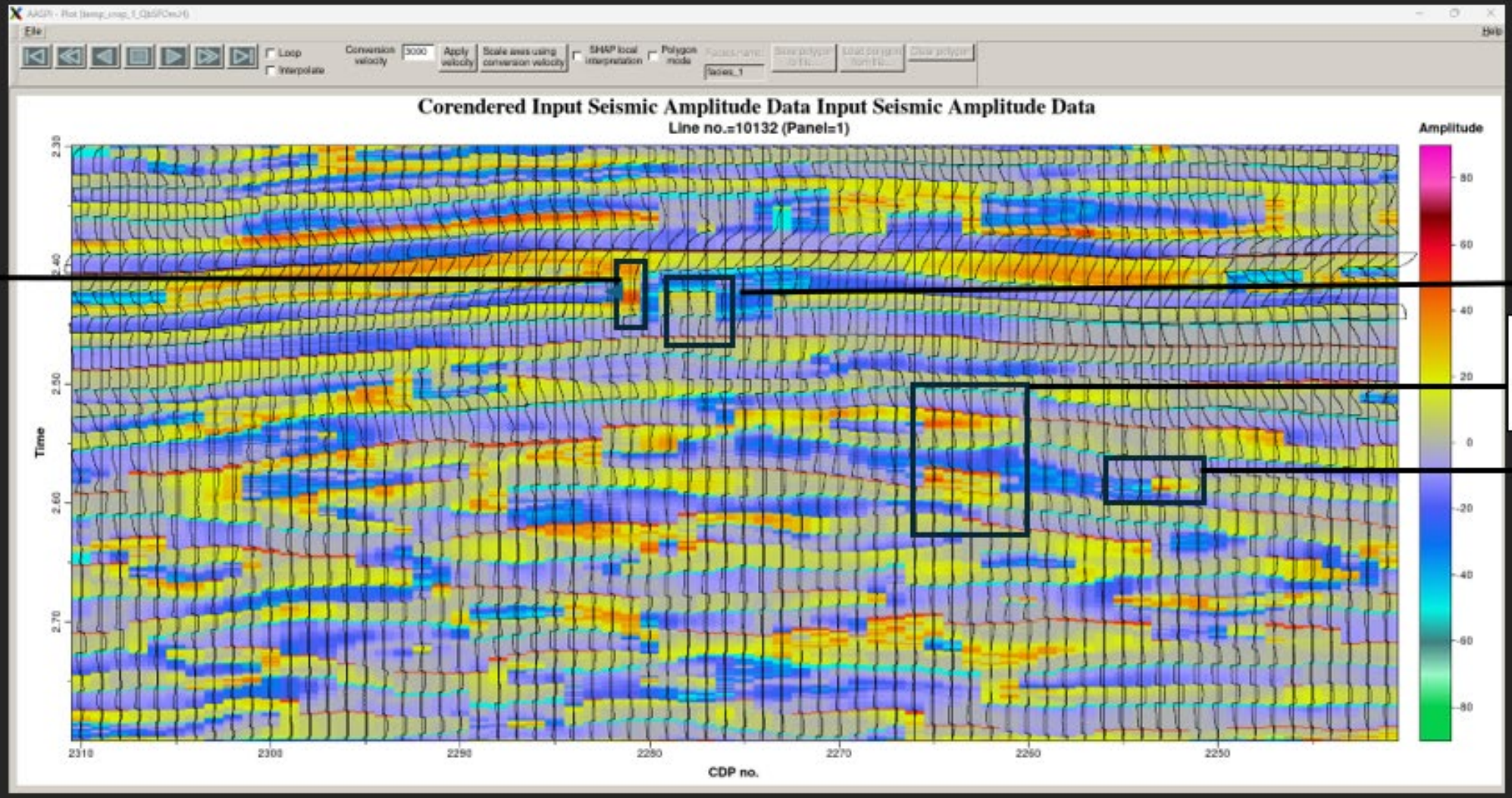
Corendered Input Seismic Amplitude Data Input Seismic Amplitude Data
Line no.=10132 (Panel=1)
Amplitude
Time
CDP no.
AVO wall
Slump Block
Commercial pay
OWC

The DQ family of attributes can be used for both GMM and GLCM machine learning. The advanced preconditioning done by DQ allows for some inversions without ML.

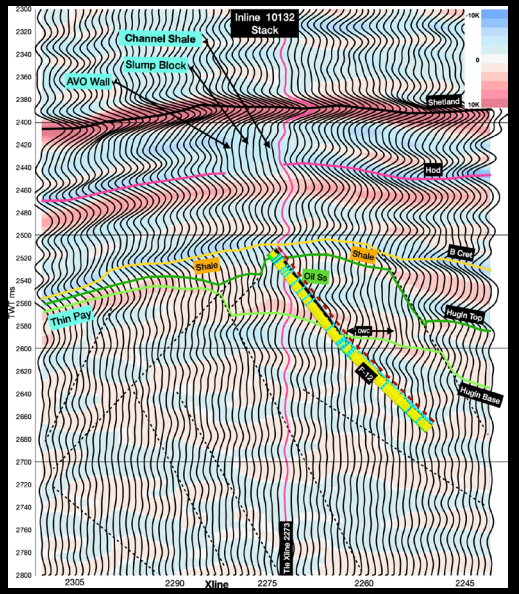

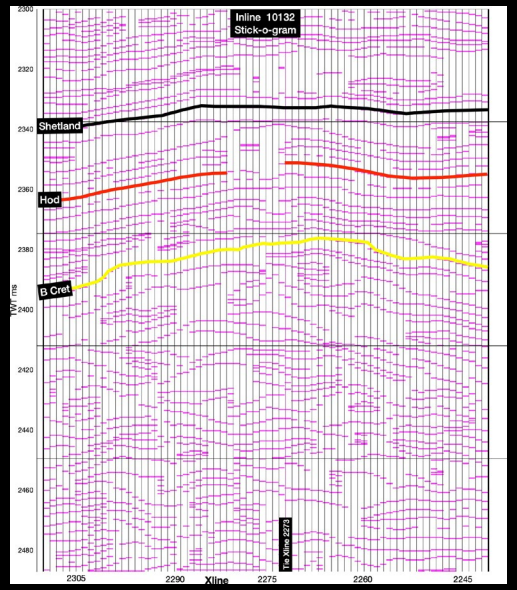

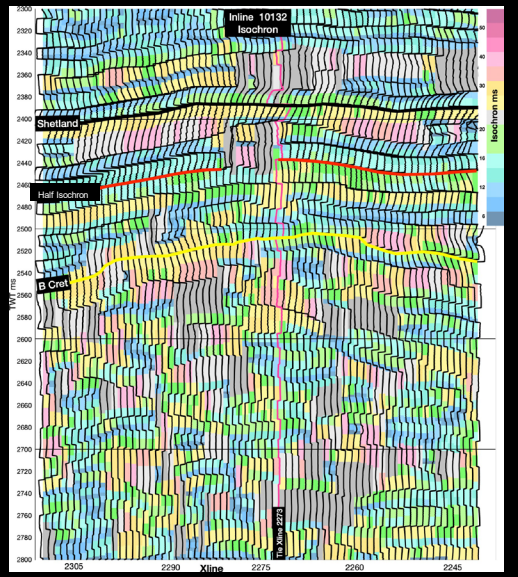

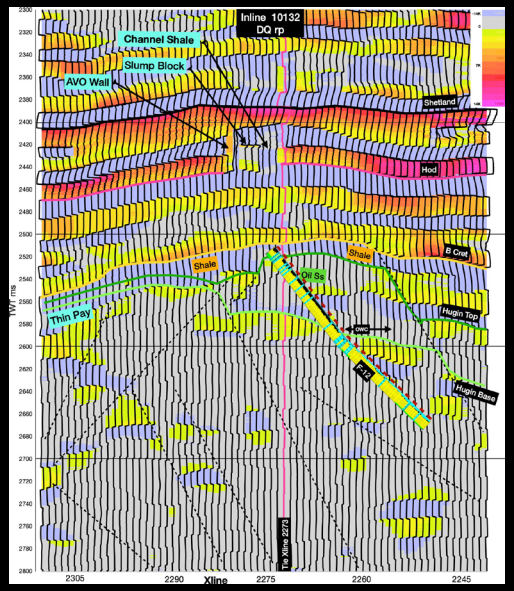

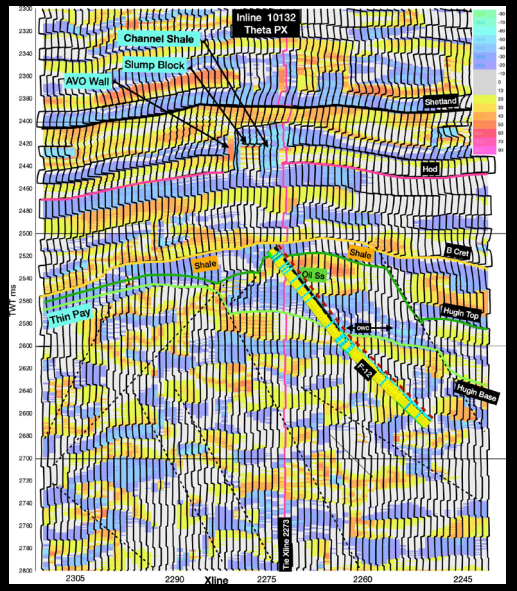

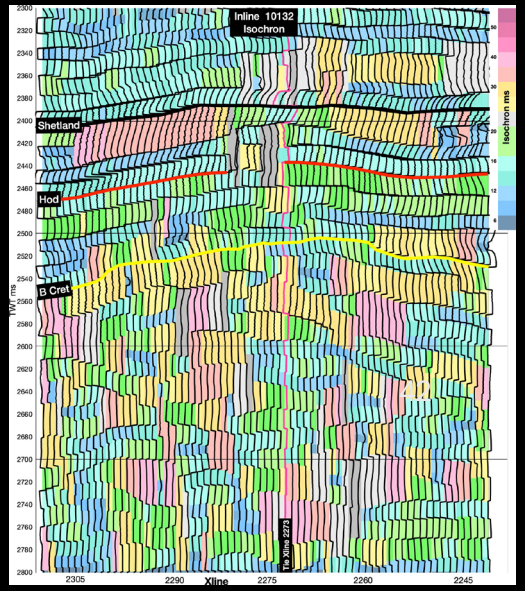

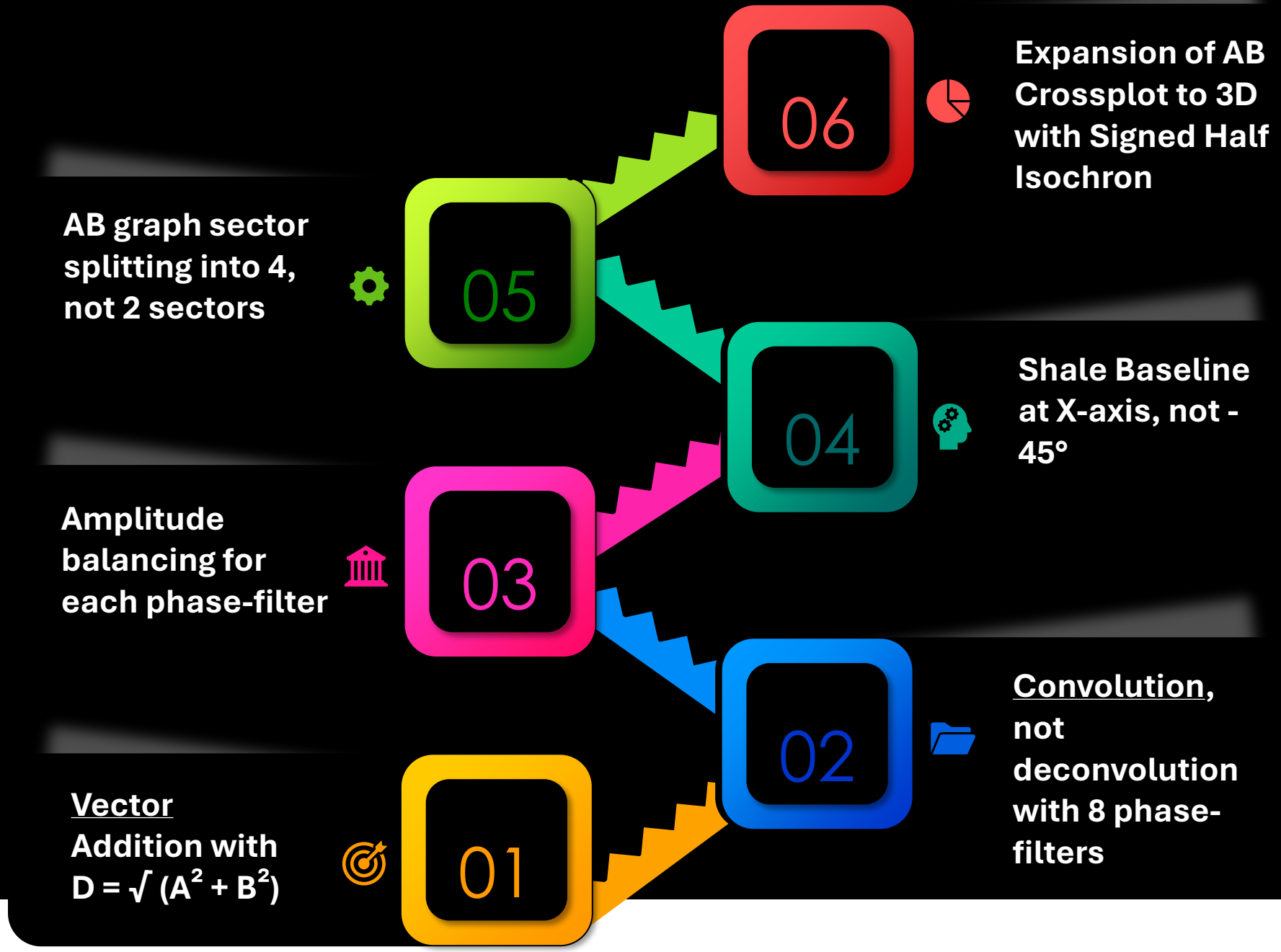
06
Expansion of AB Crossplot to 3D with Signed Half Isochron
05
AB graph sector splitting into 4, not 2 sectors
04
Shale Baseline at X-axis, not -45°
03
Amplitude balancing for each phase-filter
02
Convolution, not deconvolution with 8 phase-filters
01
Vector Addition with D = √ (A² + B²)

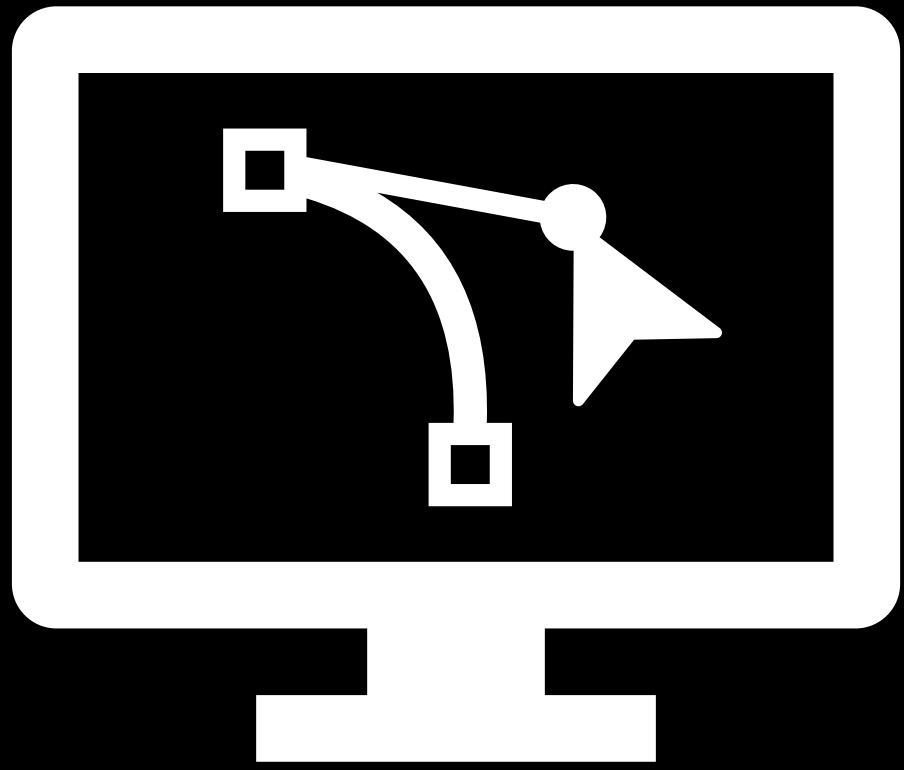

Step 3

Vector Addition with D

$= \sqrt{(A^2 + B^2)}$

Step 3

- Sand and carbonate visibility suffers in regions of Class 2 and 2p polarity reversal and phasing between the near and far offset traces.

- Regardless of the amplitude of the stack trace or the acoustic impedance (AI) curve the vector equation allows the visibility of the sand bodies from letters A to D to remain consistent.

- A vector equation is why the Hilbert amplitudes do well in an ML learning session. That equation is:

- Hilbert Envelope = $\sqrt{(A0^2 + A90^2)}$

- DQ does even better because it uses both acoustic and elastic impedance data with the same vector equation.

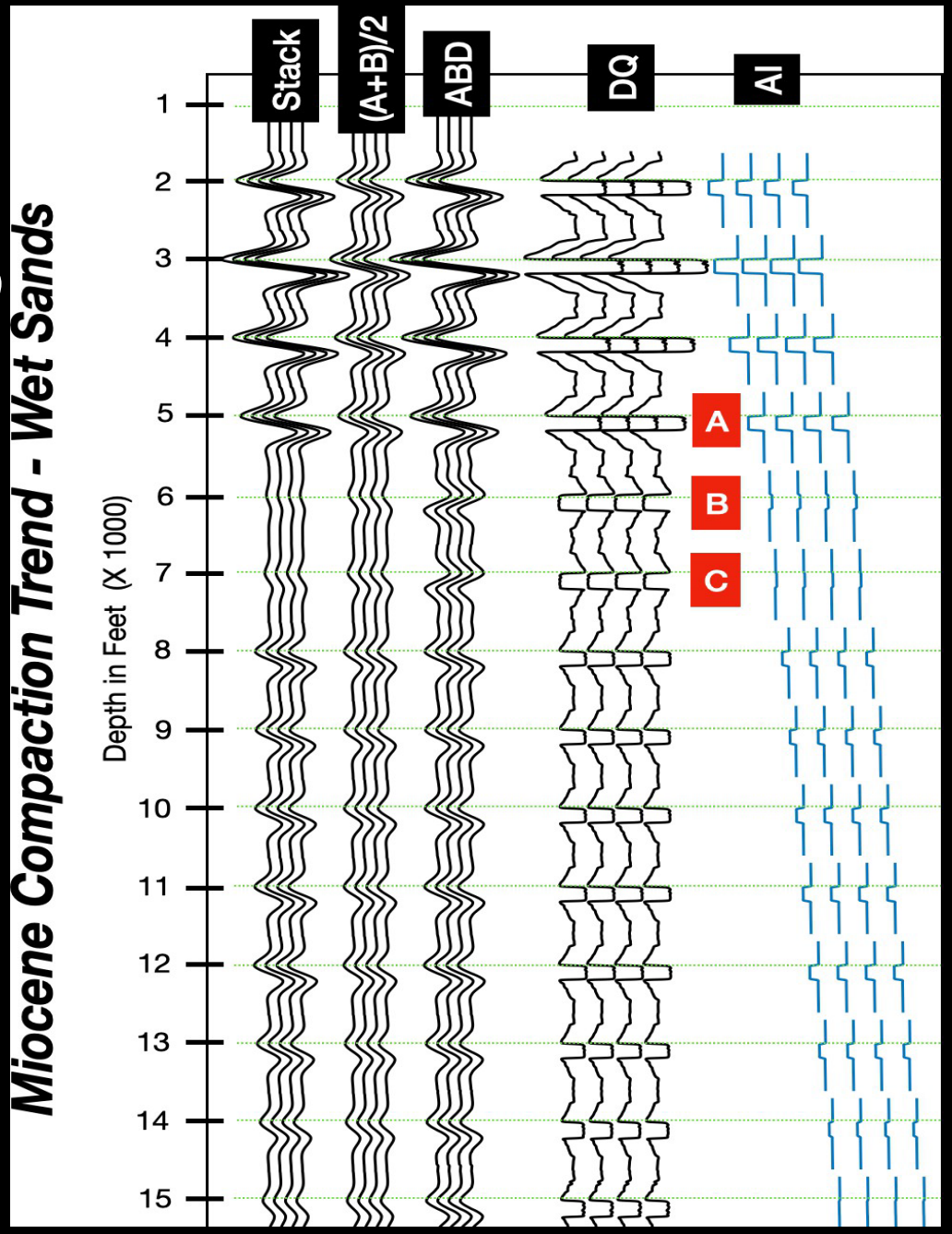

The arithmetic addition of near trace peaks with far trace troughs does not allow the stack data (left map) to return a correct presentation of the Hod horizon at the Volve field, Norway. The vector addition of the DQ processing makes the eroded channel base visible (right map).

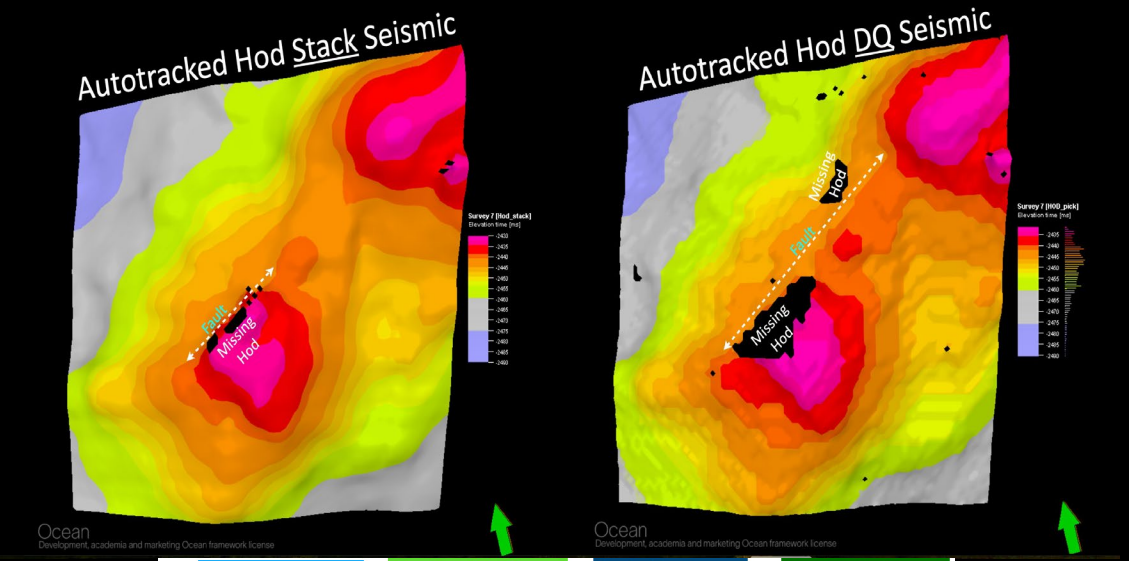

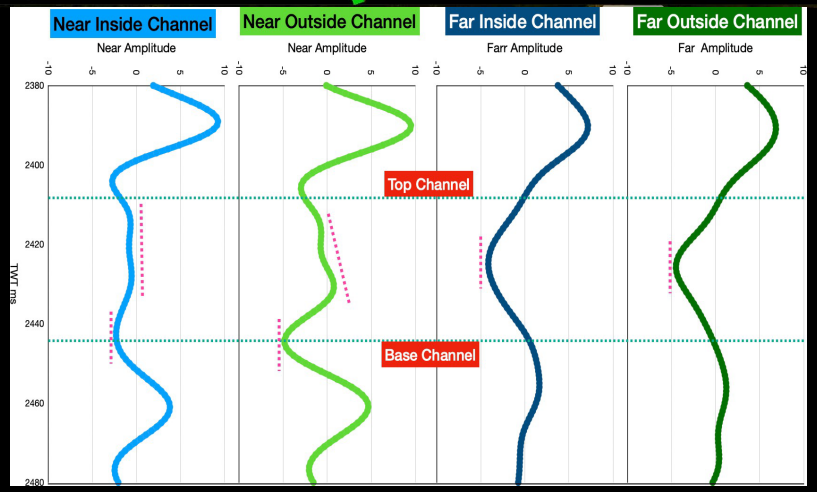

The arithmetic addition of near trace peaks with far trace troughs does not allow the stack data (left map) to return a correct presentation of the Hod horizon at the Volve field, Norway. The vector addition of the DQ processing makes the eroded channel base visible (right map).

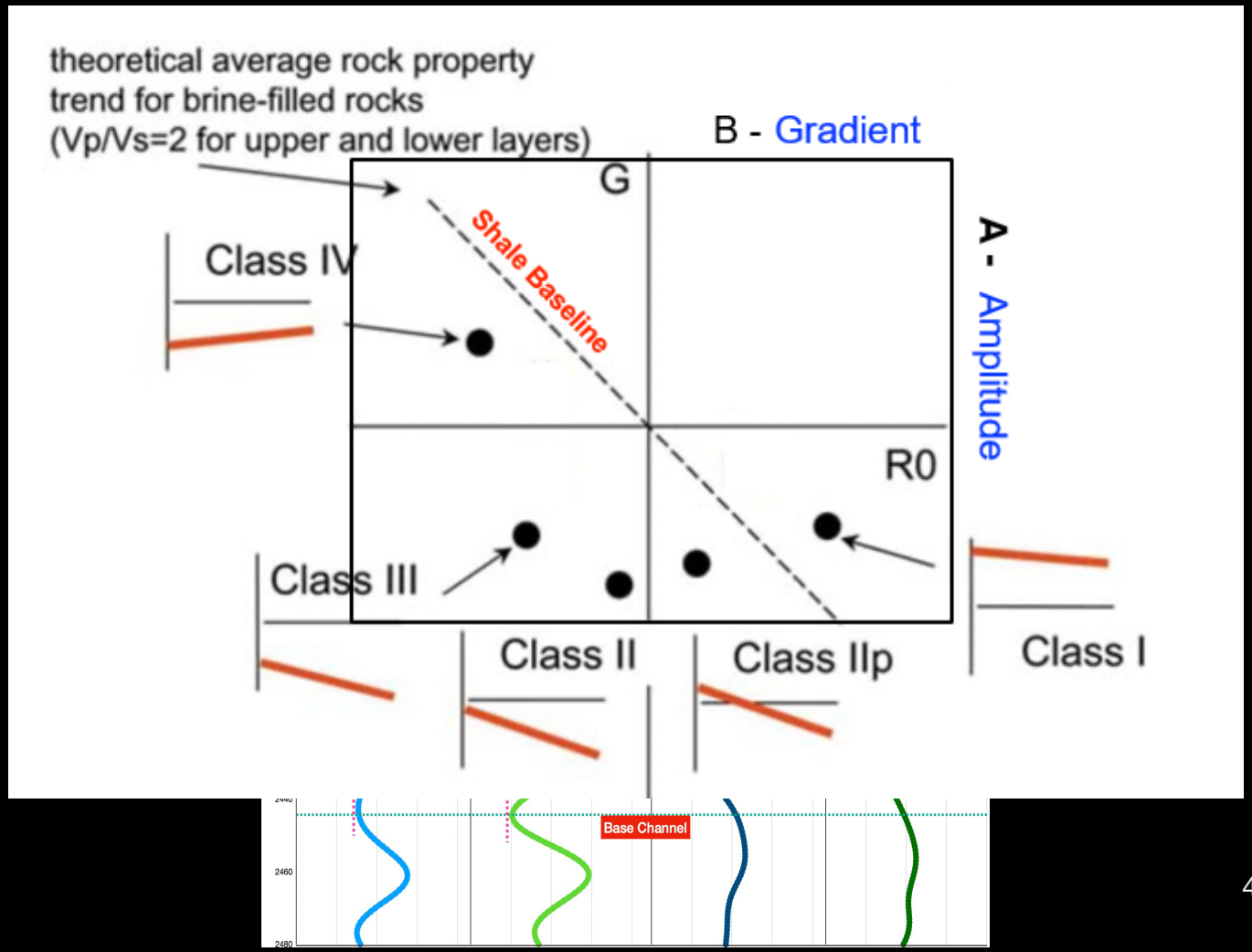

The arithmetic addition of near trace peaks with far trace troughs does not allow the stack data (left map) to return a correct presentation of the Hod horizon at the Volve field, Norway. The vector addition of the DQ processing makes the eroded channel base visible (right map).

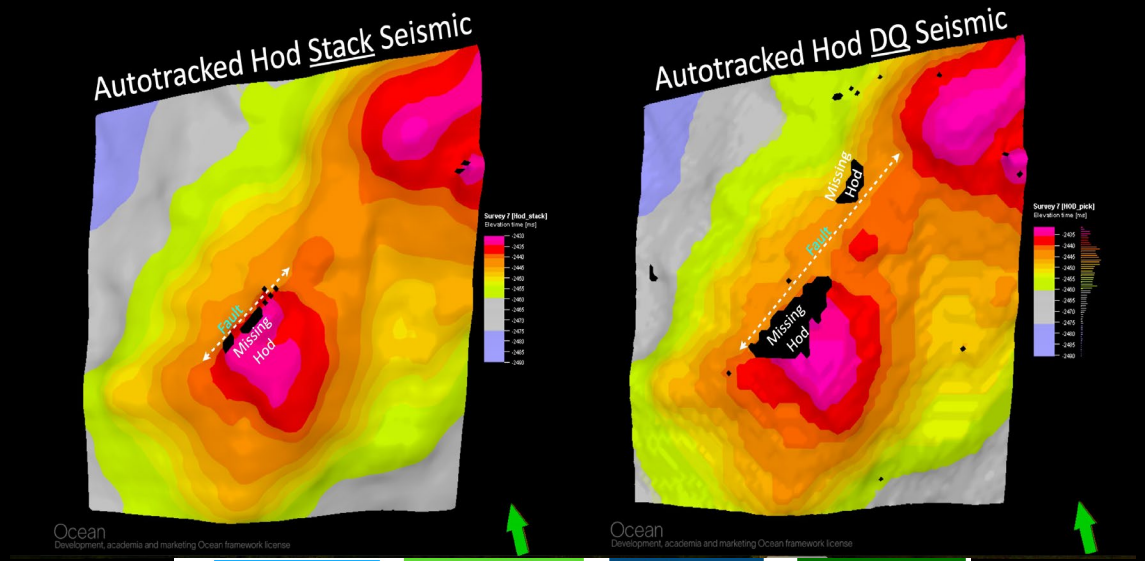

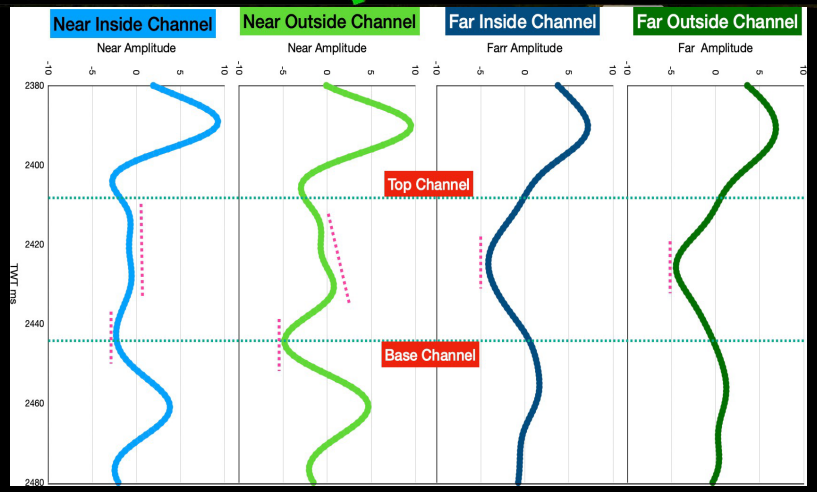

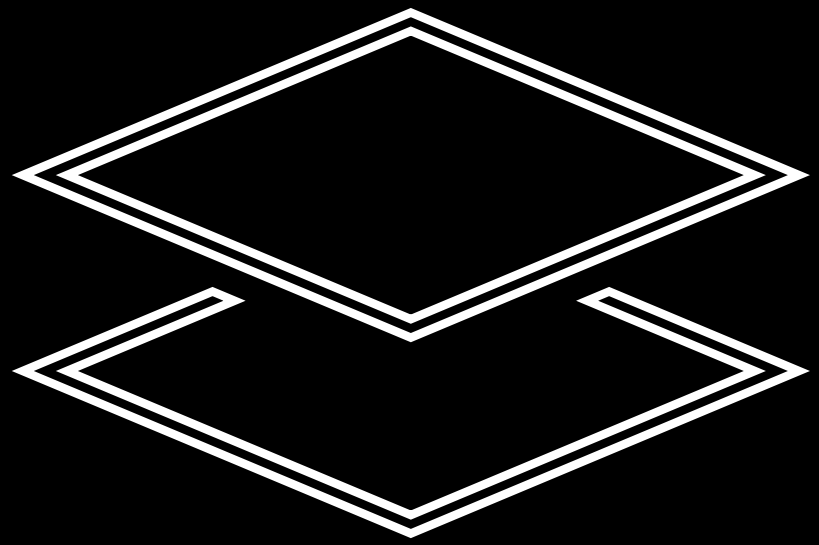

Step 4

Step 4

Convolution, not deconvolution with 8 phase-filters

The transition from sinusoidal to layer-based traces uses the 8 phase-filters. It defies four decades of industry norm and is the hardest aspect to DQ processing to understand.

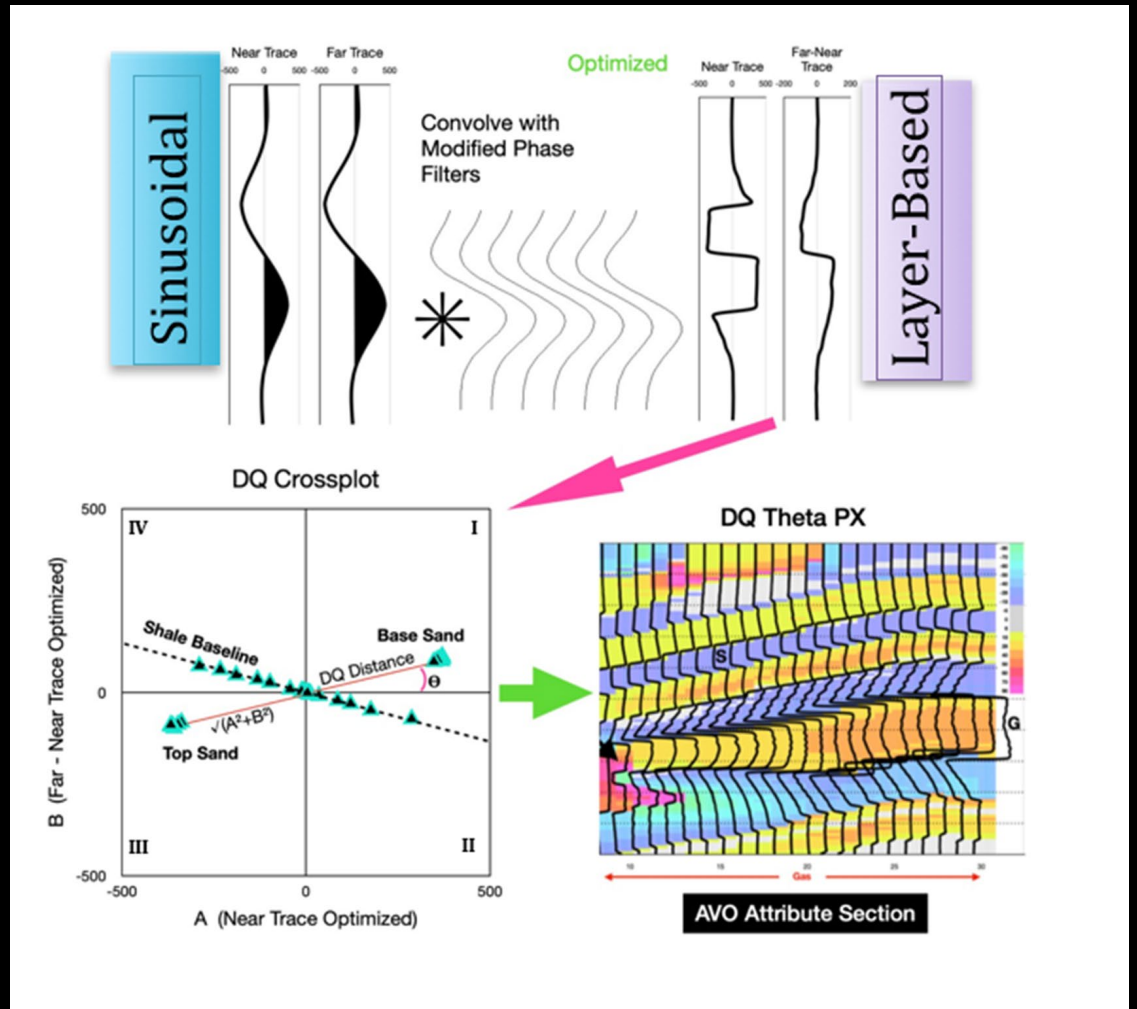

Convolution gives a more precise answer than deconvolution during acoustic impedance inversion because the extracted trace amplitude spectrum is not modified; the layering model is fully preserved. As a result, much higher resolution and smoother transitions happen compared to deconvolution-based inversion.

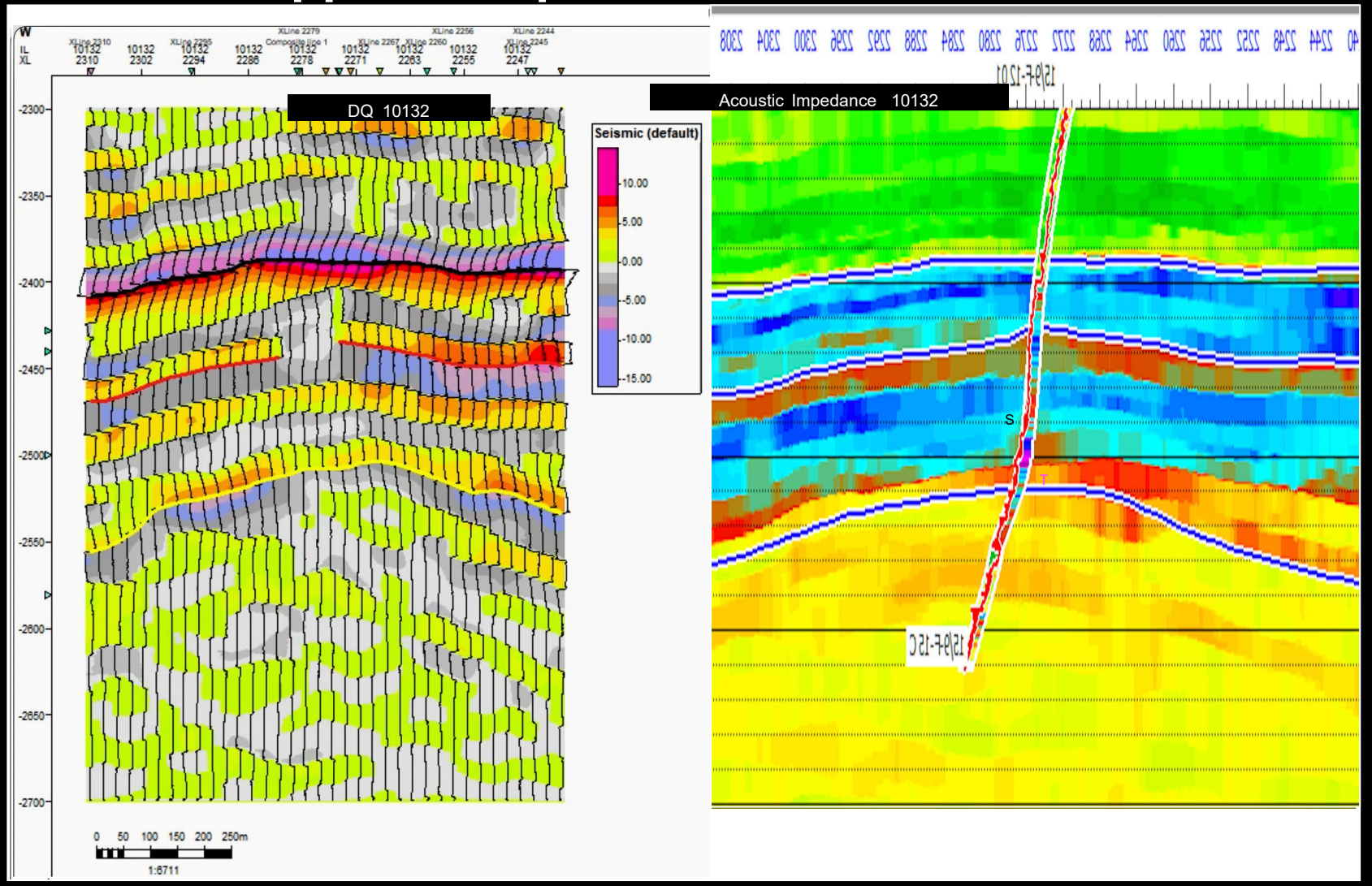

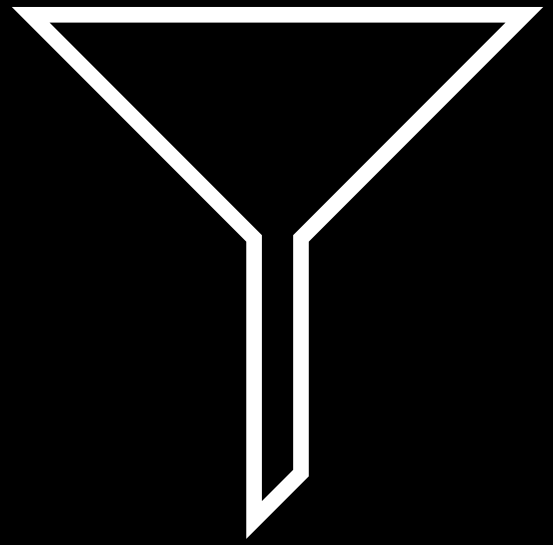

Step 5

Step 5

The pattern for applying the 8 phase-filters is how the DQ trace is able to return the shape of a porosity log. It is also necessary to scale each filter to a different amplitude as seen in the lower right graph. Until that is done, every DQ trace looks like a Hilbert transform amplitude envelope; it has an umbrella or "D" shape like #7 below.

Quadrant #	Phase Angle	Phase Filter
8	158	-22.5
1	180	0.0
2	203	22.5
3	225	45.0
4	248	67.5
5	270	-90.0
6	293	-67.5
7	315	-45.0
8	338	-22.5
9	360	0.0
2	23	22.5
3	45	45.0
4	68	67.5
5	90	-90.0
6	113	-67.5
7	135	-45.0
8	158	-22.5
1	180	0.0
2	203	22.5

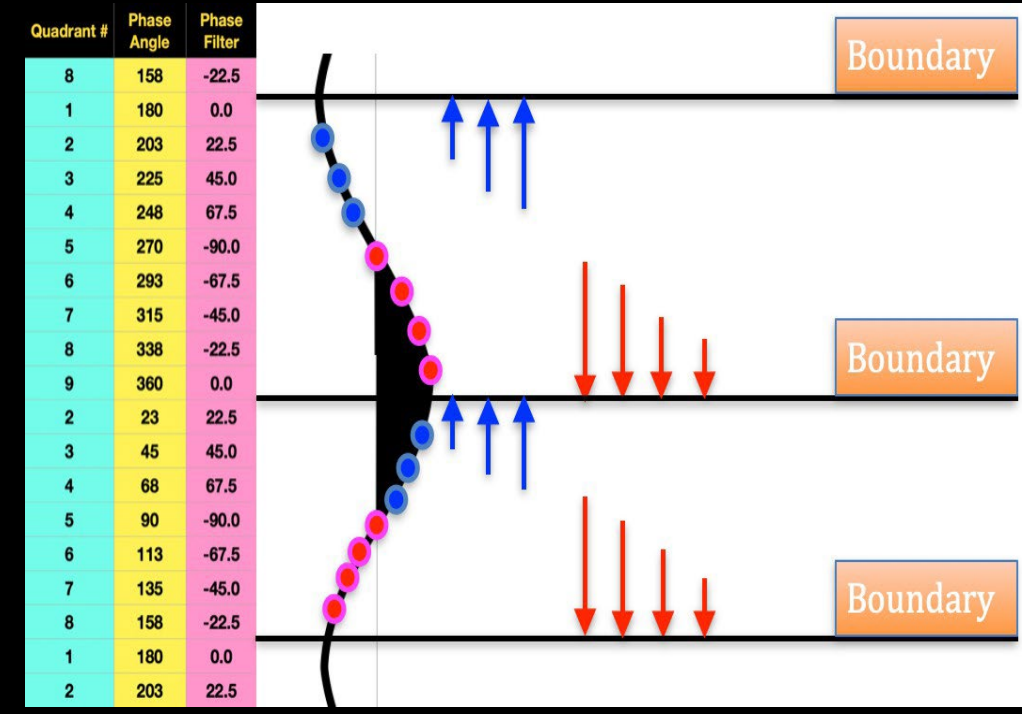

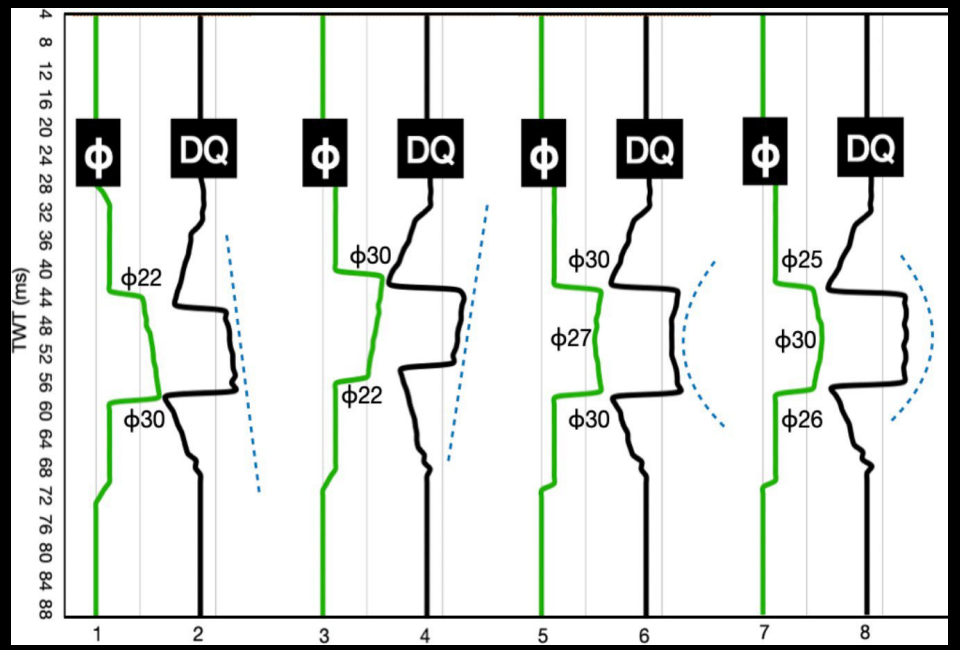

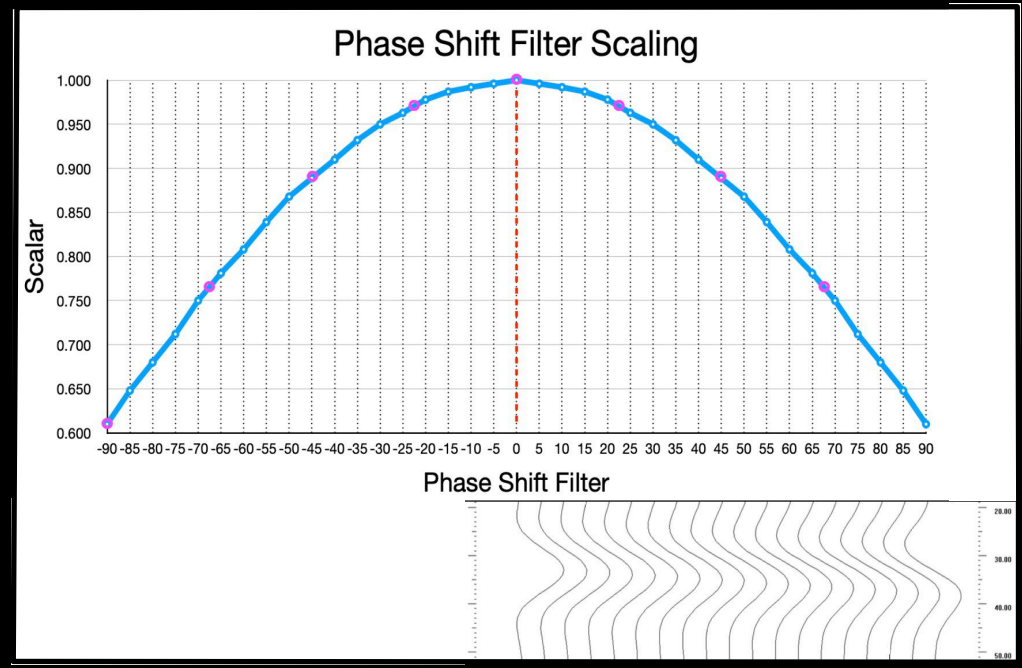

The upper right graph shows why deconvolution is not needed. A peak or a trough amplitude is linearly proportional to the magnitude of the reflection coefficient that caused it to happen. By turning all the samples into peak or trough equivalents, the relative strength of that internal sample's reflector is portrayed had it been located at the acoustic boundary. That in turn gives back the shape of the porosity log that generated the RC series.

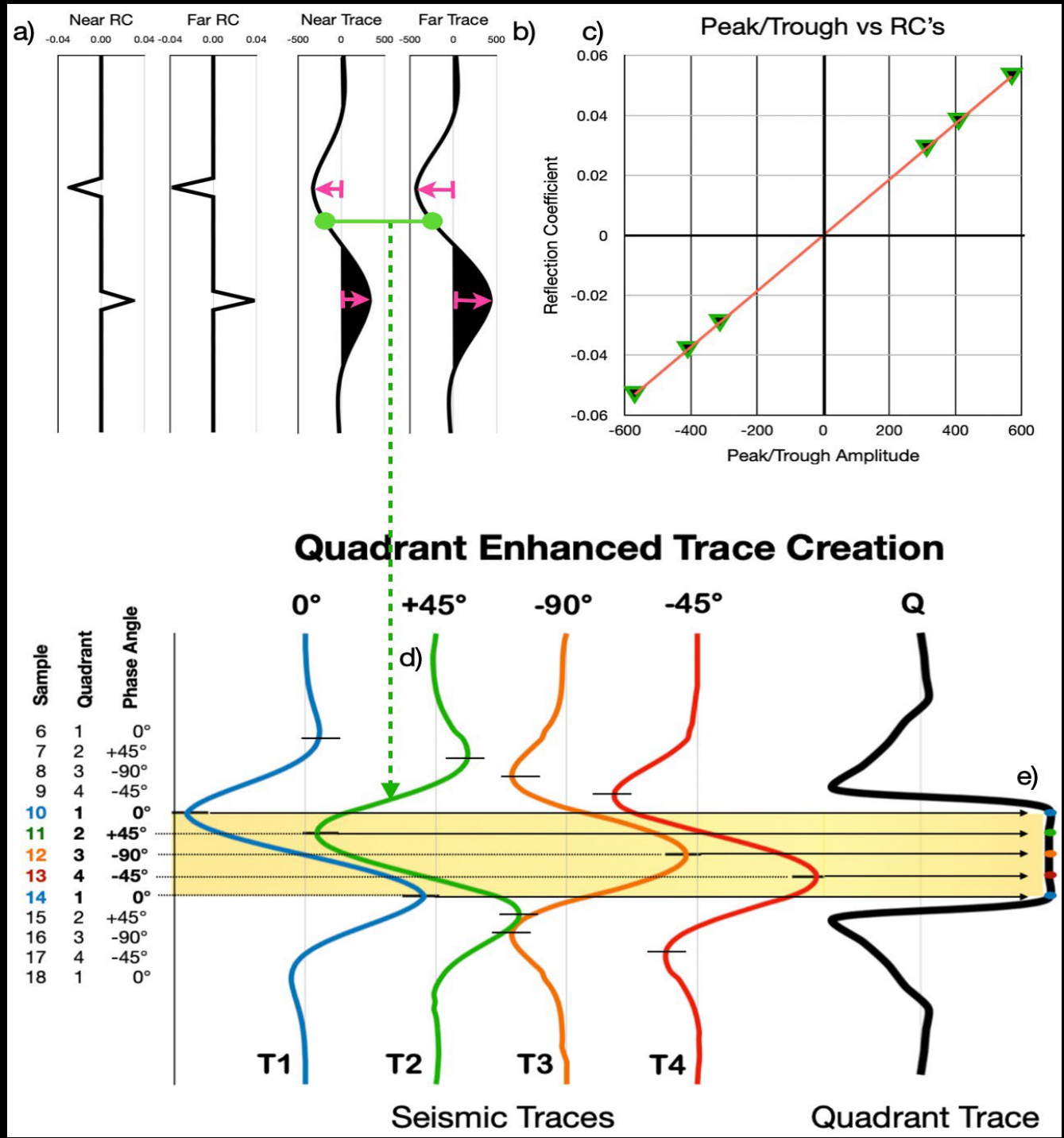

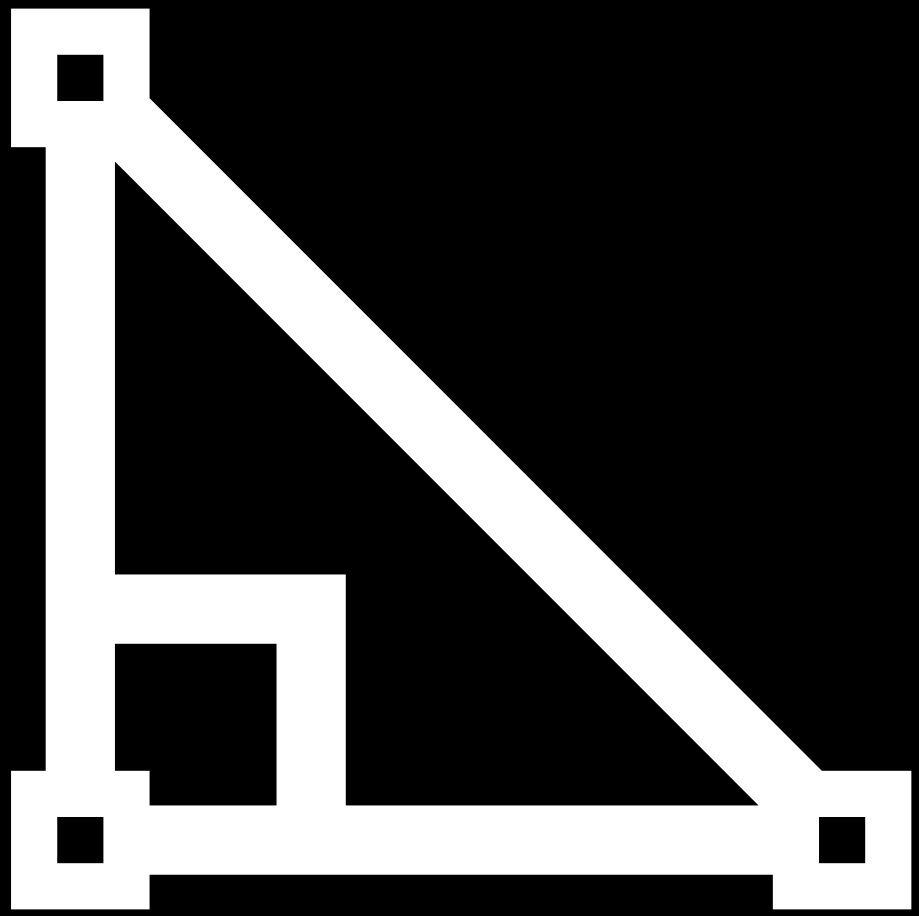

Step 6

Step 6

Shale Baseline at X-axis, not -45° AB graph sector splitting into 4, not 2 sectors

Three sets of wedge models are shown on the RDQ Crossplot. They occupy 4 sectors of the graph and the Shale Baseline is on the X-axis. Notice that both Distance and ThetaPX respond to a change in porosity.

Only Distance responds to a change in sand thickness. The A & B components both contribute to porosity prediction which is why DQ traces are called relative porosity traces.

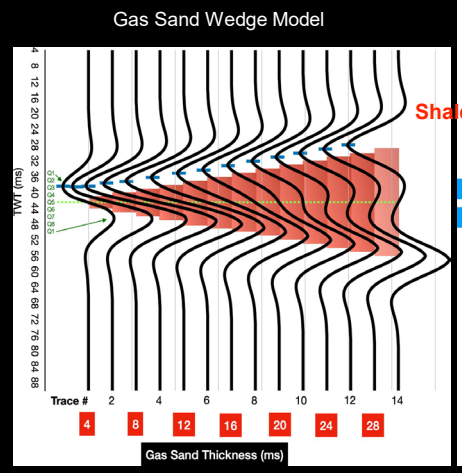

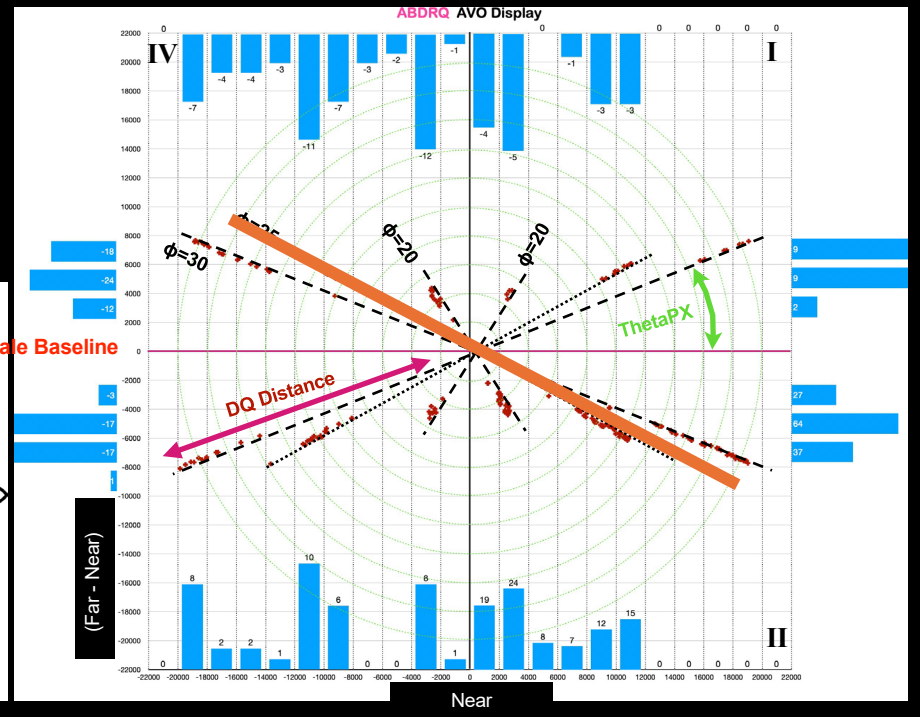

Step 6

Shale Baseline at X-axis, not -45° AB graph sector splitting into 4, not 2 sectors

Three sets of wedge models are shown on the RDQ Crossplot. They occupy 4 sectors of the graph and the Shale Baseline is on the X-axis. Notice that both Distance and ThetaPX respond to a change in porosity.

Only Distance responds to a change in sand thickness. The A & B components both contribute to porosity prediction which is why DQ traces are called relative porosity traces.

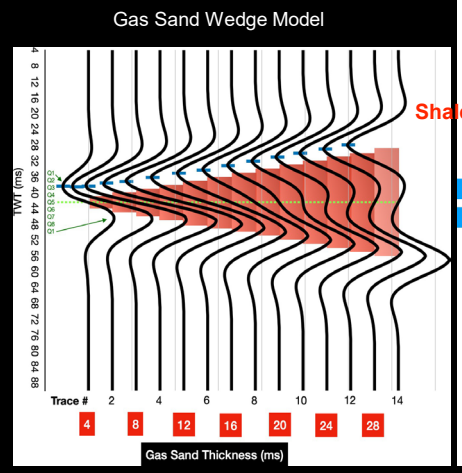

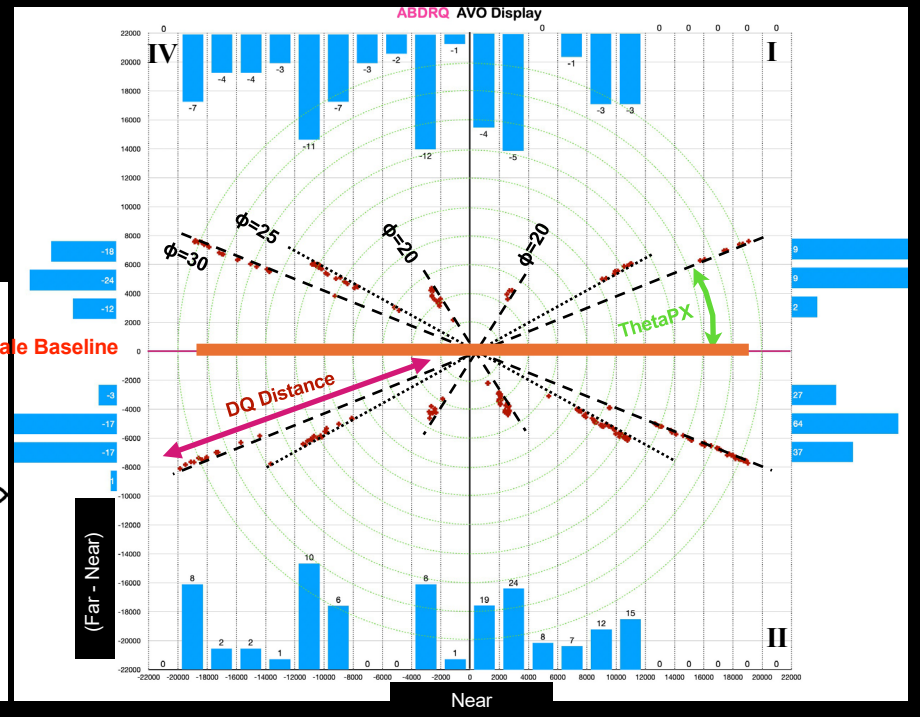

Shale Base AB graph sector splitting int

Three sets of wedge mod Crossplot. They occupy 4 Baseline is on the X-axis. ThetaPX respond to a cha

Only Distance responds to a thickness. The A & B compo contribute to porosity predic why DQ traces are called rel traces.

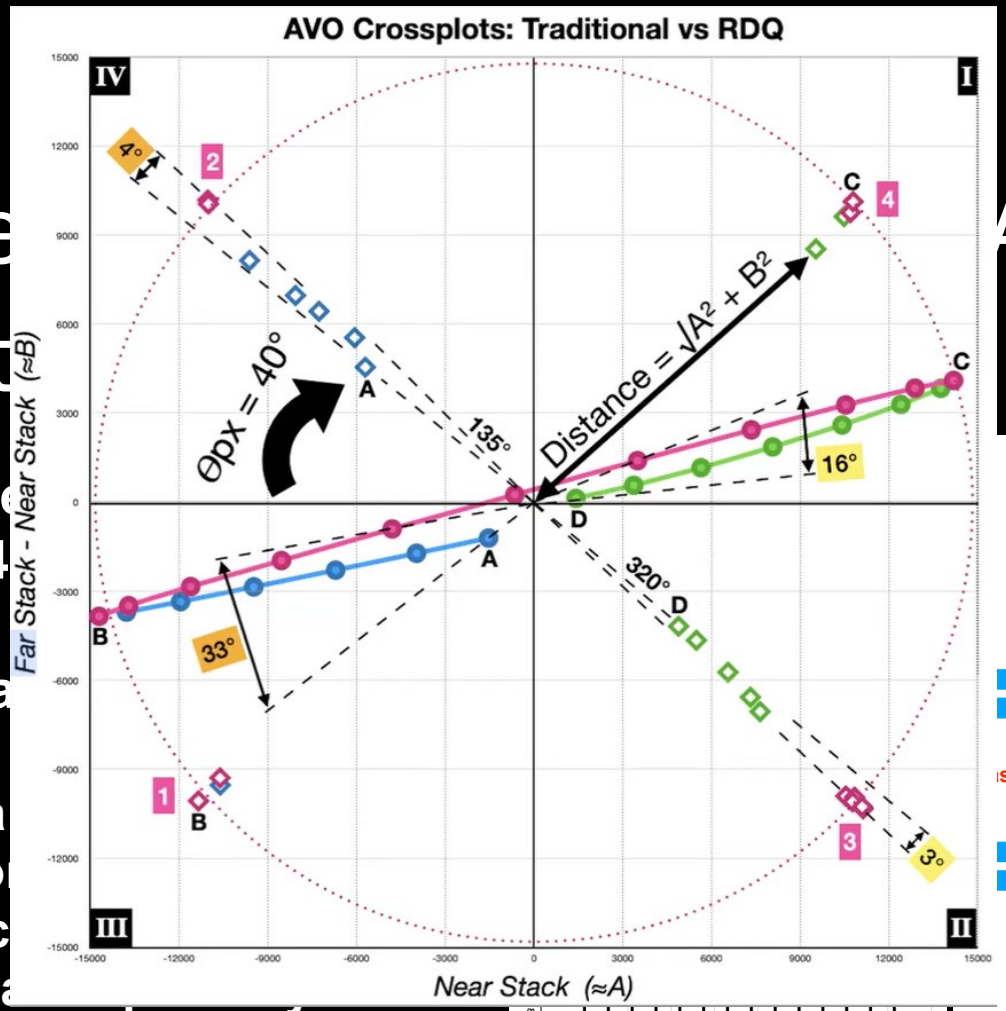

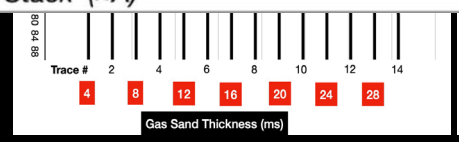

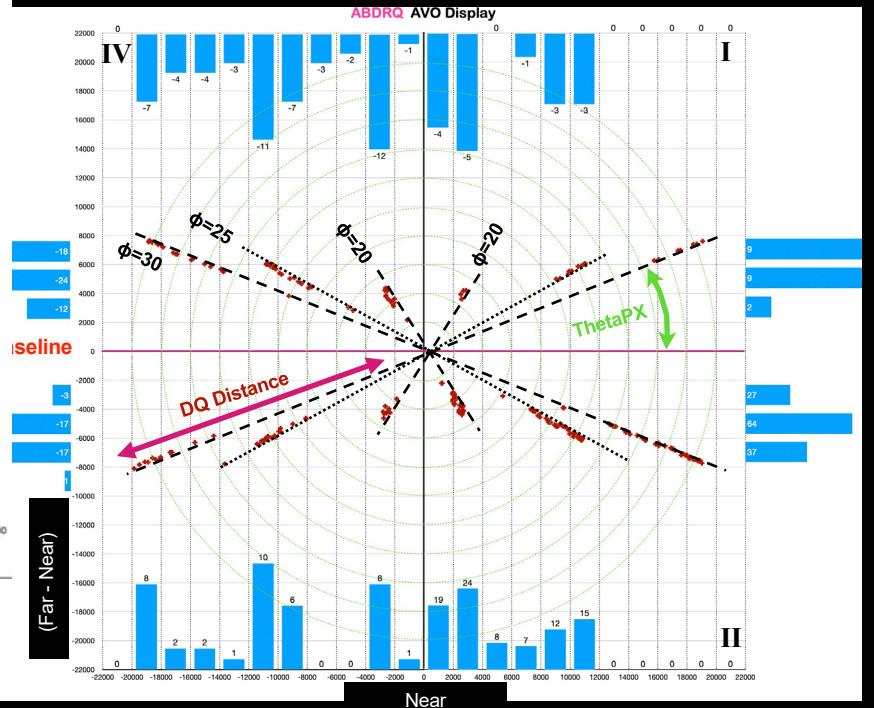

Step 6

Shale Baseline at X-axis, not -45° AB graph sector splitting into 4, not 2 sectors

Three sets of wedge models are shown on the RDQ Crossplot. They occupy 4 sectors of the graph and the Shale Baseline is on the X-axis. Notice that both Distance and ThetaPX respond to a change in porosity.

Only Distance responds to a change in sand thickness. The A & B components both contribute to porosity prediction which is why DQ traces are called relative porosity traces.

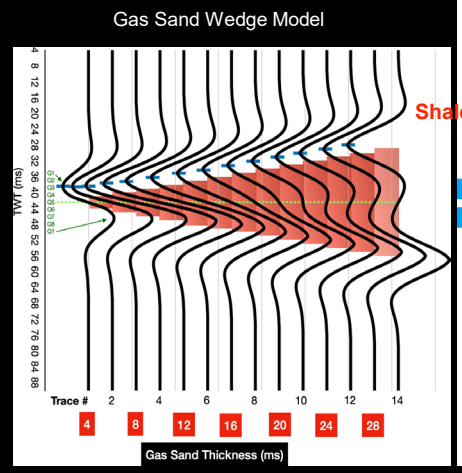

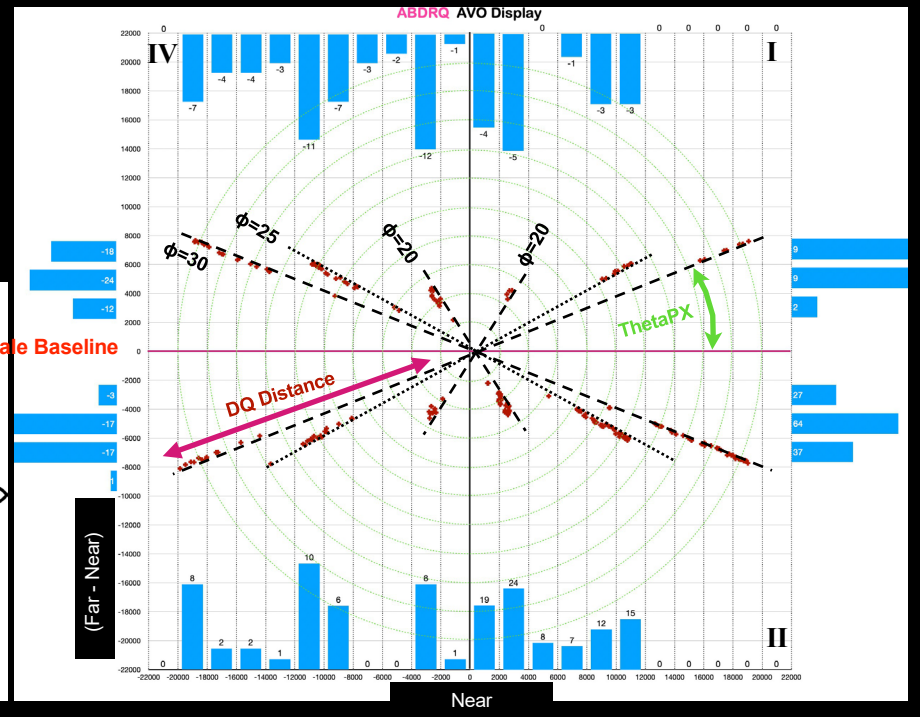

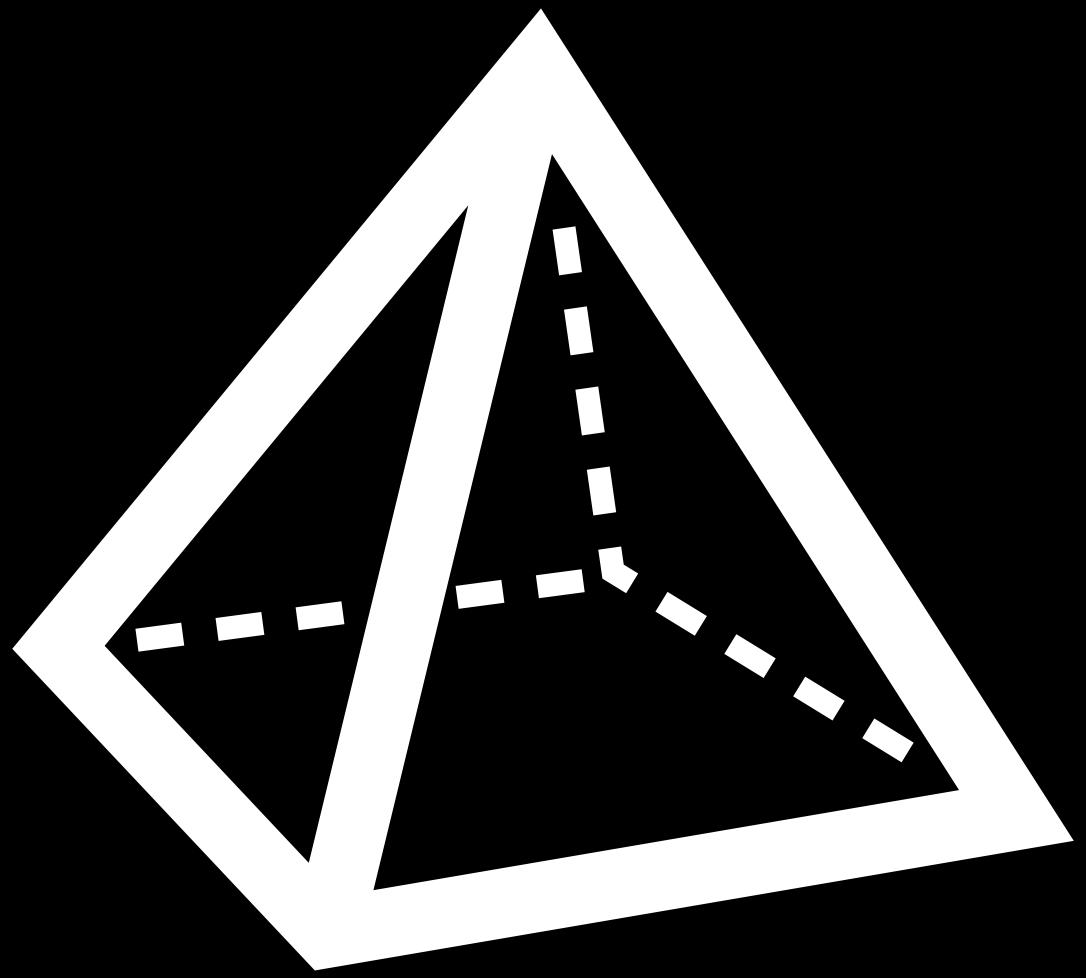

Step 7

Expansion of AB Crossplot to 3D with Signed Half Isochron

Step 7

Four patterns persist on RDQ Crossplots. Two involve tightly clustered data like letters A and B, and two involve linear data trends like letters E and D. All are desirable for
pre- inversion. The band-limited nature of seismic data causes an interval of transition to happen in “boundary shales” at letter D which is undesirable for the DQ display, but unavoidable. It is easily fixed during inversion.

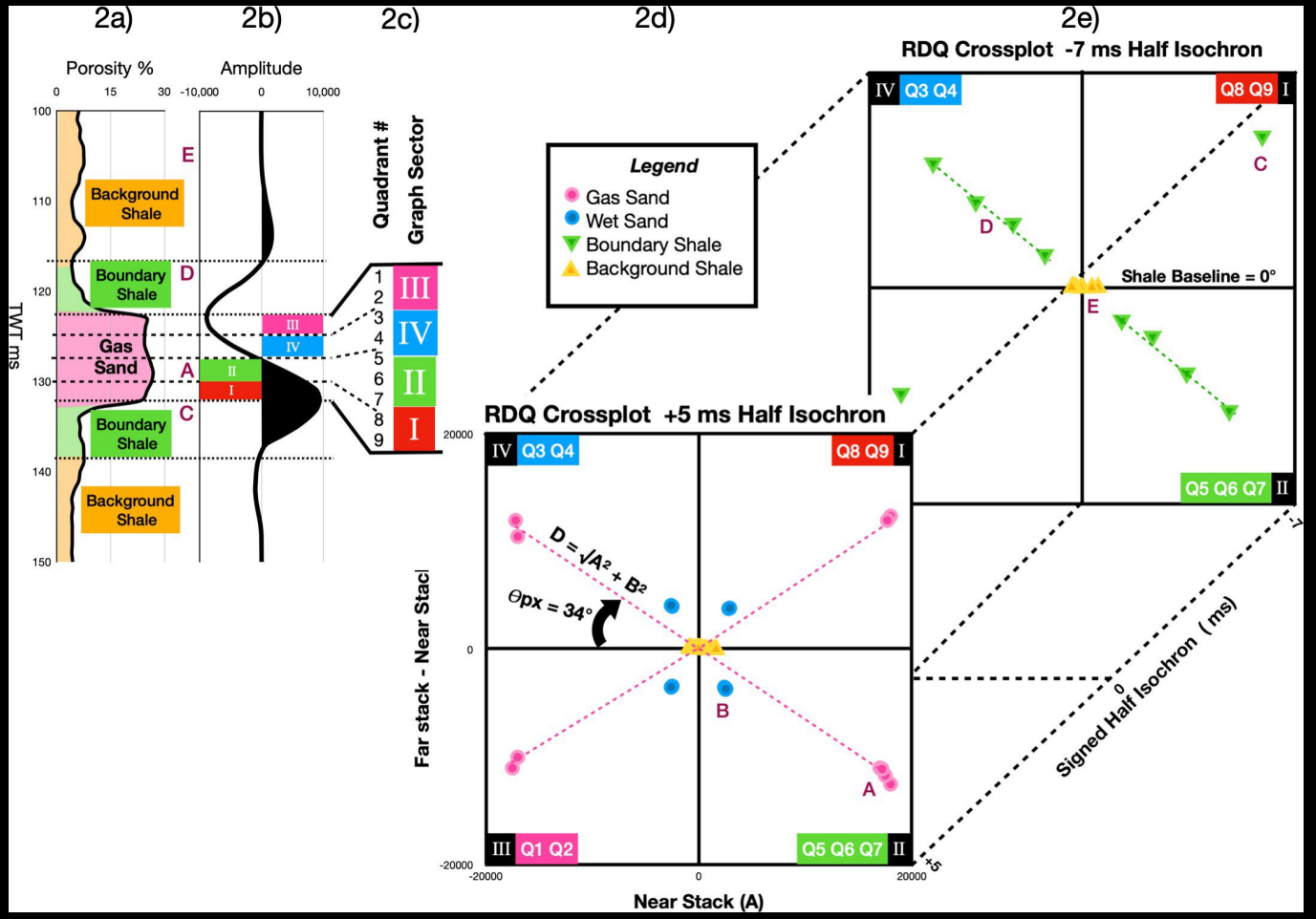

Expansion of AB Crossplot to 3D with Signed Half Isochron

Step 7

Four patterns persist on RDQ Crossplots. Two involve tightly clustered data like letters A and B, and two involve linear data trends like letters E and D. All are desirable for
pre- inversion. The band-limited nature of seismic data causes an interval of transition to happen in “boundary shales” at letter D which is undesirable for the DQ display, but unavoidable. It is easily fixed during inversion.

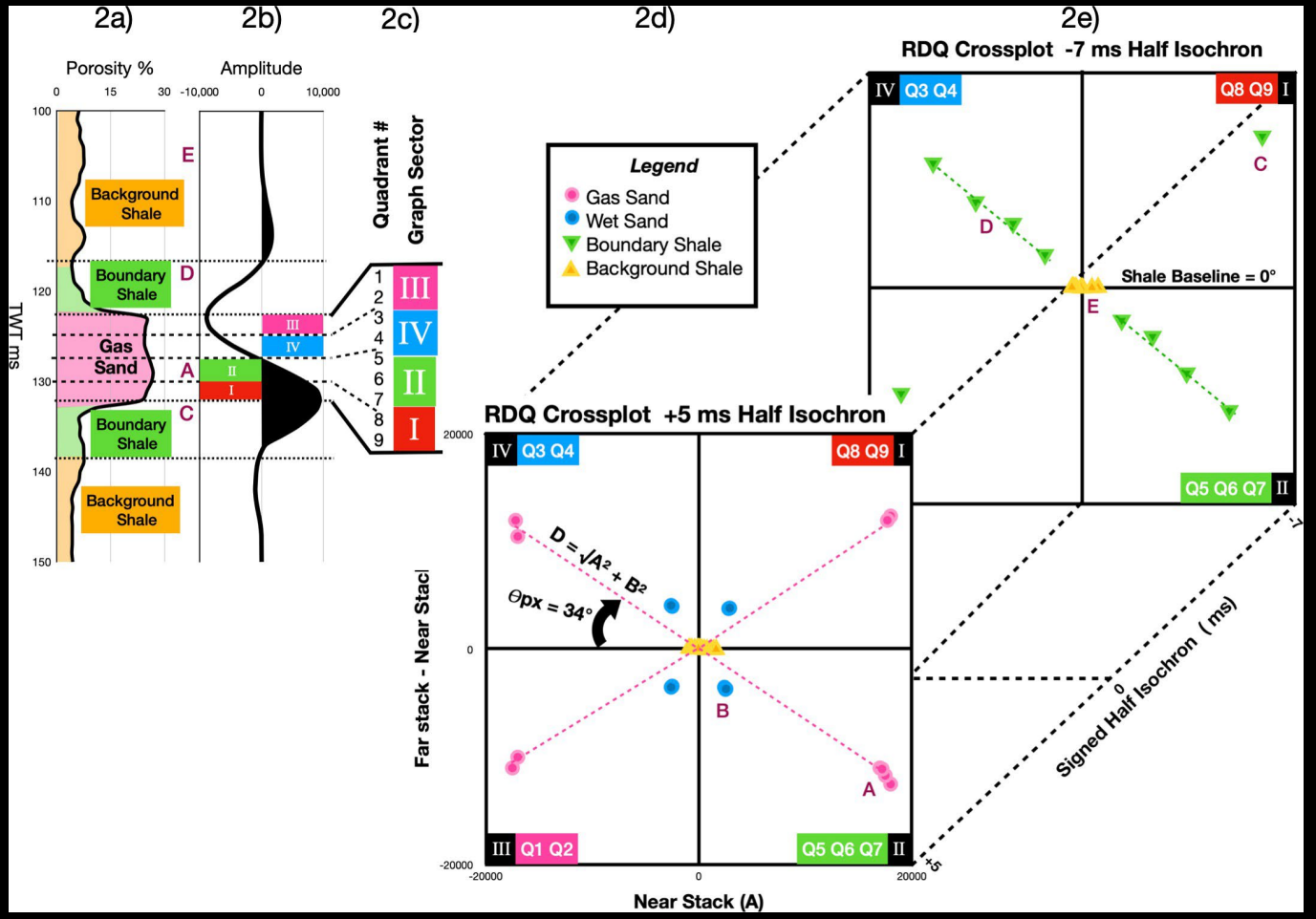

Newly published data by David Went in TLE shows acoustic impedance and shear impedance data crossplotted for a North Sea oil field as is the case for the Volve field. The break- out of patterns and trends is minimal here. Graphs a) and b) look very much like the Near & Far seismic data from Volve (letter f).

The phase-filter, optimized and rotated datapoints of the RDQ crossplot in e) have far better clustering and linear trends developed. Inversion and ML programs will have a much better chance of predicting lithology, porosity and pore fluids when the crossplot patterns are this succinct.

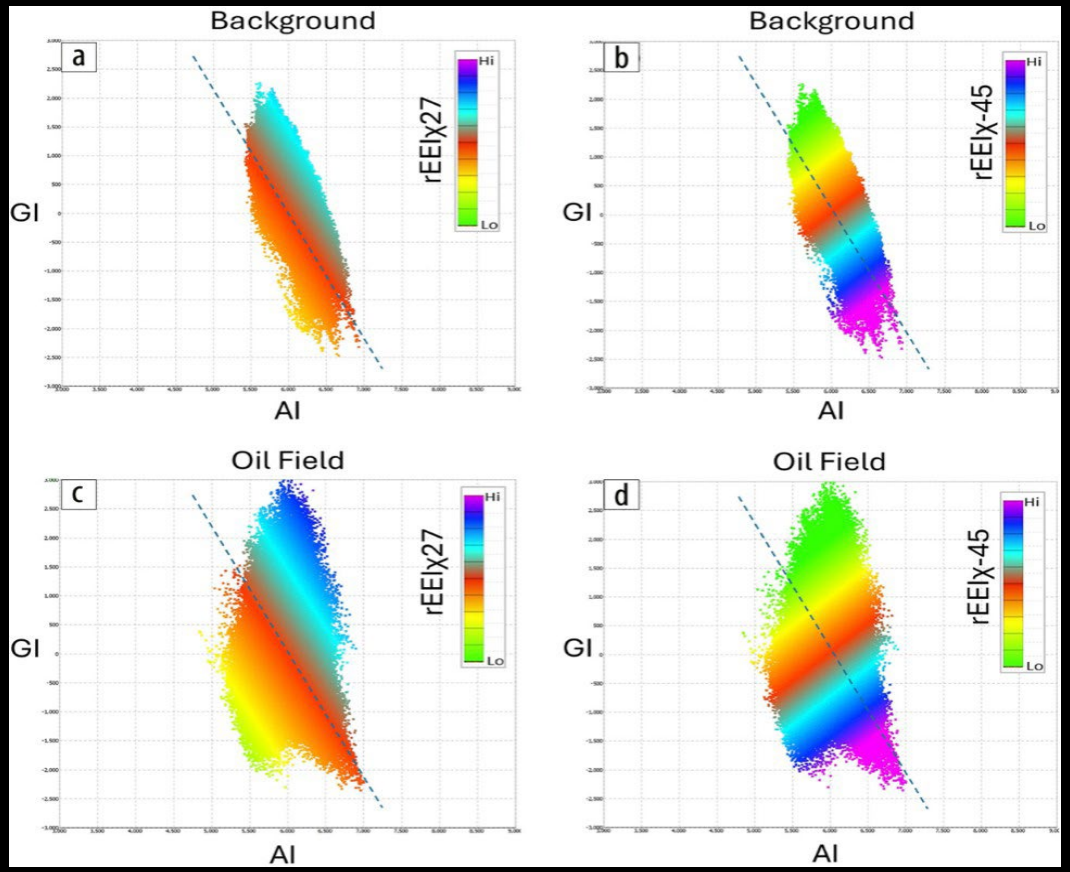

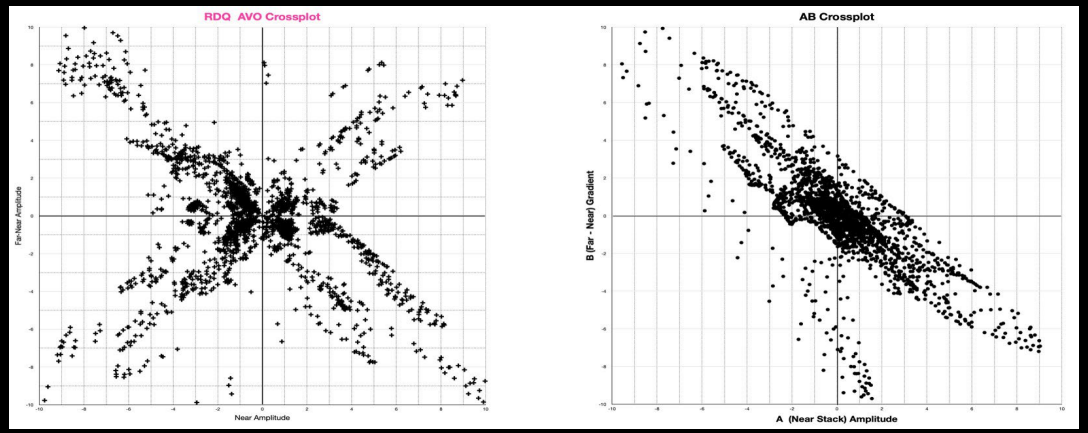

DQ Average - Shetland

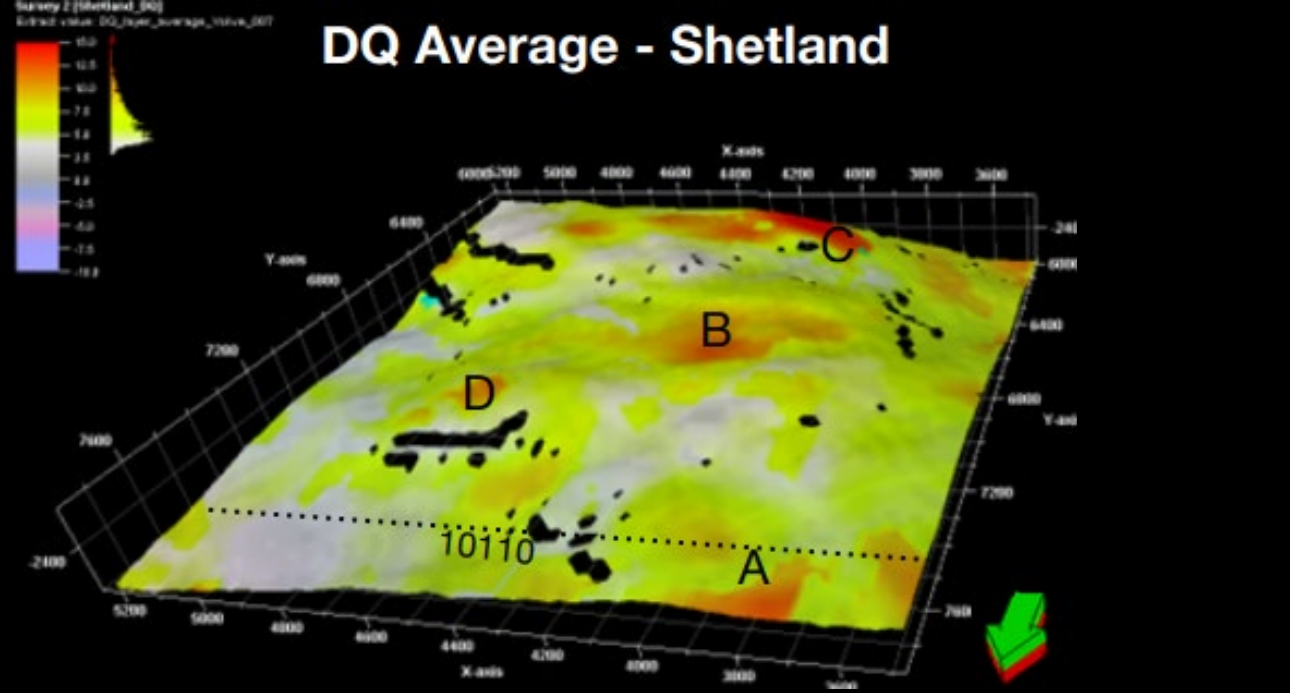

DQ Sum - Shetland

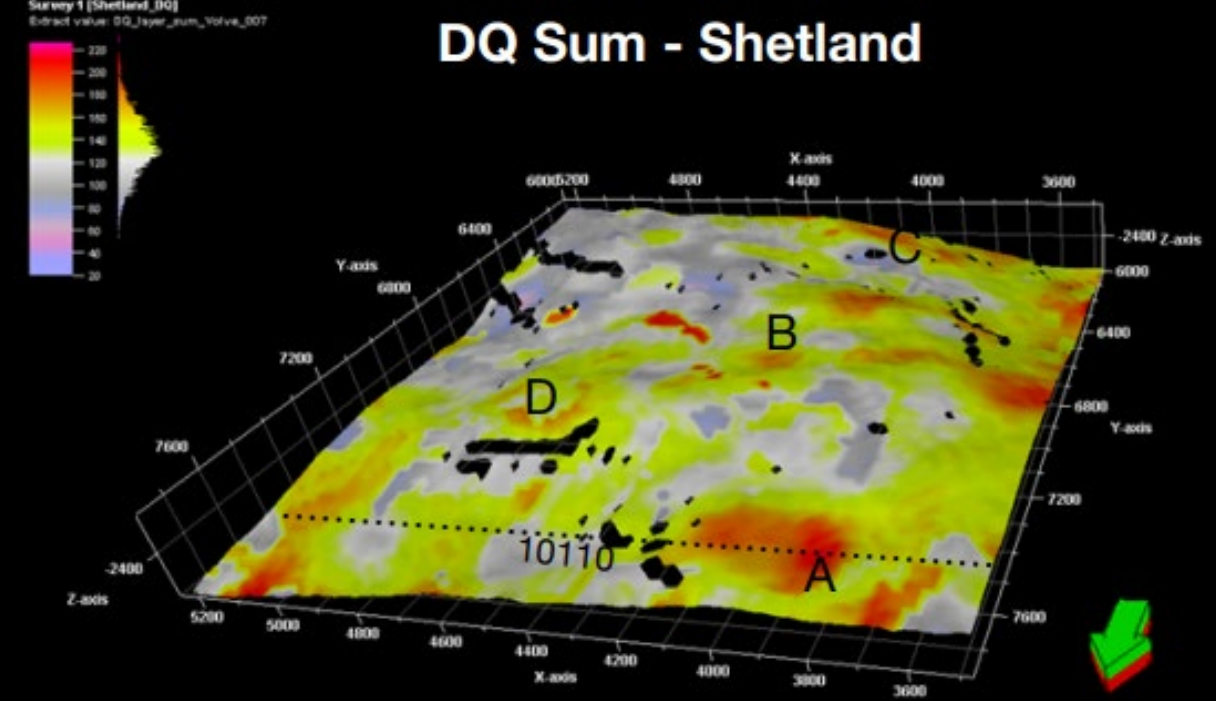

Near Stack Peak Amp - Shetland

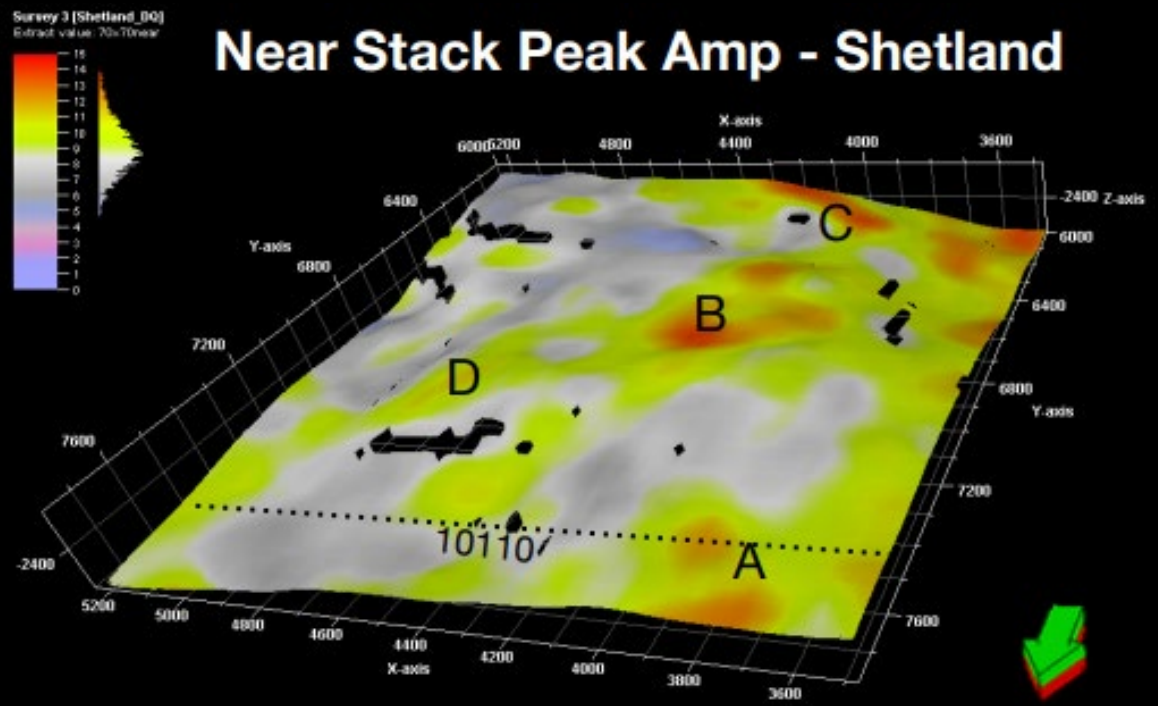

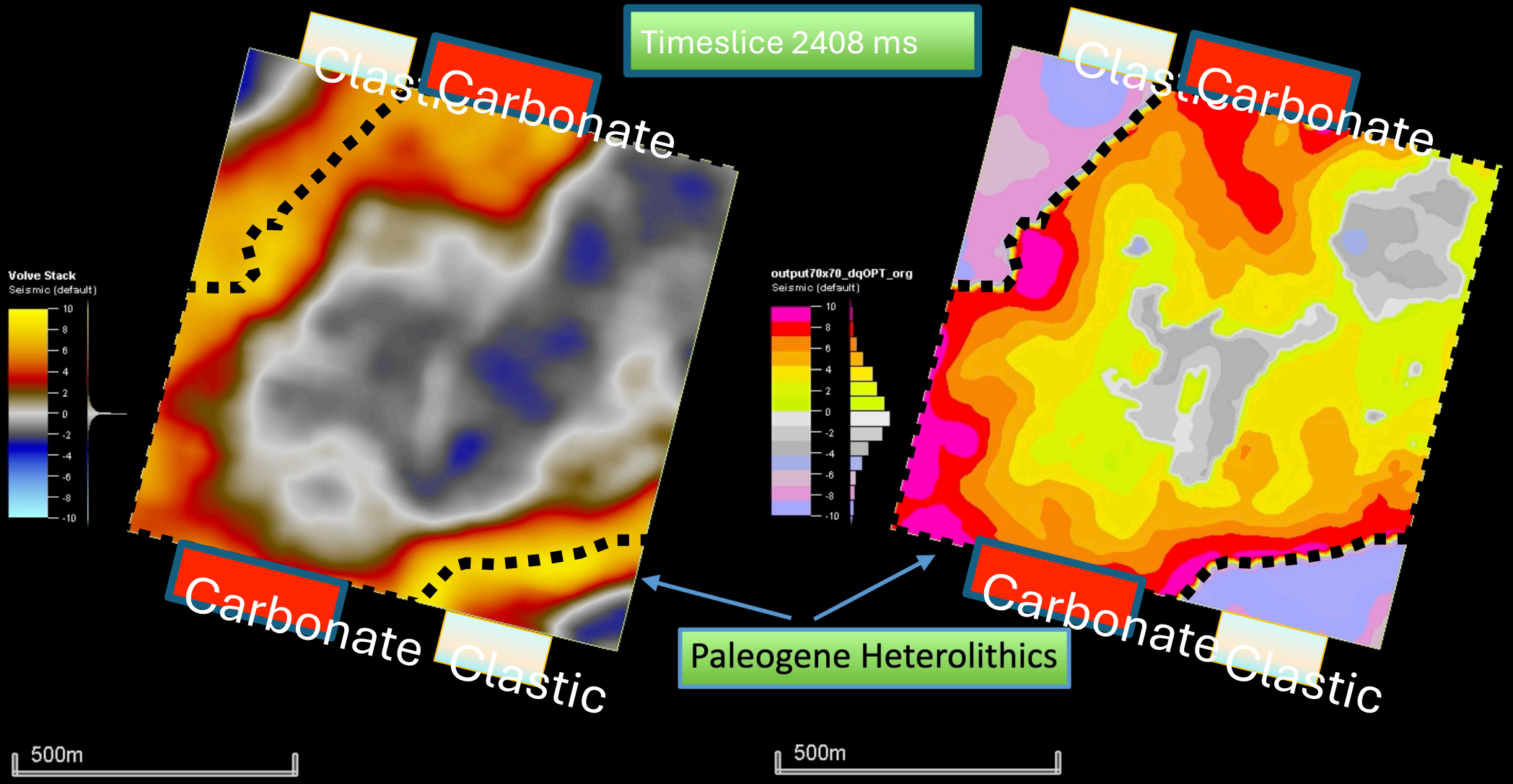
Timeslice 2408 ms
Clastic
Carbonate
Volve Stack
Seismic (default)
10
8
6
4
2
0
-2
-4
-6
-8
-10
output70x70_dqOPT_org
Seismic (default)
Carbonate
Clastic
Paleogene Heterolithics
500m
500m

Thank you!

Dr Heather Bedle
Dennis Neff
Warren Neff
Dr Marfurt
Dr Lubo
Amazing AASPI researchers

equinor

Schlumberger

AASPI sponsors:

Matador

Shell

SHARP REFLECTIONS
A CMG COMPANY

SM ENERGY

ओएनजीसी
ONGC

ConocoPhillips

GEOPHYSICAL INSIGHTS
FROM INSIGHT TO FORESIGHT

OXY

devon

BR
PETROBRAS

eog resources

DIAMONDBACK ENERGY

Dr Heather Bedle
Dennis Neff
Warren Neff
Dr Marfurt
Dr Lubo
Amazing AASPI researchers

Thank you!

Dr Heather Bedle
Dennis Neff
Warren Neff
Dr Marfurt
Dr Lubo
Amazing AASPI researchers

AASPI sponsors: